BIOLOGICALLY ENGINEERED PROTEIN-*GRAFT*-POLY(ETHYLENE GLYCOL) HYDROGELS: A CELL-ADHESIVE AND PLASMIN-DEGRADABLE BIOSYNTHETIC MATERIAL FOR TISSUE REPAIR

Thesis by

Sven Halstenberg

In Partial Fulfillment of the Requirements for the Degree of

Doctor of Philosophy

California Institute of Technology

Pasadena, California

2002

(Defended December 3, 2001)

Post tenebras lux.

(Inscription on the Reformers' Wall

at the University of Geneva, Switzerland.)

Dedicated to my parents.

ACKNOWLEDGMENTS

I thank all my current and past fellow doctoral students, postdoctoral fellows, and senior researchers in the Hubbell lab for teaching me the skills and much of the knowledge that I have acquired during my graduate years. I also thank them for creative suggestions, constructive criticism, and helpful discussions that have propelled my research. In chronological order, I would especially like to acknowledge Don Elbert for teaching me chemical synthesis, Jennifer West for teaching me cell culture, Curtis Herbert for showing me dorsal root ganglion dissections, Alyssa Panitch for introducing me to molecular biology, Petra van de Wetering for renewing and refining my chemical synthesis skills, Heike Hall for comments on manuscripts as well as helpful discussions and support, Alison Pratt for developing and sharing the "fibrin drop assay," and Ronald Schoenmakers for several key ideas and generous help that greatly contributed to this work. I also thank all of them for the friendly and spirited atmosphere that has enriched my time in the group.

At Caltech, I thank Carol Mann and Kathy Bubash for their limitless helpfulness and kindness. At the Swiss Federal Institute of Technology, I gratefully acknowledge Paul Luethi's technical help and friendliness, and, especially, Esther Singer's abundant help and support with the formal and logistical issues of life and research in Switzerland as well as other little sorrows in life.

I thank Ragna Sack of the Protein Analysis Unit, Department of Biochemistry, University of Zurich, for the amino acid analyses; Dror Seliktar of the Institute for Biomedical Engineering, ETH and University of Zurich, for the didansyl oligopeptide; and Anita Saraf of Northwestern University, USA, for help with the rheological measurements.

I thank my co-advisors at Caltech, Prof. Mark Davis, Prof. Scott Fraser and Prof. Dave Tirrell, for their advice, enthusiasm, time, and support during my visits at Caltech.

I am especially appreciative and grateful to Professor Jeff Hubbell for the opportunity to start a new and challenging, but exciting, project when I ran into problems with the first. His patience, guidance, personal support, and advice were indispensable for my research and professional growth, and inspired me to think in many new ways.

Finally, I cannot thank enough my step-grandmother and, above all, my parents for being there during times of personal and situational difficulty.

ABSTRACT

The goal of the research presented in this dissertation was to create a biomimetic artificial material that exhibits functions of extracellular matrix relevant for improved nerve regeneration.

To identify minimal factors necessary for neurite extension in a suitable model system, neural adhesion peptides were photoimmobilized on highly crosslinked poly(ethylene glycol)-based substrates that were otherwise non-adhesive. Neurons adhered in two-dimensional patterns for eleven hours, but no neurites extended. In contrast, human fibroblasts adhered and spread on regions with photoimmobilized RGDS oligopeptide, but not on RDGS peptide, suggesting that specific integrin-ligand binding accounted for fibroblast adhesion and spreading.

To enable neurite extension and nerve regeneration in three dimensions, and to address the need for specifically cell adhesive and cell degradable materials for clinical applications in tissue repair in general, an artificial protein was recombinantly expressed and purified that consisted of a repeating amino acid sequence based on fibrinogen and anti-thrombin III. The artificial protein contained integrin-binding RGD sites, plasmin degradation sites, and heparin-binding sequences. Furthermore, the protein contained six cysteine residues as grafting sites for poly(ethylene glycol) diacrylate via Michael-type conjugate addition. The resulting protein-*graft*-poly(ethylene glycol)acrylates were crosslinked by photopolymerization to form hydrogels. Human fibroblasts attached to, invaded, and apparently proliferated in the artificial hydrogel matrices three-dimensionally. Fibroblast penetration was inhibited in a concentration-dependent manner by both soluble cyclo(RGDFV) peptide and aprotinin, a serine-protease inhibitor. Inhibition of fibroblast

outgrowth by cyclic RGD peptide suggests that cellular integrins engaged in specific binding to RGD sites present in the artificial protein-*graft*-poly(ethylene glycol) hydrogels' protein core. Inhibition by aprotinin suggests that serine protease-mediated cleavage of the hydrogel matrix was the mode of cellular ingrowth.

Although three-dimensional ingrowth of fibroblasts into protein-*graft*-poly(ethylene glycol) hydrogels occurred, only surface neurite outgrowth was observed from chick dorsal root ganglia. Neurite outgrowth depended on the concentration of matrix-bound heparin, suggesting that heparin was necessary to immobilize neuroactive adhesion- and/or growth factors in the hydrogels. Toward three-dimensional neurite outgrowth in protein-*graft*-poly(ethylene glycol) hydrogels, additional heparin-binding factors can be identified or designed for intentional immobilization in future experiments.

Together, the above results show that specific biological functions can be harnessed by protein-*graft*-poly(ethylene glycol) hydrogels to serve as matrices for tissue repair and regeneration. In particular, the two design objectives, specific cell adhesion and degradability by cell-associated proteases, were fulfilled by the material. In the future, this and similar artificial protein-*graft*-poly(ethylene glycol) materials with varying protein elements for improved wound healing might serve as biosynthetic implant materials or wound dressings that degrade in synchrony with the formation of a variety of target tissues.

TABLE OF CONTENTS

CHAPTER 3

SURFACE PATTERNS OF NEURAL ADHESION PEPTIDES ON A POLY(ETHYLENE GLYCOL)-BASED SURFACE TOWARD TWO-DIMENSIONAL ARTIFICIAL NEURAL NETWORKS

CHAPTER 4

DESIGN, SYNTHESIS, AND CHARACTERIZATION OF PROTEIN-*graft*-PEG HYDROGELS

CHAPTER 6

EFFECT OF HEPARIN ON CHICK NEURITE OUTGROWTH ON PROTEIN-*graft*-PEG HYDROGELS

LIST OF FIGURES

LIST OF TABLES AND CHARTS

CHAPTER 1

General Introduction

In the United States alone, more than 200,000 nerve repair procedures are estimated to be performed annually.[1] Despite major advances in the understanding of nerve regeneration and developments in surgical techniques, complete recovery of sensory and motor function after nerve injury is rare.[2] In attempts to repair peripheral nerve injuries where the two severed nerve endings cannot be re-attached directly, the best clinical results are achieved when the nerve gap is bridged with a nerve autograft, considered the "gold standard" for peripheral nerve repair. However, to avoid the use of such an autograft, which causes discomfort and loss of function elsewhere in the patient's body, nerve guide tubes are under intense investigation to be used as implant devices that can provide a defined path as well as physical and immunologic protection for the regenerating nerve until it reaches its target, the severed distal nerve ending. From there on, the remains of the degenerated distal nerve provide sufficient information for the regenerating axons to reach their target organs. Although even empty or saline-filled nerve guide tubes can support regeneration over short distances (e.g., up to a critical injury size of 10 mm in rat sciatic nerve[3] and up to 6 mm in mice[4]), various synthetic and natural materials, including cell-loaded materials, have been tested experimentally to serve as matrices for nerve regeneration inside nerve guide tubes. Most of these materials are either deficient in their ability to significantly improve nerve regeneration beyond critical injury sizes; or various biological and physical concerns prevent their clinical use altogether, such as poor mechanical properties, a severe inflammatory response, poor nutrient supply, or potential epidemiological hazards inherent to human or animal derived substances, unless they are autologous.[5,6]

These deficiencies often apply to materials for tissue regeneration in general, and so far no "ideal" material for tissue repair is available for clinical use. Clearly, different material requirements must be fulfilled to promote regeneration of the different types of

tissue in the body, including target tissues such as cartilage, bone, skin, tissues of the peripheral and central nervous system, etc., but a better understanding and progress in the design of materials for the repair of one type of tissue will also benefit the design of biomaterials for other tissues. It is in this spirit that this doctoral research was conducted, and although Chapter 2 lists material requirements specifically for peripheral nerve regeneration, the basic principles also apply to other types of tissue. Accordingly, the materials intended for peripheral nerve repair, which will be described in Chapters 4, 5, and 6, also hold promise for the repair of tissues other than peripheral nerve.

The specific aim of this doctoral research project was to develop a synthetic alternative to human and animal derived matrices for nerve repair. However, given the promising improvements of peripheral nerve regeneration with modified or native natural materials, notably fibrin and modified fibrin-based matrices, the material developed and presented in this work was highly inspired by substances found in nature. In particular, cell-adhesiveness and cell-controlled degradability are two principal characteristics of natural extracellular matrices that are crucial for wound healing. Accordingly, our design of a material for nerve repair was aimed at achieving (a) specific, three-dimensional cellular adhesion by cell types involved in nerve regeneration as well as (b) cell-associated matrix degradation in spatial and temporal synchrony with cellular outgrowth and/or proliferation.

Since specific cellular adhesion and migration in the material were to be achieved by means of a limited number of biological signals that could possibly be incorporated, initially all efforts were directed at identifying and optimizing a combination of minimal adhesion peptides to promote neurite extension on an otherwise cell-nonadhesive surface and thereby gaining control over neuronal behavior at the level of individual neurons. Like the eventual three-dimensional matrix intended for nerve regeneration inside nerve guide tubes, the surface was that of a highly cross-linked poly(ethylene glycol) (PEG) containing material, in which the high PEG content assured low protein adsorption and zero cell adhesion, unless cellular adhesion sites were covalently immobilized on the surface.

Chapter 3 describes this work involving the photo-immobilization of cellular adhesion peptides and the patterned adhesion and spreading of human fibroblast that was achieved. However, Chapter 3 also describes the limited success with a neuronal cell type that was cultured on this patterned substrate material: Neuronal adhesion was sustained for only up to eleven hours, and neurites did not extend upon the surfaces.

Although neuritic extensions, let alone neural circuits, were never achieved on the PEG surfaces described in Chapter 3, the results with mere fibroblasts on surfaces were still promising. A three-dimensional material that would support specific fibroblast attachment and penetration still holds great potential as a matrix for nerve regeneration, because initial ingrowth of fibroblasts and Schwann cells is known to precede and promote the subsequent invasion of axons during nerve regeneration (Chapter 2). This is likely due to, both, trophic factors as well as extracellular matrix molecules that fibroblasts and Schwann cells secrete.

Extrapolating from two-dimensional cell adhesion to the intended three-dimensional neuronal cultures, subject to the biological "boundary conditions" reviewed in Chapter 2, gave rise to the design and development of a three-dimensional matrix for nerve regeneration that is described in Chapter 4. The material, a non-toxic protein-*graft*-PEG hydrogel, could be formed in direct contact with cells by photo-crosslinking PEGylated artificial protein precursors under physiological conditions. The ability to rapidly cross-link a solution of protein-*graft*-PEGacrylate precursor molecules by light and *in situ* was important so as to allow curing of the material around the severed nerve endings during surgery. In fact, the entire Chapter 4 is dedicated to the unique chemistry chosen to synthesize the protein-*graft*-PEGacrylate precursors, their crosslinking, and to the physical characterization of the resulting hydrogels.

Chapter 5 is dedicated to the biological properties and *in vitro* performance of the protein-*graft*-PEG matrices in contact with human cells. In a model system, in which fibroblast clusters were embedded inside protein-*graft*-PEG hydrogels, invasion by the

fibroblasts into this biosynthetic, highly crosslinked matrix was observed. This suggested that the material was indeed a successful representative for a truly new class of materials that are specifically biofunctional and cell-responsive. In particular, it was shown that cellular penetration of the protein-*graft*-PEG matrices was due to specific interaction with integrin-binding cell adhesion motifs that had been incorporated into the protein backbone of the hydrogels, and that cellular invasion required cell-associated proteolytic degradation in synchrony with cellular outgrowth and apparent proliferation inside the material.

While none of the neuronal cell types tested *in vitro* produced neuritic extensions inside the protein-*graft*-PEG matrices, perhaps due to poor viability or insufficient neuronal protease activity, axons extended abundantly upon the protein-*graft*-PEG hydrogels in studies with two-dimensional cultures, as elaborated in Chapter 6. Amazingly, this neurite outgrowth from chick dorsal root ganglia was independent of the presence of exogenous extracellular matrix proteins fibronectin and laminin, but depended vitally on the presence of heparin bound to the heparin-binding sites of the protein-*graft*-PEG matrix.

Since the protein-*graft*-PEG material described in this doctoral thesis fulfilled some essential requirements toward functioning as a matrix for nerve regeneration, such as suitable physical properties, apparent lack of cytotoxicity, cell adhesivity, proteolytic degradability, and ease of handling, the hope is that possible future experiments will prove the material's successful performance in supporting improved nerve repair *in vivo*. Toward this end, it might prove conducive or even necessary to pre-seed the matrix with suitable supporting cells, such as autologous Schwann cells. Such and other continuing experiments are envisioned and discussed in Chapter 7.

Beyond the context of nerve regeneration and repair, Chapter 7 also briefly touches upon the role that the general class of biosynthetic PEG-based materials might play in the future of wound healing and tissue repair. Among this class of materials the particular

protein-*graft*-PEG hydrogels described in this doctoral thesis are merely an expandable prototype.

CHAPTER 2

INTRODUCTION TO PERIPHERAL NERVE REGENERATION AND REPAIR

BIOLOGICAL BACKGROUND

Axonal Pathfinding

Axonal pathfinding during development or the regeneration of nerves *in vivo* is governed by complex interactions of a neuron's growth cone with its environment. Cell-cell interactions, cell-extracellular matrix interactions, gradients of inhibitory or neuroinductive molecules and growth factors, as well as electrical stimuli all provide possible cues for the growth cone's complicated task of establishing the correct connections among neurons in the brain or between neurons and their target organs in the periphery of the body. In culture, however, a cell adhesive substrate and the presence of sufficient growth factors in the culture medium alone can support outgrowth of neurites and the formation of synapses. Within dense three-dimensional substrates, neuronal outgrowth also requires proteolytic activity, unless the substrate material is porous or fibrillar and, thus, effectively allows for unobstructed two-dimensional outgrowth within the pores or along the material's fibers. However, such conditions do not exist at the site of a nerve injury, where a dense fibrin clot and even scar tissue may form, nor within the remains of a distal nerve piece where, after axotomy and Wallerian degeneration, Schwann cells shape and populate a dense extracellular matrix surrounded by basal lamina or endoneurial tubes.[2]

An informative review of the molecular and cellular events ensuing after nerve crush or axotomy, i.e., the complete severance of an axon, and of early approaches to enhance peripheral nerve regeneration via nerve guide tubes, can be found in the reviews by Seckel, 1990,[2] and Fawcett and Keynes, 1990.[7] The following overview is based on their work.

Wallerian Degeneration of the Distal Nerve Stump

In the distal nerve stump, myelin, which surrounds nerves in the healthy peripheral nervous system, begins to deteriorate 96 hours after axotomy (Figure 2.1.B).

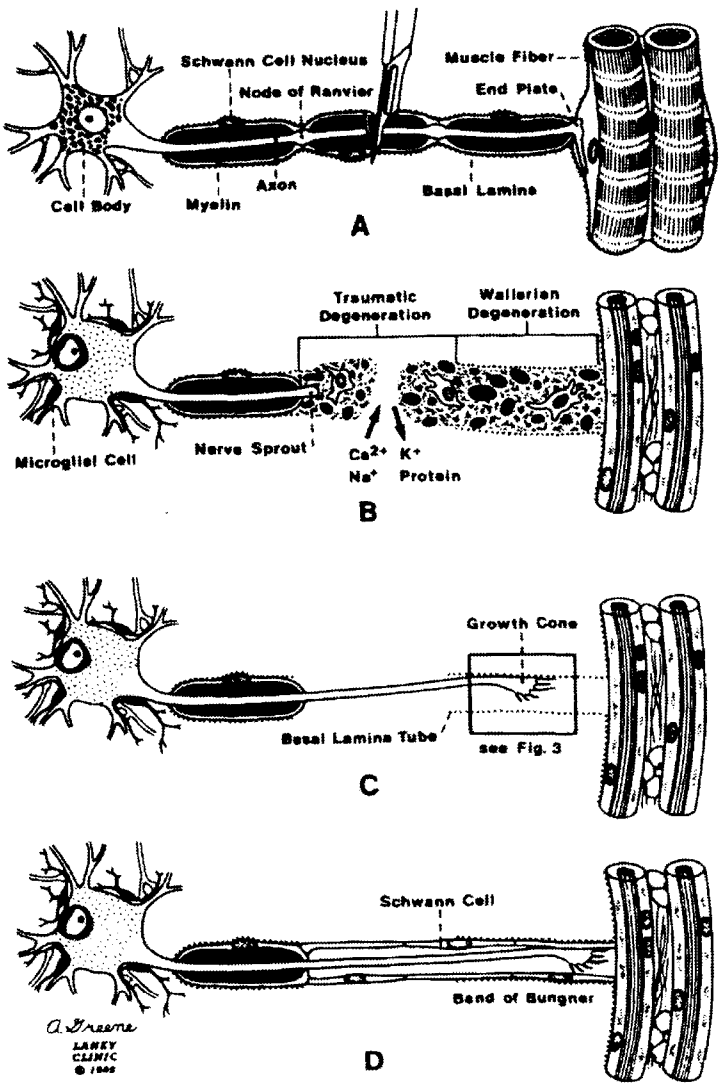

Figure 2.1 A-D: Spontaneous Regeneration of Peripheral Nerves after Axotomy

Schematic of a single myelinated neuron regenerating after axotomy. An actual nerve consists of thousands of such axons, bundled into fascicles and surrounded by basal lamina and endoneurium. (from Seckel, 1990)[2]

Schwann cells proliferate and, together with invading macrophages, remove the myelin debris by phagocytosis. During this process, the basal lamina tubes and endoneurium, which are connective tissues that ensheathe the myelinated nerve fibers, persist. Schwann cells align longitudinally within the confines of the basal lamina and form continuous columns of cells called endoneurial tubes or bands of Büngner.[8,9,10] At later stages, Schwann cells also deposit collagen along both surfaces of the basal lamina tube, while the basal lamina itself consists of collagens, laminins, fibronectin, heparan sulphates, proteoglycans, and enactin.[11,12]

Axonal Regeneration From the Proximal Nerve Stump

In the peripheral nervous system, axons that survive rapid traumatic degeneration near the tip of the proximal nerve stump (Figure 2.1.B) have the capacity to re-sprout spontaneously after axotomy (C). In fact, the injury leads to a dedifferentiation of the injured neurons toward a more plastic or embryonic state that permits growth.[13,14,15] This may be due to the loss of certain trophic factors from the periphery that usually maintain the differentiated, mature state of a functional neuron.[16]

Extracellular Adhesion Molecules

Besides the necessity of certain neurotrophic factors to sustain neuronal survival (not directly subject of this thesis, but reviewed elsewhere),[17,18,19] supporting cells and regenerating growth cones require adhesion molecules that provide adhesion sites for mechanical attachment, signalling for vital second messenger pathways toward proper gene expression and differentiation state, and directional cues for continued outgrowth. Adhesion molecules can be divided into cell-cell adhesion molecules (cell adhesion molecules) and cell-matrix adhesion molecules (extracellular matrix adhesion molecules).

Cell Adhesion Molecules

Since the aim of this research project was to design a matrix that would support ingrowth of both neuronal and supporting cells, and since those supporting cells were expected to provide the cell-cell interactions necessary for sustained neurite outgrowth, the main objective of the matrix was to provide equivalents of the necessary extracellular matrix molecules that are required for cellular adhesion during nerve regeneration. Therefore, the focus of the following section will be on extracellular matrix molecules, particularly those that function in neuron-matrix adhesion. For an overview of cellular adhesion molecules such as neural cell adhesion molecule (N-CAM), neuroglia CAM (NgCAM or L1), the fasciclins, N-cadherin, etc., the reader is referred to introductions by Jessel, 1991,[20] and Nicholls *et al.*, 1992,[21] or to studies by Daniloff *et al.*, 1986,[22] and Martini and Schachner, 1988,[23] that focus on neural adhesion molecules expressed, e.g., by Schwann cells, in response to injury and ensuing repair.

Extracellular Matrix Adhesion Molecules and Their Cellular Receptors

The extracellular matrix (ECM) is a complex set of collagens, noncollagenous glycoproteins, glycosaminoglycans and proteoglycans. ECM adhesion molecules among these constituents play important and defining roles in the development and regeneration of neurons after injury. During peripheral nerve regeneration, especially those adhesion molecules that are contained in the basal lamina tubes, which persist or are maintained even after Wallerian degeneration, provide crucial ligands and directional cues for growth cone attachment and outgrowth. Ligands for cell surface-associated integrin receptors (reviewed specifically in the context of the peripheral nervous system by Previtali *et al.*, 2001),[24] and the integrin-binding RGD motif in particular,[25] are the most prominent and abundant factors in the ECM that enable neuronal attachment and extension. The RGD domains in laminin,[26] fibronectin,[26] collagen type I and IV,[27] and thrombospondin[28] have all been directly implicated in neurite outgrowth.

Especially laminin, a large (900 kDa), three-chain (A, B1, B2), cross-shaped glycoprotein found in basement membranes, functions as a very potent substrate for neurite outgrowth *in vitro*. Laminin contains a number of additional, non-integrin binding sites. Although some uncertainty remains regarding the relative significance of its domains in mediating attachment and/or outgrowth, and about the specificity of some of the corresponding laminin receptors,[29] it seems clear that at least the following sites in laminin are functionally relevant for neuronal cell and growth cone adhesion: a domain in the B1 chain containing the amino acid sequence YIGSR;[30,31] a nearby heparin-binding and cell adhesion-promoting site in the globular region of the B1 chain with amino acid sequence RYVVLPRPVCFEKGMNYTVR;[32] and a site at the end of the long arm in the A chain containing the amino acid sequence IKVAV.[33,34,35]

As far as the corresponding cellular receptors for laminin's adhesion domains are concerned, a 67 kDa non-integrin receptor has been identified in peripheral neurons that seems to mediate specific binding to the YIGSR-containing active site of laminin.[36,37] Similarly, an IKVAV-specific 110 kDa receptor for neurite outgrowth has been known for several years[38] and been localized in the hippocampus among other regions of the brain,[39,40] suggesting that interactions between laminin and this receptor play a role in controlling axonal guidance during development, or in repair during regeneration.[40]

It is remarkable that, instead of requiring the entire laminin molecule or its local three-dimensional context, neuronal cell-surface receptors also interact specifically with some short synthetic oligopeptides that are functional elements of the above-mentioned domains. Such interactions may not have the full signalling or binding capacity that the native corresponding protein domain has, but short oligopeptides can –to an extent– fulfill the function of the entire domain that they are derived from and, thus, mimic the domain's role as a ligand, for instance. For example, neurons adhere and extend upon defined regions of oligopeptides containing the isolated YIGSR motif,[30,31,41,29,42] as demonstrated, for example, with synthetic, photo-immobilized CDPGYIGSR peptide by Clemence *et al.*,

1995,[43] and others. Likewise, an immobilized synthetic RGD peptide based on the RGD-site of the laminin A chain was active in cell attachment, spreading, migration and neurite outgrowth.[26]

One further laminin-derived peptide sequence that is important for neurite outgrowth, at least in hippocampal cells, is RDIAEIIKDI.[44] This peptide was potent not only in eliciting neurite outgrowth, but also necessary to induce a mature neuronal phenotype of embryonic hippocampal neurons in culture.

Regarding the role of many other extracellular adhesion proteins such as agrin, the tenascins and the thrombospondins, the reader can find comprehensive lists and summaries in the reviews by Reichardt and Tomaselli, 1991,[45] Martini, 1993,[46] Venstrom and Reichardt, 1993,[27] and others.

Proteoglycans represent another important class of adhesion molecules that require mentioning especially in the context of the project presented in this thesis. Proteoglycans are macromolecules composed of glycosaminoglycan chains covalently bound to a protein core. An unusually large number of proteoglycans is expressed in the nervous system, and they are expressed by both neurons and glia.[27] Their functions include roles both as receptors and components of neuronal extracellular matrix that can actively promote neurite outgrowth. An important feature in the context of the materials presented in this doctoral thesis is that proteoglycans' glycosaminoglycan side chains (such as highly negatively charged heparin) provide binding sites for adhesion molecules –such as laminin[47,48]– and growth factors,[49,50] and thus act as indirect modulators of cellular adhesion and growth factor action. One directly neurite-promoting heparan sulfate proteoglycan, that is basal lamina-associated, is perlecan,[51] and its receptors even include integrins.[52]

Some proteoglycans, such as certain chondroitin sulfate proteoglycans,[53,54] can also inhibit neural cell migration and neurite outgrowth, especially at high concentrations.[55] As a consequence, some approaches to nerve repair have involved nerve grafts that were stripped of chondroitin sulfate proteoglycan by incubation with appropriate matrix

metalloproteinases prior to implantation.[56] Proteoglycans may inhibit cell migration and neurite outgrowth by binding to the cell surface, thereby sterically hindering other cell adhesion receptors, or by binding matrix proteins and thereby masking cell attachment sites.[27,57]

As far as the results of the research presented in this thesis are concerned, the balance between enough and too much of the glycosaminoglycan heparin turned out to be of significant importance (Chapters 5 and 6).

Proteolytic Activity of the Growth Cone

In addition to matrix interactions and chemotaxis, extending axons require proteases, in particular plasmin, to penetrate first the cellular debris and initial fibrin clot that they encounter at the site of the injury and, then, to invade and penetrate the remains of the distal nerve piece, when the distal stump is reached. In accordance with numerous *in vitro* studies, Siconolfi and Seeds, 2001,[58] have recently shown that the induction of the plasminogen activator system accompanies peripheral nerve regeneration *in vivo* after sciatic nerve crush in mice. The plasminogen activators (PAs), tissue plasminogen activator (tPA) and urokinase plasminogen activator (uPA), two serine proteases, convert inactive plasminogen to its proteolytically active form, plasmin, which is also a serine protease. Mice lacking tPA, uPA, or plasminogen genes showed delayed functional nerve recovery after sciatic nerve crush.[59]

Plasmin has broad activity by virtue of its ability to cleave many, but not all, peptide bonds carboxy-terminal to basic residues lysine and arginine. In particular, in fibrinogen's α-chain, plasmin cleaves between residues Arg^{104}-Asp^{105}, Arg^{110}-Val^{111}, and Lys^{206}-Met^{207}.[60] Of these cleavage sites, Arg^{104}-Asp^{105} and Arg^{110}-Val^{111} were chosen to be part of recombinant protein pentamer [A] (Chart 4.1, Chapter 4) in order to confer specific

degradability by plasmin to protein[A]-*graft*-PEG hydrogels, the subject material of this thesis.

Although plasminogen's most prominent role is in fibrinolysis in the blood, where it has a circulating concentration of 2 μM, plasminogen is also present in the extracellular/extravascular space of most tissues. However, in tissues, plasminogen activation to plasmin is highly localized to cellular surfaces or to the surface of neuritic growth cones, because uPA, the relevant PA in cell migration and matrix remodelling, binds to a well characterized receptor (uPAR) on cell surfaces.[61] Plasminogen activation and plasminolysis are, thus, limited to the immediate cellular proximity[62] and the direction of neurite outgrowth. Potent and abundant serine protease inhibitors such as α2-plasmin inhibitor and α2-macroglobulin constantly curb plasminolysis and prevent plasmin activity altogether when it diffuses away from the cell surface or neuritic growth cone. Another serine protease inhibitor, and therefore inhibitor of plasmin, is aprotinin. Aprotinin, also known as pancreatic trypsin inhibitor, is a small protein (6.5 kDa) that has high structural complementarity with its target enzymes and engages them in strong electrostatic interactions, thus blocking their proteolytic activity. In the context of this thesis project aprotinin was used to establish a negative control (Chapter 5) for the plasmin degradability of the protein[A]-*graft*-PEG materials presented in Chapter 4.

SURGICAL REPAIR OF TRANSECTED NERVES

Sprouting axons have to be able to reach the distal stump in order for nerve regeneration and eventual reinnervation of the target organ to occur. Therefore, the proximal and distal stumps should ideally be in direct contact, and must not be separated by an insurmountable distance nor be obstructed by ingrowth of scar tissue or poor alignment of the nerve's microstructure. Otherwise, possible consequences include a backward

change in direction of the axonal sprouts, axonal branching into surrounding tissue, or the formation of a neuroma,[63,64] which clinically are all catastrophic results.

To overcome nerve gaps due to large injuries, and evade obstruction by scar tissue between the two nerve stumps, surgical intervention is usually necessary after peripheral nerve lesions. Fine *et al.*, 2000,[65] provide an up-to-date summary of the materials as well as clinical and experimental advances in peripheral nerve repair, upon which the following overview is largely based.

End-to-End Repair

When axotomy results from a "clean cut" and the nerve endings merely retract, it is often possible to reconnect the severed nerve fascicles directly using microsurgical techniques. Presently the most commonly used suture material in end-to-end repair is fine monofilament nylon.[65] Similarly, fibrin glue materials have been used for many years in experimental nerve repair.[66] One experimental system even uses poly(ethylene glycol) to fuse axons of transected nerves in earthworms.[67,68]

These procedures cannot be performed when injury leads to a large nerve gap or when a large segment of the nerve is crushed. Also, after a complete transection it is always difficult to achieve good surgical reconstruction of the former microstructure and to avoid mismatching individual nerve fiber connections. Since many neurons are "forced" to regenerate along endoneurial tubes that lead to inappropriate targets, nerve reattachment might not even necessarily be the best option toward optimal functional recovery.

Autologous Nerve Grafts

Nerve autografts are employed when nerve retraction or nerve tissue loss preclude direct end-to-end repair. Autologous grafts typically originate from the patient's sural nerve (a nerve in the lower leg) or other sensory nerves. Since autografts continue to

provide the best clinical results, as a natural biomaterial they are considered the "gold standard" in peripheral nerve repair, and the associated functional losses elsewhere in the body are often regarded as acceptable. Nevertheless, major advances in the understanding of nerve regeneration, in surgical techniques, and in material design are producing ever improving alternatives to autologous nerve grafts.

Entubulation Repair

To circumvent the use of a nerve autograft while still providing the necessary guidance for axonal outgrowth toward the distal stump, both severed nerve endings can be placed into the openings of a tubular nerve guide (or nerve guidance channel). This also entails the advantage that regenerating axons are free to find their own entry points into the distal nerve stump as opposed to being poorly aligned with mismatched fibers or tissue during surgical end-to-end repair. For a brief history and some trends using this procedure see Suematsu, 1989.[69]

Even empty or mere saline-filled tubes support regeneration according to the following four stages[70] (Figure 2.2):

1. Day 1: Clotting molecules, mostly fibrinogen, enter the tube.
2. Week 1: An acellular fibrin matrix forms.
3. Week 2: Cells that will become perineural-like supporting cells migrate in first, followed by Schwann cells and endothelial cells.
4. Originating only from the proximal stump, axons grow in at a rate of 1 - 2 mm per day with myelination following after a five-day lag.

Eventually, axons enter the distal stump and, ideally, at long last reinnervate the appropriate target organs.

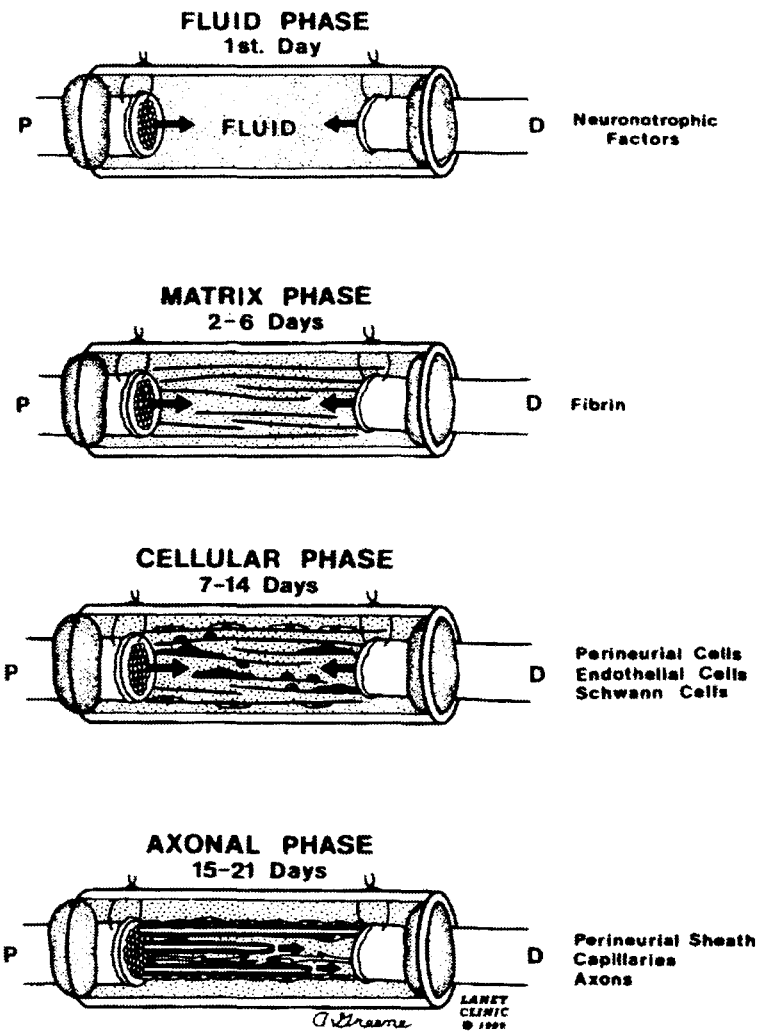

Figure 2.2: Nerve Regeneration Through a Nerve Guide Tube

Schematic drawings of the stages during nerve regeneration through a nerve guidance channel. Shown are the proximal (P) and distal (D) nerve endings inside a nerve guidance tube, and the ensuing events toward regeneration (on day 1, days 2-6, days 7-14, and days 15-21). (from Seckel, 1990)[2]

The use of a nerve guide tube offers the advantage that the space between the nerve stumps is largely protected from scar tissue ingrowth and the properties of the tube itself, such as roughness,[71,72] permeability[73] and overall dimensions,[74] can influence axonal regeneration and organization.

After initial failures with a variety of poorly biocompatible materials such as magnesium, rubber, gelatin, bone and parchment paper, some of which were used as early as the late nineteenth century, advances with polymeric materials have led to the experimental and clinical use of a variety of materials as nerve guide tubes (Table 2.1).

Table 2.1: Examples of the Most Common Nerve Guidance Channel Materials (*based on* Fine *et al.*, 2000)[65]

POLYMERIC MATERIALS

NONRESORBABLE

Nonporous

- Ethylene vinyl acetate copolymer (EVA)
- Poly(tetrafluoroethylene) (PTFE)
- Polyethylene (PE)
- Silicone elastomers (SE)
- Poly(vinyl chloride) (PVC)

Microporous

- Gortex, expanded poly(tetrafluoroethylene) (e-PTFE)
- Millipore (cellulose filter)

Semipermeable

- Poly(acrylonitrile) (PAN)
- Poly(acrylonitrile) poly(vinyl chloride) (PAN/PVC)
- Polysulfone (PS)

BIORESORBABLE

- Poly(glycolic acid) (PGA)
- Poly(L-lactic acid) (PLLA)
- PGA/PLLA blends
- Polycaprolactone (PCL)
- Polyesther urethane

METALS

- Stainless steel
- Tantalum

BIOLOGIC MATERIALS

- Acellular muscle[75]
- Artery
- Collagen
- Hyaluronic acid derivatives
- Mesothelial tubes
- Vein

As an example for the effect of a nerve guide's physical properties, Aebischer *et al.*, 1990,[71] and Valentini and Aebischer, 1993,[72] noted that use of tubes with highly porous, rough walls resulted in isolated fasicles of nerves dispersed within a loose connective tissue stroma. In contrast, smooth-walled, impermeable PTFE tubes led to a discrete cable delineated by an epineurium and located within the center of the guidance channel. In tubes containing alternating sections of smooth and rough luminal surface texture, an immediate change from single-cable to numerous fascicle morphology occurred at the interface of the smooth and rough segments.

Considering the fact that sciatic nerve regeneration through empty or saline-filled tubes is limited to maximal gap sizes of 10 mm in the rat and 6 mm in mice, entubulation repair offers the additional advantage that the nerve guidance channel can be filled with neurotrophic and neurite-promoting factors that accelerate and extend axonal outgrowth beyond those length limits. Support matrices inside the nerve guidance channels are necessary to load, provide, or anchor these factors. Suitable matrices might also include materials pre-seeded with cells that fast-forward regeneration to the cellular phase (Figure 2.2). Therefore, intense research efforts have aimed to develop nerve guide matrices for accelerated axonal outgrowth through nerve guidance channels toward the repair of ever larger nerve injuries. Furthermore, improved <u>functional</u> recovery is a major concern that can be addressed by providing directional structure to a nerve regeneration matrix, the idea being that the fasciculation found in a nerve can best be preserved or reinstated during axonal extension if the matrix has an intrinsic axial alignment or micro-compartmentalization.

TOWARD NEW MATRICES FOR PERIPHERAL NERVE REGENERATION

In light of the known biological mechanisms and stages of nerve regeneration, the proposed approach to embed the matrix in a nerve guidance channel, and under the constraints of some general considerations relating to implant materials, a material for nerve regeneration should fulfill the following requirements:

1.) A stable matrix should homogeneously fill the entire lumen of the nerve guide tube to avoid uneven axonal outgrowth that might lead to poor structural regeneration of the new nerve. Furthermore, the material should be of sufficient mechanical strength and integrity to support axonal ingrowth and extension over a period of several weeks. Covalently crosslinked materials might therefore be of advantage.

2.) The matrix should contain or otherwise present the necessary neuronal adhesion sites as well as growth and trophic factors that guarantee the fastest possible ingrowth and optimal conditions for survival of supporting cells and neuronal processes. Although the primary objective is axonal outgrowth through the material, adhesion-, growth-, and guidance signals perhaps cannot, and do not have to be, exclusively aimed at neurite outgrowth. In fact, much like during spontaneous regeneration through empty nerve guides, it appears to be desirable that supporting cells grow into the material first to facilitate and promote subsequent neurite outgrowth. As a minimum requirement, supporting cells should be able to follow axonal extensions to guarantee myelin formation and the assembly of new endoneurial and basal lamina tubes that make up functional nerve cables.

3.) Unless a highly porous material is chosen, the matrix material itself must be penetrable by cells and axons. When the regenerated nerve piece is fully restored, the artificial matrix is no longer needed and should be resorbed. Taken these two requirements together, an ideal matrix seems to be one that allows cells to penetrate by their own cellular enzymatic activity, so that matrix degradation will occur in perfect synchrony with cellular or axonal

outgrowth. Such a matrix must therefore contain cleavage sites that can be cleaved by neuronal proteases. Since the relevant mode of cell migration and matrix penetration by neuronal cells is plasminolysis (see above), the matrix for nerve regeneration in this project was designed to contain plasmin cleavage sites that allow complete degradation and solubilization of the matrix's crosslinked backbone when cleaved by plasmin (Chapters 4 and 5).

4.) In order to place any matrix into a nerve guidance channel and to embed the nerve endings inside the channel's openings during the entubulation surgery, it is desirable to start with a liquid precursor that can rapidly be transformed into the final, solid matrix material. For embedding of the nerve endings in the channel openings, the transformation even has to occur *in situ*, i.e., under physiological conditions, and neither excessive heat nor toxic by-products must be generated. Also, the transformation reaction should not lead to reactions or modifications of the surrounding tissue, although the transformation may have to occur in direct contact. Eventually, the material should fill out any given space completely and create a snug closure, so no other extracellular matrix or fibrin clot deposition can occur that could lead to deviating neurite outgrowth or undesirable ingrowth of non-neuronal cells. Also, good closure at the tube opening favors better alignment of the regenerating axons.[76]

5.) Like any implant material, the matrix constituents and degradation products must be non-toxic and non-immunogenic.

6.) The matrix should either be homogeneous or patterned longitudinally to help regenerating axons grow in better alignment, because tight and organized axonal alignment is associated with better structural and functional recovery of nerve.[7] This consideration is an argument against materials that are porous on the micron scale (see material requirement 3.), in which the presence of large amorphous pores and channels might lead to deviations and "scrambling" of axons, events that slow outgrowth and are counterproductive to fasciculation and good functional recovery.

Overview of Matrices for Nerve Regeneration and Tissue Repair

Table 2.2: Classes of Materials for Peripheral Nerve and Other Tissue Repair

Category	Material Description/ Source	Author	Degradation Mode	Gelation Mode	Biological Signals	Problems
natural, mammalian/ autologous	(processed) mammalian ECM	various	enzymatic (cellular)	self-assembly, enzymatic (fibrin)	ECM-based adhesion, induction	viral/prionic if animal-derived
natural, modified	immobilized additions to ECM gels	Hubbell, Schense, Sakiyama	enzymatic (cellular)	self-assembly, enzymatic (fibrin)	adhesion, induction, trophic	viral/prionic, immuno-genic(?)
natural, pre-seeded w/ cells	ECM with autolog. cells	e.g., Aebischer, Navarro	enzymatic (cellular)	self-assembly, enzymatic (fibrin)	cell-cell adhesion, trophic	manufacture time, state of autolog.cells
natural, non-mammalian	agarose, alginate, etc.	e.g., Aebischer, Navarro	slow, uncontrolled[i]	physical interaction	adhesion peptides	limited amt. of biol. information
biosynthetic[ii]	modified PLLA matrices	e.g., Langer	hydrolysis	solvent-cast foam	adhesion peptides	limited biol. information, acidity
biosynthetic[ii]	modified PEG gels	Hern, Elbert, Hubbell	slow hydrolysis	photo-polymerized *in situ*	adhesion peptides	limited biol. information
biosynthetic[ii]	cross-linked PEG gels	Sperinde, Griffith	(unclear!)	enzymatically cross-linked	adhesion peptides possible	limited biol. information, undegradble.
biosynthetic[ii]	modified p(NIPAAm-*co*-AAc)	Stile, Healy	(unclear!)	thermo-reversible solidification	adhesion peptides	limited biol. information
bioartificial[iii]	artificial recombinant proteins	McGrath, Tirrell, *et al.*	(eventual unspecific proteolysis)	e.g., self-assembly, cast coatings	potentially unlimited	solubility, some not X-linkable
enzyme-sensitive biosynthetic[ii]	peptide-PEG hydrogels	West, Hubbell	specifically cell-protease-sensitive	photo-crosslinkable	adhesion peptides possible	very limited amt. of biol. information
enzyme-sensitive biosynthetic[ii]	peptide-PEG hydrogels	Pratt, Hubbell	specifically cell-protease-sensitive	self-forming covalent cross-links	adhesion peptides	slow gelation, relatively lmt. biol. info.
enzyme-sensitive bioartificial[iii] & synthetic	artificial protein-co-PEG gels	this doctoral thesis	specifically cell-protease-sensitive	photo-crosslinkable	adhesion motifs, addtn'l. domains	high cost, immuno-genic(?)

[i] reference: Bouhadir *et al.*, 2001[77]

[ii] Meant to say that the material is entirely synthetic, but with biologically active parts or functions.

[iii] Meant to say that the material is biologically produced but artificial in nature.

Note: - Brackets denote a prediction or judgment not necessarily examined or stated by the authors.
- Shaded boxes highlight desirable features in the context of peripheral nerve repair.

The above table summarizes the classes of materials that are described and analyzed in more detail in the subsequent sections. Given the prolific efforts of many research groups to create new, and improve old, biomaterials for tissue repair and regeneration, note that the list is certainly not complete. Instead, the intention was to categorize and judge the materials in terms of their usefulness as matrices for improved peripheral nerve regeneration. Also, some overlaps exist, as materials might belong to several categories at the same time.

Natural, Acellular Matrices for Nerve Regeneration

In order to accelerate regeneration and to increase the distance over which regeneration can occur, the following natural substances have been tested as pre-filling materials for nerve guidance channels mostly in rat models involving sciatic nerve transection:

- longitudinally oriented fibrin gels[78]
- fibronectin in the form of fibronectin/fibrinogen composite cables[79,80]
- matrigel, a gel containing collagen type IV and other ECM components (for collagen type IV, see: *Extracellular Matrix Adhesion Molecules and Their Cellular Receptors*, above)[81,82]
- viscous laminin gels[81,82]
- glycosaminoglycans[81,82]
- muscle basal lamina (essentially acellular muscle)[83,84,85,86]

Blends or combinations of some of these materials have been used with great success such as the impressive peripheral nerve regeneration across an 80-mm gap in a dog model, where the sciatic nerve was bridged simply by a polyglycolic acid (PGA)-collagen tube filled with laminin-coated collagen fibers.[87]

However, inappropriate physiochemical properties of the materials listed above (such as, for example, the highly negative charge of proteoglycans) may interfere with the regeneration process.[65] Another general problem with the use of these materials is their poor mechanical strength (except for muscle basal lamina grafts). A merely viscous, but not crosslinked gel, such as laminin gel or glycosaminoglycan solutions, might have an initial conducive effect on the speed of regeneration, but the material usually does not last or retain its structural integrity long enough to support regeneration through long nerve guidance channels. Liquid fillings, therefore, seem flawed in terms of providing the necessary mechanical support that is desirable for good alignment and structural regeneration of a nerve. To take advantage of fibrin's relatively good mechanical properties and add to its limited neuroinductive and neurotrophic features, Schense *et al.*, 2000,[88] covalently incorporated bioactive peptides into fibrin matrices and, as a result, significantly enhanced neurite extension in rat models. This approach was also used by Sakiyama-Elbert and Hubbell, 2000,[89,90] and Sakiyama-Elbert *et al.*, 2001,[91] to immobilize heparin and heparin-binding growth factor, or to incorporate growth factor directly within fibrin matrices. This design prevented the loss of the exogenous growth factor by diffusion.

Despite the advances with natural matrices toward improved nerve regeneration, serious problems generally exist with the intended use of human- or animal-derived materials for implantation. If ECM-derived materials have to be purified from the patient's own tissue or blood first, crucial hours or even days might be lost before the entubulation surgery can be performed. On the other hand, taking tissue- or blood-derived substances from a donor or animal entails greater risks of inflammation, immunological reactions, and disease transmission.[5,6] A pre-filled, shelved, and ready-to-use nerve guide is desirable that is reliably free of viral and prionic agents.

Cell-Containing Matrices

Another important approach toward improved nerve regeneration is to pre-seed matrices (usually consisting of ECM molecules such as collagen, fibronectin and laminin) with autologous support cells, above all Schwann cells.[92,93] The intention of this approach is to provide neurotrophins[94] and neural adhesion molecules[22,23] that Schwann cells express, and by which they promote neurite extension naturally. Although significant improvement in the number and degree of myelination of regenerated neurons has been made by this approach compared to acellular guides, Schwann cells require actual nerve injury to dedifferentiate and upregulate the expression of neurotrophins and adhesion molecules.[95] Therefore, and due to the harvesting and *in vitro* expansion procedure, the differentiation state of re-implanted Schwann cells may be very different from the differentiation state desirable in the context of nerve regeneration. In addition, harvesting, purifying and expanding Schwann cells in culture costs valuable time and requires the sacrifice of a nerve piece elsewhere in the body.

Functionalized Natural, But Non-Mammalian-Derived Materials

In order to circumvent the use of human- and animal-derived materials, intense research has focused on the functionalization of other naturally occurring gels and polyelectrolytes such as agarose and alginate. The aim of such efforts is to modify these materials in ways so that they mimic ECM and, thus, promote rapid and functional nerve regeneration. The goal of avoiding the use of whole ECM adhesion molecules completely is realized by using bioactive oligopeptides derived from ECM adhesion molecules that confer adhesive and neuroinductive properties in a highly specific and controlled fashion. For instance, agarose gels[96,97] covalently functionalized with laminin-derived peptide CDPGYIGSR, but not non-sense peptide CDPGRGSYI, significantly increased the number of myelinated axons inside an agarose-filled nerve guidance channel in a rat model

for nerve regeneration.[98,99] For other recent experimental work on alginate gels as a matrix for nerve regeneration, see Sufan *et al.*, 2001,[100] and Kataoka *et al.*, 2001.[101]

Biosynthetic and Bioartificial Materials

Another class of materials, the use of which avoids human- or animal-derived materials, are **biosynthetic materials**, that is, entirely synthetic materials upon which biologic activity is conferred by immobilizing synthetic, but biologically active molecules such as synthetic adhesion peptides, sugars, antibiotics, bacterially expressed gene products, etc. Examples of biosynthetic materials include the following:

- PLLA-based: poly(lactic acid-*co*-lysine) matrices grafted with RGD peptide, that promote bovine aortic endothelial cell adhesion and spreading[102,103,104]
- PEG-based: *in situ* forming poly(ethylene glycol) gels grafted with adhesion-peptides, that promote attachment and spreading of targeted cell types (such as human dermal fibroblast and human umbilical vein endothelial cell),[105,106] and that exhibit reduced acid formation during hydrolysis compared to PLLA-based matrices
- p(NIPAAm-*co*-AAc)-based: thermo-reversible poly(N-isopropylacrylamide-*co*-acrylic acid) hydrogels can be delivered to the body in a minimally invasive manner, and can be modified to contain biomimetic peptides;[107] these hydrogels support spreading and proliferation of osteogenic cells.[108]

Since the amount of biological information that can be incorporated in these non-biological systems is limited despite the extensive use of biomimetic peptides, Tirrell and co-workers have developed a growing number of **"bioartificial" matrices** from artificial, recombinantly expressed proteins.[109] Such protein materials consisting of well-defined bacterial expression products do not come with the risk of viral or prionic contamination, and thus represent an attractive and versatile alternative to animal-derived matrices. In fact,

by combining functional domains of known enzymes and proteins, the amount of biological functions that artificial proteins and the resulting protein-materials can fulfill is limited only by the repertoire that Nature herself has at her disposal. Moreover, by including even non-natural amino acids in bacterial expression systems,[110] non-natural features can also be added, such as aryl bromide functionality, for instance, useful for derivatization of brominated proteins via metal-catalyzed coupling reactions.[111] Other material features that have been achieved in the resulting "protein designer materials" include the following: temperature- or pH-tuned self-assembly,[112] precisely pre-determined supramolecular structures,[113,114,115] cell adhesivity targeted to specific cell types,[116,117] introduction of reactive terminal alkene functionality,[118] etc. Promise with these bioartificial materials in the context of nerve regeneration lies in the fact that strongly neuroinductive and neuroadhesive ECM analogues can be envisioned that contain optimal and precisely defined concentrations and types of neuroactive domains.

In the case of matrices that are not actively and specifically degraded, such as peptide-grafted PLLA foams, which simply hydrolyse, it remains unclear what the temporal fate of the matrix material will be during and after regeneration, as matrix degradation does not necessarily occur in synchrony with cellular invasion and neurite outgrowth. Even in the case of highly porous matrices, the material might locally obstruct and retard axonal outgrowth because of inhomogeneities. Furthermore, if degradation, phagocytosis, dissolution, or other forms of removal do not occur rapidly enough, some matrix material might be compressed into dense regions that remain void of axonal ingrowth forever. On the other hand, matrices that disappear too fast by whatever form of resorption serve no purpose at all, as the extending axons find no support for continued outgrowth altogether.

Enzymatically Degradable Synthetic Materials

In order to create non-mammalian-derived materials that do not suffer from undefined and, therefore, uncontrolled degradation or lack thereof, synthetic materials can be rendered degradable in response to specific proteases. Toward this end, researchers have incorporated protease-sensitive oligopeptides into side groups and core chains of polymeric matrices. The origins of this approach appear to coincide approximately with the advent of facilitated Fmoc-based peptide synthesis.[119]

Pioneers in this field were Kopecek and co-workers, 1980,[120] who prepared copolymers of N-(2-hydroxypropyl)methacrylamide, in which synthetic polymer chains were joined by crosslinks containing oligopeptide sequences degradable by papain, a thiol protease derived from papaya. While Kopecek proceeded to develop polymer-based drug delivery systems that respond to the ambient presence of proteases, such as lysosomal enzymes,[121] other groups used peptide sequences to attach therapeutic agents that are released only in the presence of bacteria or cells that secrete specific proteases, which can cleave the particular peptide sequences used.[122,123]

The next step toward synthetic materials that are, as a whole, degradable by local protease activity during cellular migration, was to place enzymatic degradation sites at the crosslink sites of fully crosslinked materials. This was achieved by West and Hubbell, 1999,[124] who synthesized telechelic block copolymers of protease-sensitive oligopeptides (APGL for collagenase, VRN for plasmin) and PEG so that the resulting hydrogels (following terminal acrylation and photo-polymerization) were specifically degradable by plasmin or collagenase, two enzymes relevant for cell migration and ECM remodeling. Limitations of this system included the laborious addition of single amino acids, the inability to reliably purify polydisperse amino-acid-derived PEG, and the limited amount of biological information that could be incorporated by a synthetic method involving the stepwise addition of single amino-acids.

Methods of Matrix Formation

Another important concern regarding materials in tissue engineering is the method of implantation. It is often desirable to inject or spread a liquid precursor at the site of a wound and transform it to a solid, gel-like state *in situ*. As mentioned among the list of material requirements for a nerve guide matrix, this feature would be useful when filling a nerve guidance channel and embedding the nerve endings in the tube openings during surgery. Examples of materials that allow for an *in situ* transformation include the following:

- fibrinogen, which forms fibrin (see above) after cleavage by thrombin, followed by covalent crosslinking with inherent factor XIIIa
- Healy and co-workers' thermo-reversible poly(NIPAAm-*co*-AAc)-based gels[107,108] (see above)
- PEG gels developed by Sperinde and Griffith, 1997,[125] that result from a transglutaminase cross-linking reaction of glutaminamide-functionalized PEG and poly(lysine-phenylalanine).

In contrast to these physical or enzymatic gelation processes, Hubbell and co-workers (e.g., West and Hubbell, 1999,[124] above) have developed photo-chemical crosslinking schemes that enable a rapid liquid-to-solid transformation of their PEG acrylate systems relatively independent of pH in a physiological range, and with gelation times on the order of seconds. This is a very useful transformation speed for the anticipated surgical use of their matrices.

A New Class of Protease-Sensitive and Self-Forming Materials

In continuation of West and Hubbell's work, Pratt and Hubbell[126,127] produced self-forming hydrogels by mixing multithiol-containing oligopeptides with acrylate-terminated PEG chains under physiological conditions. The oligopeptides represented protease-sensitive amino-acid sequences, which were cleavable by cell-associated enzymes and, thus, permitted penetration of cells into these hydrogels in model systems both *in vitro* and *in vivo*. Furthermore, cellular infiltration depended on the presence of RGD adhesion sequences that were incorporated by reacting a small fraction of the PEG diacrylate chains with monothiol-containing RGD peptides prior to hydrogel formation. The resulting hydrogels thus represented matrices that were both specifically degradable and specifically adhesive to target cells.

Some concerns remain regarding the relatively slow gelation kinetics (on the scale of tens of minutes) of these materials as well as the strong pH-dependence of the crosslinking reaction, as acidic conditions –such as present at the site of a wound– further slow the kinetics. A more serious potential problem, however, is the required solubility of all hydrogel precursors, in particular the oligopeptides' solubility, since many peptides of potential interest (such as hydrophobic IKVAV) are likely to precipitate even more readily in the presence of PEG. Furthermore, despite the possibility to confer biological activity via tethered adhesion- and other peptides, the amount of biological information that can be incorporated in purely synthetic materials remains limited, especially in the context of nerve regeneration, where many more, and perhaps larger adhesive, trophic and neuroinductive factors are likely to be necessary.

AIM OF THIS PROJECT

In light of the above considerations, the aim of the doctoral research project presented in this thesis was to develop homogeneous matrices for tissue repair, specifically peripheral nerve, that

- present a basic set of relevant cell adhesion sites as well as sites for the immobilization of additional cell-type specific adhesion sites and trophic factors. The integrin-binding RGD motif was chosen as a permanent element of the matrices, and a heparin-binding site was incorporated to immobilize heparin and, in turn, heparin-binding neuroactive agents such as neural growth and adhesion factors.
- are degradable by cell-associated enzymatic activity. To match the relevant mode of axonal outgrowth during nerve regeneration, plasmin-degradation sites were incorporated in the matrix.
- are non-animal derived. Instead, the protein backbone of the matrices was bacterially expressed, then purified; and the bulk of the material consisted of poly(ethylene glycol) that was grafted to the protein backbone by Michael-type conjugate addition.
- have sufficient mechanical strength to support cellular ingrowth. Therefore, the material was to be covalently crosslinked at a high crosslink density.
- can rapidly form *in situ* from a liquid precursor, so as to act as a glue or sealant for the nerve guide openings, and to be potentially injectable. Light-induced radical polymerization of terminal acrylate groups was chosen to crosslink the precursor.
- consist of constituents and degradation products that are non-toxic and non-immunogenic. The core protein sequence was therefore based on human protein sequences, and poly(ethylene glycol) was chosen as the bulk constituent because of its well-established immunocompatibility.[128]
- are transparent to enable microscopic analysis of anticipated three-dimensional cell cultures. The high water content of PEG matrices and their anticipated homogeneous sub-micron architecture were expected to ensure this feature.

Chapter 4 will describe the design and creation of matrices with these intended features in detail, and Chapters 5 and 6 will describe their performance in models for tissue and nerve regeneration.

CHAPTER 3

SURFACE PATTERNS OF NEURAL ADHESION PEPTIDES ON A POLY(ETHYLENE GLYCOL)-BASED SURFACE TOWARD TWO-DIMENSIONAL ARTIFICIAL NEURAL NETWORKS

INTRODUCTION

As a prelude to the work in three dimensions to be described in Chapters 4, 5, and 6, the aim of the work presented in this chapter was to photo-immobilize multiple cell adhesion peptides in a patterned fashion on an otherwise protein- and cell-adhesion resistant surface in order to effect localized adhesion, directed neurite outgrowth, and controlled synapse formation among groups of individual neurons in two dimensions. The envisioned neural circuits were intended to provide *in vitro* models of neuronal behavior including development, nerve regeneration, and learning, and to allow for applications such as biosensors and bioelectric devices.

The adhesion-resistant culture substrate was a highly crosslinked polymer network of trimethylolpropane triacrylate (TMPTA) and pentaerythritol tetraacrylate (PETA) copolymerized with poly(ethylene glycol) α-monoacrylate ω-monoethylether (PEGMA). Due to the high content of pending PEG chains, the advantage of this substrate material compared to many other surfaces was its persistent resistance to protein adhesion, therefore ensuring the preservation of a defined and controllable surface. In an initial test of principle, UV light-induced functionalization of this substrate was achieved with photolabel-derivatized RGDSG peptide in simple patterns, to which human fibroblasts adhered RGD-specifically. To achieve the adhesion of dissociated cells from the dorsal root ganglia (DRG) of embryonic chicks, which include sensory cells that belong to the class of pseudo-unipolar neurons whose axons have a central and a peripheral branch,[129] regions on the substrate material had to be derivatized with a combination of five peptides

based on the receptor-binding domains of laminin and N-cadherin as well as a heparin-binding domain of anti-thrombin III.

In summary, this work was aimed at (a) providing an example of precise control of cellular function via surface-immobilized bioactive peptides, (b) providing further insight into the function of the adhesion ligands LRGDN, YIGSR, IKVAV, HAV, and KAF(βA)KLAARLYRK in controlling neuron and neurite morphology, and (c) enabling the formation of designed neuronal circuits for neurobiological investigation. Toward these goals, this study was –to my knowledge– the first attempt to employ multiple bioactive peptides simultaneously to create a patterned surface with highly defined biological signals on an otherwise non-adhesive culture substrate.

The results of this work foreshadowed some of the results with fibroblast cultures in three-dimensional systems that will be presented in Chapters 4 and 5, and yielded valuable clues for effecting and understanding the neurite outgrowth on the materials described in Chapter 6.

MOTIVATION FOR NEURONAL CULTURES ON PATTERNED SURFACES

The computational, cognitive, adaptive, and creative capacity of the brain is unparalleled even by the most advanced computers of our age. Accordingly, a further understanding of the cellular and molecular mechanisms underlying the development, information processing, and plasticity, i.e., learning, of the brain would continue to promote the design of advanced computational methods and devices.[130,131] Moreover, devices that already incorporate neuronal components as computational units are under investigation (e.g., by Curtis *et al.*, 1994;[132] Kovacs *et al.*,1994;[133] etc.). While brain slice preparations have revolutionized the study of synaptic transmission, neuronal integration and long-term potentiation,[130] the operation of the nervous system is only understood to a

limited extent at the level of single cells. We know little about the importance of (1) cell connection patterns, (2) synapse position and type, (3) cell shape (including arborization) and signal propagation, summation, etc., in one cell, or alternatively, (4) the differentiated state of the cell or (5) the previous electrical history of the cell.[132] Insights of this kind are difficult to obtain because of the complexity and relative inaccessibility of individual cells in the living brain. In addition, studies involving individual cells *in vivo* are sometimes hard to reproduce, as many factors influencing neuronal performance remain uncontrolled, if not completely unknown.

Control of the organization of neurons in defined and reproducible networks in culture promise the potential for new systems of study and for major technical innovation.[130] Toward the goal of culturing neurons in precise, reproducible and meaningful networks, the following requirements have to be met:

A. Long-term viability of neurons in culture.

B. Well defined and invariable culture substrates that can be patterned.

C. Directed growth of neural processes along defined pathways.

D. Controlled neuronal polarity by orienting the growth of the axon and dendrites.

E. Formation of functional synapses between patterned neurons.

F. Retention of differentiation state and transmitter phenotype of patterned neurons.

(*based on* Cotman *et al.*, 1994;[130] *modified*)

The primary focus of the research described in this chapter was to contribute to an improvement and understanding of the issues pertaining to requirements A - C, which might lead to progress and insights regarding D, E and F. That is, insights about the establishment of neuronal polarity, synapse formation, and determinants of neuronal differentiation *in vitro* will be gained by studying the growth and behavior of neurons in culture as a function of precisely controlled surface chemistry and geometry. For instance,

questions for which answers were sought in this chapter include the following: Which peptides, if any, can support neuronal attachment and which can promote neurite extension on an otherwise non-adhesive substrate? Can combinations of different adhesion peptides on such a surface mimic the extracellular matrix and, thus, improve viability and determine the differentiation state and morphology of neurons in culture?

If eventually even only simple neuronal circuits could be constructed reliably and reproducibly, and could be maintained for prolonged periods of time in contact with electric devices that measure electric activity of the neurons, these circuits would constitute a source for new applications in bio-sensing and bio-computing. Also, knowledge of the minimal requirements for neuronal cultures would provide improved design criteria for three-dimensional, biosynthetic materials that support neurite extension and, thus, nerve regeneration (Chapters 4, 5, and 6).

PREVIOUS WORK WITH PATTERNED SURFACES

Chemically Patterned Surfaces

The patterning of surfaces lies at the heart of any effort to guide neural growth in two dimensions. The idea is to outline regions and "paths" for cell attachment and neurite extension on surfaces that are otherwise adhesion resistant or non-permissive of neural growth. Ground-breaking progress in chemical patterning of surfaces has been made by Whitesides and co-workers (e.g., Kumar, 1994).[134] Based on stamping or contact printing, self-assembled monolayers (SAMs) of alkanethiolates can be adsorbed on a gold surface in a patterned fashion on scales as small as 0.2 μm. An elastomeric stamp bearing the desired pattern is used to transfer alkanethiols with desirable functional end groups to the surface of an evaporation-deposited gold film. A pattern consisting of chemically differentiated regions can thus be created at submicron-scale resolution. The limits on the

resolution of these patterns arise only from the maximum resolution of the pattern that has to be generated on the PDMS film by a sequence of photolithographic and polymer casting techniques.

Other approaches to patterning SAMs have included photochemical methods that were applied directly to the surface. Stenger et al., 1992,[135] for example, generated covalently attached monolayers of trimethoxy alkyl silane on glass that were further derivatized in a patterned fashion by localized activation with UV irradiation through a photomask followed by the appropriate solution chemistry on the activated end groups.

An abundance of other patterning techniques has since been developed, including, for example, microfluidic systems, patterns involving concentration gradients of functional groups, and selective patterning controlled by ambient conditions such as pH.

Shortcomings of Chemically Patterned Substrate Materials

The abundance of surface patterning techniques presently available has given rise to impressive short-term control over the organization of various cell types on culture substrates by virtue of surface chemistry and geometry,[136-137] but most of the culture substrates used do not permit long-term control over the properties of the surface, as protein adsorption, desorption, denaturation, and proteolysis remain unpredictable variables. For instance, even when human or bovine serum albumin is pre-adsorbed on certain regions of a surface to render those regions resistant to cell adhesion by blocking them from other, adhesion-promoting, proteins such as fibronectin or laminin, unwanted cell adhesion and neurite outgrowth have been observed depending on albumin's surface conformation.[138] In addition, over time proteolysis and/or desorption of albumin from the surface allows for adsorption of adhesion proteins that are naturally present in serum containing media.

The problem of unwanted cell adhesion and uncontrolled neurite outgrowth even arises in protein free media, because cells that are cultured for long periods of time start to

release their own extracellular matrix proteins, which will adsorb to the culture substrate and then promote uncontrolled adhesion and spreading. Meaningful results of experiments involving neurons in culture are thus limited to the first few hours after cell seeding, when protein deposition and non-specific adhesion to blocked surfaces are probably still insignificant. While inhibitors of protein synthesis and secretion have been used to control the protein environment in cell cultures, such additions introduce new complications by depriving cells from potentially vital and experimentally crucial factors.

Biospecific Patterned Surfaces

Recent attempts of surface patterning and functionalization have been aimed at obtaining better defined culture substrates by employing short adhesion peptides based on extracellular-matrix proteins such as laminin, collagen, fibronectin and others (see Chapter 2). Since short adhesion peptides are often less prone to proteolytic degradation and denaturation on surfaces, their use circumvents some of the complications resulting from using whole proteins to define surface properties. However, the problem of surface changes due to uncontrolled protein adsorption remains. Nevertheless, the advantage of employing individual adhesion- and outgrowth-promoting peptides is that the specific response to a particular isolated peptide can be tested. The effect of individual neuronal adhesion peptides, for example, has been described for several cell types on the YIGSR-containing oligopeptide GYIGSRY by Massia and Hubbell, 1993;[42] for NG 108-15 neuroblastoma × glioma cells in response to surface-immobilized oligopeptide CDPGYIGSR by Clémence, et al., 1995;[43] and for embryonic hippocampal neurons on oligopeptides RDIAEIIKDI and CDPGYIGSR by Matsuzawa et al., 1996.[44]

To establish the specific and exclusive effect of isolated bioactive peptides on the long-term growth and development of neurons in culture, and to enable the creation of a biologically well defined and patterned culture substrate free of interfering proteins for long periods of time, a substrate is required that does not permit any protein adsorption. Such a

substrate with the desired protein adsorption-resistant properties was developed by Drumheller and Hubbell[139,140,141] and was used in this study.

The Poly(Ethylene Glycol)-Containing Substrate Material

Besides resistance to protein adhesion, the substrate material must be mechanically robust and stable, non-toxic for cell culture purposes, and preferably translucent to allow microscopic analysis *in situ*. These requirements were met by glassy, translucent, highly crosslinked polymer networks formed by copolymerization of trimethylolpropane triacrylate (TMPTA) copolymerized with poly(ethylene glycol) diacrylate (PEGDA). The PEG-based surface of these films was electroneutral and had a low interface energy with water. The hydrated high-molecular PEG chains at the water interface likely exhibited high segmental mobility and thus were thought to render the surface highly protein-repellent and cell non-adhesive.[142,143] Other important qualities of this substrate material consisted in its mechanical strength, small amount of swelling in both organic solvents and water (as a result of the high degree of crosslinking), and the films' optical properties: Since the films were completely translucent, light microscopy of cell cultures on the films was possible.

Modification of the Poly(Ethylene Glycol)-Containing Substrate Material

When the original protocol based on TMPTA and PEGDA, as reported by Drumheller and Hubbell, 1994,[139] gave rise in my hands to films of insufficient cell adhesion resistance, further experiments indicated that only films made with poly(ethylene glycol) α-monoacrylate ω-monomethylether (PEGMA, Figure 3.1) exhibited a similar resistance to cell adhesion as previously reported by Drumheller and Hubbell.[139] These results suggest that the degree of acrylation in what Drumheller and Hubbell believed to be poly(ethylene glycol) diacrylate might actually have been significantly lower, such that a

fraction of the polymer used had actually been poly(ethylene glycol) monoacrylate, giving rise to the observed resistance to cell adhesion of the films.

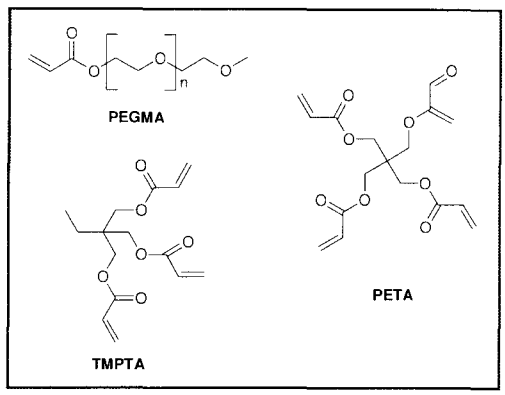

Figure 3.1: Constituent Molecules of Polymer Networks

Poly(ethylene glycol) α-monoacrylate ω-monomethylether (PEGMA), mol. wt. 5000, trimethylolpropane triacrylate (TMPTA), pentaerythritol tetraacrylate (PETA).

Entropic considerations support this conclusion, in that polymer chains linked at only one end (as is the case with PEGMA) can achieve a much larger number of molecular configurations compared to a polymer linked at both ends (as would have been the case with PEGDA) (Figure 3.2).

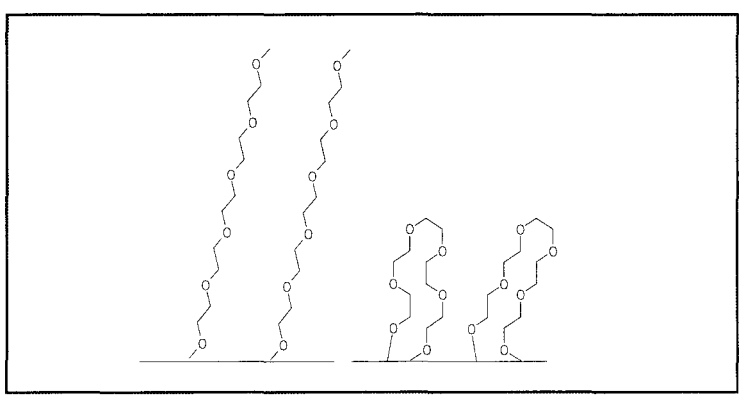

Figure 3.2: Non-Adhesive Nature of Network Surface Due to PEGMA

Schematic of substrate surface resulting from use of PEGMA (left) versus PEGDA (right).

The larger number of attainable molecular configurations translates into a more favorable entropic state in the absence of adsorbed proteins as compared to the presence of adsorbed

proteins, which would limit chain mobility. In addition, PEG chains linked at only one end may generate more steric hindrance to protein adhesion, because such PEG chains reach out farther into the hydrous phase and "dangle" more freely (also Figure 3.2). Cell adhesion to the PEG-based substrate was thus prevented by obstructing the adsorption of adhesion-mediating proteins.

Another improvement of the substrate material was achieved with respect to its mechanical properties. Initially, the combination of TMPTA and PEGMA (instead of an unknown mixture of PEGMA and PEGDA) produced films that were very prone to cracking during the photoinitiated polymerization step. Cracking during polymerization can be explained by tensile forces between polymerizing domains that arose when the Van der Waals distance between polymerizing molecules suddenly shrank to the distance of covalent bonds that were formed. Domains in which polymerization was occurring thus started to contract, while interstitial regions with fewer crosslinking became prone to cracking (Figure 3.3).

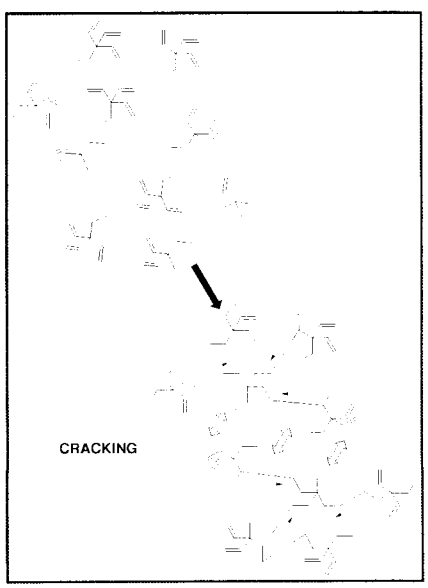

Figure 3.3: Cacking During Formation of Highly Crosslinked Polymer Networks

Schematic illustration of suggested reason for cracking in films made with TMPTA and PEGMA (not shown) only: As domains of polymerization contract, mechanical failure results in regions of little or no crosslinking. (TMPTA is represented schematically.)

Mechanical failure can only be prevented when the degree of crosslinking is large enough throughout the material, so that tensile forces due to the volume change of reaction can be withstood. This was achieved by the addition of pentaerythritol tetraacrylate (PETA), which by virtue of its four acrylate end groups evidently seemed to increase the density of covalent bonds formed such that despite shrinking, the films cracked substantially less, while completely retaining their adhesion-resistant character.

Photopatterning

Very convenient choices of bifunctional photocrosslinkers for the immobilization of biomolecules on polymeric surfaces are benzophenones and certain arylazides, some of which can be UV photoactivated at wavelengths above 320 nm. Biological activities of photo-immobilized biomolecules are, in general, not affected by the conditions used for light activation.[144-43] Inspired by the work of Huebsch et al., 1996,[145] the photocrosslinker N-succinimidyl-6-[4'azido-2'-nitrophenylamino]hexanoate (SANPAH) (Figure 3.4), which forms a reactive nitrene upon irradiation, seemed particularly convenient for the functionalization of the substrate films. SANPAH can easily be radiolabeled with ^{125}I for future experiments to determine the surface concentrations of ^{125}I-SANPAH-immobilized peptides on substrate surfaces.

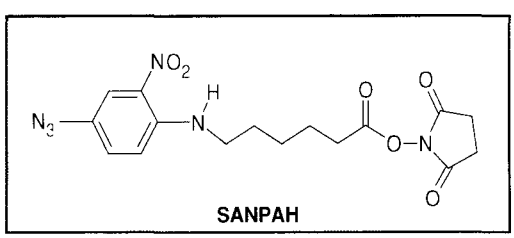

Figure 3.4: Molecular Structure of SANPAH

SANPAH can be attached to the N-terminus of any peptide via the formation of an amide bond that replaces the succinimidyl ester shown in Figure 3.4. Because of the strong

resistance to cellular adhesion of the substrate material,[139] a larger molar amount of adhesion peptides had to be immobilized per unit area to elicit cell adhesion and spreading than is necessary on other substrates such as silanated glass.[146] The problem that arises from this fact is that during the immobilization reaction a very large concentration of photolabelled peptide was required at the surface of the substrate material, so that a sufficient number of peptides would be covalently bound to promote a biological response. This difficulty was overcome by applying a solution of photolabelled peptide onto the films in defined regions, and allowing the peptide to dry upon the substrate, followed by short irradiation to avoid high temperatures.

MATERIALS AND METHODS

Synthesis of poly(ethylene-glycol) α-monoacrylate ω-monomethylether

Poly(ethylene glycol) α-monoacrylate ω-monomethylether (PEGMA), mol. wt. 5000, was prepared from PEG monomethylether, mol. wt. 5,000 (Fluka, Switzerland, M_n ca. 5000 according to supplier). PEG was dried by azeotropic distillation in benzene for 1 hr using a distillation column. After cooling to less than 50 °C under argon, triethylamine (2.2 eq., Aldrich) was added. Addition of acryloyl chloride in two half-portions (4.0 eq. total, Aldrich) separated by 10 min initiated the reaction. The reaction continued with stirring overnight in the dark at room temperature under argon. The resulting pale yellow solution was filtered and the reaction product precipitated by dropwise addition of the solution to diethyl ether in an ice bath. After recovery by filtration, the precipitate was washed with diethyl ether and dried *in vacuo*. ^{1}H NMR spectrometry in $DCCl_3$ resulted in the following characteristic peaks: 3.6 ppm (94.38 H, PEG), 4.3 ppm (t, 1.93 H, -CH_2-$C\underline{H}_2$-O-CO-CH=CH_2), 5.8 ppm (dd, 1.00 H, CH_2=$C\underline{H}$-COO-), 6.1 ppm, 6.4 ppm (dd, 2.08 H, $C\underline{H}_2$=CH-COO-). Quantitative acrylation was evident from comparison of the

peak at 3.6 ppm to the acrylate-associated peak at 5.8 ppm and applying the M_n reported by the supplier.

Photoinitiated Formation of Highly Crosslinked Networks

As explained above, the adhesion-resistant substrate material for this study were films of a highly crosslinked network of trimethylolpropane triacrylate (TMPTA, Aldrich) and pentaerythritol tetraacrylate (PETA, Aldrich) copolymerized with PEGMA (Figure 3.1) in the presence of photoinitiator benzil dimethyl ketal (BDMK, Aldrich), which was based on earlier materials by Drumheller and Hubbell.[139-141]

Briefly, 0.8 g PEGMA were dissolved in 1.8 mL TMPTA and 0.2 mL PETA by heating the mixture to 100 °C. After addition of 26 μL BDMK solution (300 mg/mL in TMPTA), the homogeneous mixture was filled into a circular space formed by a PTFE gasket (1-mm thickness, ~14-mm diameter; Small Parts) clamped between two clean glass coverslips (Corning). After re-heating to 100 °C in a pre-warmed oven with a glass window (Bioblock), a 100-W medium-pressure mercury vapor UV light source (Blak-Ray, UVP) was shone through the oven window for 1 min, thus exposing the coverslip assembly to a flux of 10 mW/cm^2 perpendicular to the opening in the PTFE gasket. The resulting polymer films were gently removed from the assembly and postcured under UV irradiation for 1 min.

Automated Fmoc-based Peptide Synthesis on Solid Supports

Oligopeptides RGDSG, RDGSG, KAF(βA)KLAARLYRKA, GGGYIGSR, GGGIKVAV, and HAV were synthesized on solid polystyrene support with a "Pioneer" peptide synthesizer (Applied Biosystems, USA) by automated solid phase peptide synthesis using 0.4 g peptide amide resin (NovaSyn TGR, Novabiochem-Calbiochem AG, Switzerland) per peptide. Synthesis occurred by standard 9-fluorenyl-methyloxycarbonyl

(Fmoc) chemistry,[119] using solvents from Applied Biosystems (Warrington, England) and all other reagents from Novabiochem-Calbiochem. The N-terminal Fmoc group was removed by a final de-protection cycle to free the N-terminal amine for further reaction. After synthesis, the peptide resin was washed with MeOH and dried in a vacuum chamber overnight.

Photolabelling of Peptides

Under exclusion of light, peptide resins from different syntheses were separately placed in N,N-dimethyl formamide (DMF) containing a two-fold excess of the photolabel SANPAH and activator N-hydroxybenzotrizole (HOBt) per theoretical peptide, based on the protocol by Huebsch et al.[40], 1996. After reacting for 2 h, the resin was recovered by vacuum filtration through fritted glass funnels and washed with 10 resin volumes of DMF, then 5 volumes of MeOH, and dried. Peptides were cleaved from the resin and deprotected for 4 h by shaking the resin in 10 mL of a solution containing 8.8 mL trifluoroacetic acid (TFA, Fluka, Switzerland), 0.5 mL phenol (Aldrich), 0.2 mL triisopropylsilane (Aldrich), and 0.5 mL water. Precipitation of the orange photolabelled peptides occurred when the filtration flow-through was added drop-wise to chilled diethyl ether (~40 mL). The deep orange precipitate was recovered by vacuum filtration (0.2 μm pore-sized PTFE membrane filters, Gelman Sciences) and washed with three ~5 mL portions of diethyl ether. The final filtrate was dried in a vacuum chamber overnight and then sealed under argon for temporary storage at –20 °C.

Photolabelled peptides RGDSG and RDGSG were purified by preparative C_{18} chromatography (Prep Nova-Pak 19 x 300 mm column; Waters, USA) using a BioCAD 700E chromatograph (PerSeptive Biosystems). Separation of peptides from impurities was achieved by applying a gradient of acetonitrile in 0.1% TFA. The resulting eluate fractions were freeze-dried and analyzed by matrix-assisted laser desorption ionization-time of flight (MALDI-TOF) mass spectroscopy using the "Voyager Elite 122" spectrograph (Applied

Biosystems, USA) and, as MALDI matrix, alpha-cyano-4-hydroxycinnamic acid (Aldrich). Before storage at –20 °C, verified and identical peptide fractions were combined, dried in a vacuum chamber overnight and finally sealed under argon for storage.

Surface Patterning

20 mM solutions of photolabelled peptides in DMF were prepared for direct application to the substrate films. On the surface of at least two films per experiment, circular ~3-mm areas were covered with 1-2 µL of separate solutions of photolabelled adhesion peptides and allowed to dry in the dark. After exposure to a 100-W medium-pressure mercury vapor UV light source (Blak-Ray, UVP) for 10-20 s, all films were rinsed with DMF three times, followed by extraction in DMF over night. The DMF was then gradually exchanged by deionized water, and the DMF extracted by deionized water over 6-8 h with frequent exchanges of fresh deionized water.

Culture of Human Foreskin Fibroblasts

After pre-incubation of the films in fibroblast culture medium for 1 h, fibroblasts were seeded at confluence onto the peptide-treated surface of the substrate films inside 24-well tissue culture well plates (1 mL medium with cells per well). Well established techniques[147] were used for cultures of neonatal human foreskin fibroblast (hFFs, Clonetics(Cambrex) via BioWhittaker Europe, Belgium) of passage numbers up to 14. hFFs were cultured in Dulbecco's Modified Eagle Medium (DMEM, with 1000 mg/L glucose, 110 mg/L sodium pyruvate, 862 mg/L L-alanyl-L-glutamine) supplemented with 10% *(v/v)* heat-inactivated fetal bovine serum and 1X antibiotic-antimycotic (all Life Technologies, Scotland).

After 5 h, the films were rinsed with DMEM, the cells fixed with formalin (10%, Sigma), and stained with hematoxilin (Sigma). Microscopy and image processing were performed

using a Zeiss inverted confocal light microscope (Axiovert 135, Zeiss, Germany) in conjunction with a Hamamatsu Color Chilled 3CCD Camera (Hamamatsu, Japan) and LeicaQWin image processing software (Leica Imaging Systems Ltd., 1997).

Culture of Dissociated DRG Cells

Day 8 chick embryos were taken from Lewis Brown chicken eggs. DRGs were dissected according to standard protocols described elsewhere[147] and then kept in a small petri dish with supplemented DMEM/F12 medium (DMEM/F12 medium with 1% (*v*/*v*) insulin – transferrin – selenium supplement (100X), 1% (*v*/*v*) ABAM (100X), 0.5% (*v*/*v*) chick embryo extract, 60Å ultrafiltrate, all Gibco; 100 ng/mL nerve growth factor, Sigma) at 37 °C for up to 30 min until dissociation. DRGs were dissociated by incubation at 37 °C with trypsin-EDTA for 5 min followed by gentle trituration with a 1 mL plastic pipette tip. The dissociated DRG cells were centrifuged (700 g, 3 min, room temp.), resuspended to 50000 cells per mL, and seeded onto the peptide-treated surface of pre-incubated polymer films inside 24-well tissue culture well plates (1 mL medium with cells per well). After 5 h, the medium was gently replaced with fresh, pre-warmed DMEM/F12 medium. Microscopy and image recording were done *in situ* in approximately three-hourly intervals.

RESULTS AND DISCUSSION

Adhesion Resistance of Unmodified Substrate Surfaces

Despite the "adhesive challenge" presented to the PEG-containing polymer films by seeding hFFs at confluence and culturing on the surface for 5 h, the substrate material was completely resistant to cell adhesion (Figure 3.5).

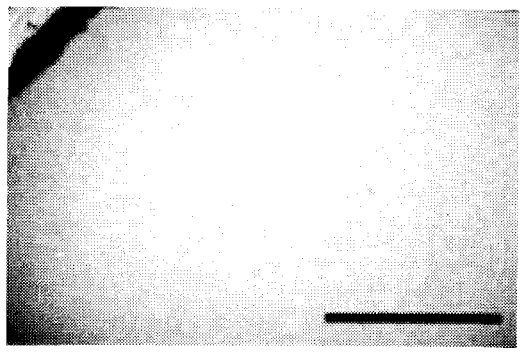

Figure 3.5: The Substrate Material's Resistance to Cell Adhesion

Photograph of an untreated substrate film after hFF culture for 5 h followed by rinsing with DMEM, fixing and staining. No cells adhered anywhere on the surface. (Scale bar = 1 mm)

Derivatization of Peptides with Photoactive Groups

Analysis of SANPAH-labelled peptides RGDSG and RDGSG (mol. mass both 765.6) after UV exposure in water (to convert the nitrene groups [$-N_3$] to amines [$-NH_3$] so as to avoid unknown degradation or reaction products from the nitrene group during analysis) yielded dominant peaks at molecular mass = 740.6 for both peptides. This is in perfect agreement with the expected molecular mass for these species.

Surface Patterns

Even after photo-immobilization of SANPAH-labelled peptides and subsequent extraction with DMF and deionized water, an orange-purple stain was visible in the same region where the peptide had been placed. Also, despite UV exposure and solvent exchanges, the films remained glassy and clear, mostly free of cracks, and appeared not to swell at all, based on visual inspection.

Specific Integrin-Mediated Cell Adhesion to Regions of RGD Peptide

Figures 3.6 and 3.7 show fixed and stained fibroblasts after 5 h in culture on RGDSG-grafted substrate material. The cells adhered and spread exclusively on peptide-treated regions. Surfaces that had been treated with control inactive peptide RDGSG,

shown in Figure 3.8, remained completely non-adhesive, similar to untreated films (Figure 3.5).

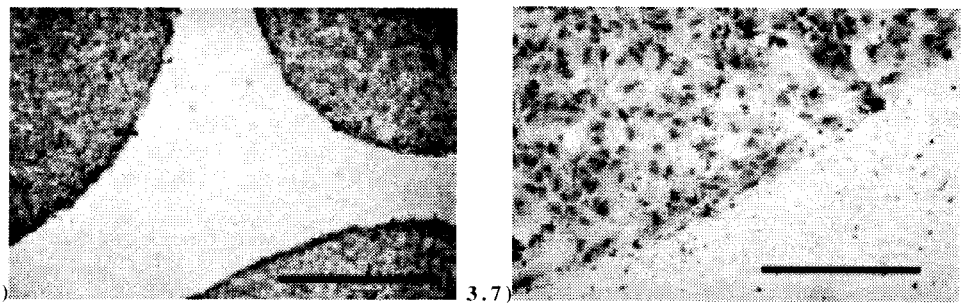

Figure 3.6: hFF Patterns Due to Adhesion to Regions Containing RGD-Peptide

hFFs cultured on a peptide-grafted substrate film for 5 h: Cells only adhered and spread in regions with immobilized adhesion peptide RGDSG; other regions remained completely cell non-adhesive. (Scale bar = 1 mm)

Figure 3.7: Exactness of Cellular Adhesion to Regions of RGD-Peptide

Close-up microscope image of stained fibroblasts cultured a locally bioactivated substrate film for 5 h. Cells adhered and spread precisely to regions with immobilized adhesion peptide RGDSG; other regions remained completely non-adhesive to cells. (Note the well-defined border between cell adhesive and cell non-adhesive surface regions.) (Scale bar = 100 μm)

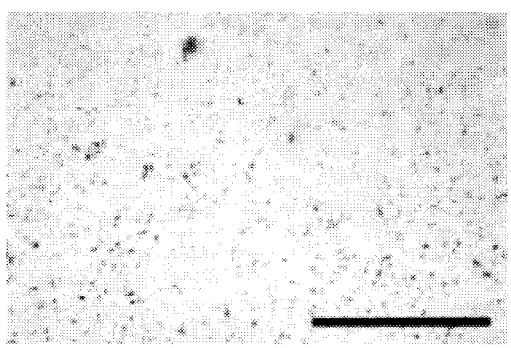

Figure 3.8: Cell Adhesion and Spreading Requires Integrin Binding to RGD-Peptide

Substrate film grafted with control peptide RDGSG. Cells did not adhere anywhere on the surface. Fixing with formalin apparently caused some protein precipitation and deposition onto the surface. (Scale bar = 100 μm)

These results strongly suggest that hFF adhesion was enabled by specific integrin-mediated binding to the RGDSG-peptide, which contains the tetrapeptide RGDS known to support fibroblast attachment and to inhibit fibronectin binding to platelets if present in solution.[148]

If the presence of adhesion peptide RGDSG had merely modified the surface in a biologically unspecific way, e.g., by changing the surface charge, the presence of RDGSG, which is very similar to RGDSG, would have been expected to elicit cell adhesion also. Instead, only RGDSG promoted cell attachment and spreading. The fact that the presence of the control peptide did not support cell adhesion strongly suggests that the observed hFF adhesion to the RGDSG-grafted surface was indeed integrin-mediated and, thus, biologically specific.

Figure 3.9 illustrates another striking detail: In the region depicted, the droplet of peptide solution that had been applied to the film to deposit RGDSG peptide, left behind "striata" of peptide (in terms of surface concentration) in the process of drying. Assuming that the amount of peptide grafting was proportional to the local concentration of photolabelled peptide, the resulting "striated concentration pattern" of adhesion peptide gave rise to fibroblast adhesion that conformed intimately to the striata of photo-immobilized, peptide.

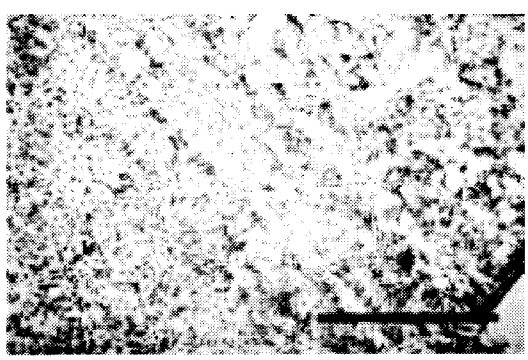

Figure 3.9: Cellular Adhesion Conforming to Concentration Patterns

hFFs cultured for 5 h that adhered in a "striated" fashion, conforming to the local differences in surface concentration of photo-immobilized adhesion peptide RGDSG. (Scale bar = 500μm)

Patterned DRG Cell Adhesion to Multiple Peptides

Cells from dissociated embryonic chick DRGs, presumably mostly pseudo-unipolar sensory neurons, attached to surface regions grafted with a combination of peptides

RGDSG, GGGYIGSR, KAF(βA)KLAARLYRKA, HAV, and GGGIKVAV (Figure 3.10), but not to regions without peptides nor regions with any of these peptides alone (images not shown).

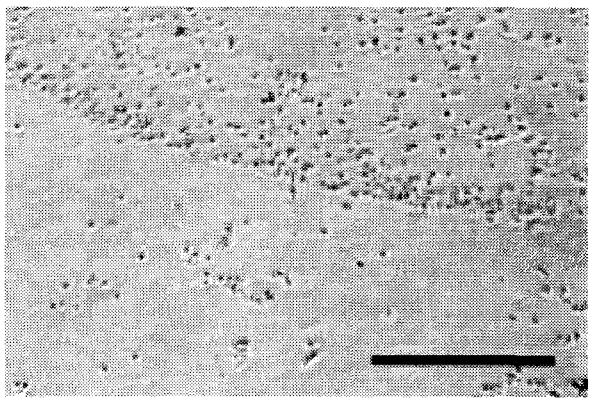

Figure 3.10: Patterned Adhesion of Dissociated Chick DRG Cells

Dissociated chick DRG cells seeded onto a regionally peptide-grafted substrate film. After 5 h the cells only adhered to regions containing immobilized adhesion peptides RGDSG, GGGYIGSR, KAF(βA)KLAARLYRKA, GGGIKVAV, and HAV; other regions only supported a minimal amount of adhesion in clusters of cells. (Scale bar = 100 μm.)

Many paired combinations of receptor ligands RGDSG, GGGYIGSR, HAV, and GGGIKVAV also did not support cell adhesion, suggesting that the heparin-binding site KAF(βA)KLAARLYRKA was a necessary contributor. A possible reason for this is that a surface-bound heparin-binding site can function as an adhesion site for cell-surface proteoglycans and, thus, contribute to cell adhesion to the surface. Furthermore, heparin-binding sites can bind heparin from the culture medium which, in turn, can help immobilize heparin-binding growth factors and extracellular matrix (ECM) proteins on this otherwise protein-resistant substrate material. Relevant growth factors and ECM proteins are conducive to the adhesion of neural cells to any substrate.

Adhesion by dissociated DRG cells to peptide-grafted regions only persisted for about 6 hours, after which no cells remained attached. No neuritic extensions were observed at any time. Possible reasons for the lack of continued attachment and lack of

neurite outgrowth include an insufficient concentration of peptides immobilized, a suboptimal combination or ratio of adhesion ligands, insufficient overall ligand- and signalling capacity of the peptides immobilized, loss of adhesion peptides due to hydrolysis of peptide-grafted PEG chains, and surface rearrangements that reduce binding to tethered adhesion peptides.

CONCLUSION

Surfaces otherwise resistant to protein- and cell adhesion can be grafted with specific cell-receptor ligands to effect highly localized surface attachment and spreading. This principle was demonstrated for the PEG-containing substrate material by hFFs, which attached via specific integrin-binding to surface regions photo-grafted with RGD peptide.

While the creation of highly defined and functional neural circuits for neurobiological investigation was the ultimate, but unaccomplished goal of this part of the project, it was also an important, more direct aim of the work in this chapter to investigate the function of the receptor-ligands RGD, YIGSR, IKVAV and HAV and of the heparin-binding peptide KAF(βA)KLAARLYRKA. Although neurite extension on the PEG-containing films was not supported even by regions grafted with the combination of all five of these adhesion ligands, the conducive effect that the heparin-binding peptide had led to its inclusion in the protein backbone of the protein-*graft*-PEG gels described in Chapters 4, 5, and 6.

CHAPTER 4

DESIGN, SYNTHESIS, AND CHARACTERIZATION OF PROTEIN-*graft*-PEG HYDROGELS

OVERVIEW

To address the need for bioactive materials toward clinical applications in wound healing and tissue regeneration, an artificial protein was created by recombinant DNA methods and modified by grafting of poly(ethylene glycol) diacrylate. Subsequent photopolymerization of the acrylate-containing precursors yielded protein-*graft*-poly(ethylene glycol) hydrogels. The artificial protein contained repeating amino acid sequences based on fibrinogen and anti-thrombin III, comprising an RGD integrin-binding motif, two plasmin degradation sites, and a heparin-binding site. Two-dimensional adhesion studies (Chapter 5) showed that the artificial protein had specific integrin-binding capability based on the RGD motif contained in its fibrinogen-based sequence. Furthermore, heparin bound strongly to the protein's anti-thrombin III-based region. Protein-*graft*-poly(ethylene glycol) hydrogels were transparent and plasmin degradable, had Young's moduli up to 3.5 kPa, and –as will be described in Chapter 5– supported three-dimensional outgrowth of human fibroblasts. Cell attachment in three dimensions resulted from specific cell-surface integrin binding to the material's RGD sequence. Hydrogel penetration by cells involved serine-protease mediated matrix degradation in temporal and spatial synchrony with cellular outgrowth. Protein-*graft*-poly(ethylene glycol) hydrogels represent a new and versatile class of biomimetic hybrid materials that hold clinical promise in serving as implants to promote wound healing and tissue regeneration.

INTRODUCTION

Design of Protein-graft-PEG Hydrogel

Advances in tissue repair call for implant materials that permit cell specific adhesion, that degrade in spatial and temporal synchrony with cellular infiltration and proliferation, and that do not elicit an immune response.[149,150] Such materials should also display sufficient mechanical stability to be useful in surgical applications. Fibrin, formed as a result of injury, is the initial, naturally occurring wound healing matrix. As such, fibrin serves as a useful therapeutic material itself, but also presents a model for semi-synthetic and synthetic analogs, which can potentially be more specifically tailored to various applications and can be produced without the complexities associated with human blood products.

Toward the use of bio-functional materials in wound healing and tissue regeneration, the goal of this study was to obtain a biosynthetic material that could mimic the natural extracellular matrix in two important features: cell attachment and specific proteolytic remodeling. Genetic engineering techniques were employed to design and produce a specific bio-functional component inspired by fibrin that would confer these properties. As mentioned in Chapter 2, where surface-immobilization of a heparin-binding sequence contributed to neural cell adhesion, heparin-binding sites can bind heparin and, thus, help immobilize growth factors and ECM proteins that are conducive to the adhesion of neural cells to a given substrate. Therefore, as a third feature, we sought to incorporate affinity for heparin into the biosynthetic material, thus providing for immobilization of heparin and, in turn, for heparin-binding growth factors as well as potentially other designed exogenous agents that possess affinity for heparin.[89,90] An amino acid sequence based on a heparin-binding domain of the protein anti-thrombin III (ATIII) was incorporated to accomplish this.[151] Grafting PEG chains with terminal acrylate groups to this recombinant protein then enabled the formation of a three-dimensional protein-*graft*-polymer matrix that can be cured *in situ*.

Specifically, the recombinantly expressed, repeating 26 amino acid sequence of human fibrinogen (α chain, residues L^{94}-I^{119})[60] that is at the core of the multifunctional protein constituent (Chart 4.1, shaded) contains an RGD cell adhesion site (underlined) and two adjacent plasmin degradation sites (indicated by up arrows ↑).

Chart 4.1: Fibrinogen- and ATIII-based Recombinant Protein Pentamer [A] and Non-Functional Control Pentamer [B]

Chart 4.1: Fibrinogen- and ATIII-based Recombinant Protein Pentamer [A] and Control Pentamer [B]

In [A], the RGD cell adhesion site is underlined and the two adjacent plasmin degradation sites are indicated by up arrows (↑). In [B], the non-functional RGG domain is underlined and the loss of plasmin degradability is indicated by the symbol §. In both constructs, the amino acid sequence based on human fibrinogen is shown shaded; cysteine residues are outlined; and the thrombin-cleavable (↓) hexa-histidine tag is spelled out fully as **HHHHHH**.

Amino acid codes: alanine (A), arginine (R), asparagine (N), aspartic acid (D), cysteine (C), glutamic acid (E), glutamine (Q), glycine (G), histidine (H), isoleucine (I), leucine (L), lysine (K), methionine (M), phenylalanine (F), proline (P), serine (S), threonine (T), tryptophan (W), tyrosine (Y), valine (V).

The RGD motif was included to enable integrin-mediated cell attachment,[25] while the plasmin sites enabled cell-controlled degradation via cell-associated plasmin activity that represents one of the relevant modes of matrix penetration during wound healing.[62] Furthermore, a 14 amino acid heparin-binding sequence (*cursive*) derived from anti-thrombin III (ATIII; residues K^{121}-A^{134})[151] was recombinantly fused with the fibrinogen sequence in order to provide the heparin binding sites. Finally, repeating constructs of the above-described cassette, with multiplicity five (recombinant protein pentamers), were designed to contain six intermittent cysteine residues (outlined) that allowed for grafting

of PEG chains with terminal acrylate groups at the cysteines' thiol groups, thereby rendering the protein pentamer covalently photo-crosslinkable to form an elastic hydrogel. A thrombin-cleavable (↓) hexa-histidine tag (HHHHHH) exists near the protein construct's N-terminus in order to facilitate purification of recombinant protein pentamers, their mutant variants, as well as their derivatives. Two different recombinant protein pentamers were designed: One all-active construct with functional RGD and plasmin degradation sites (Chart 4.1, protein pentamer [A]); and an analogous recombinant protein pentamer (Chart 4.1, protein pentamer [B]) containing non-functional RGG domains (underlined) and ten point mutations resulting in arginine-to-glycine substitutions that led to loss of plasmin degradability (indicated by the symbol §).

Chapter 5 will describe that human cells interact specifically with the artificial matrix described above. The observed cellular responses, namely three-dimensional cell attachment and proteolytic penetration, are promising of controlled and improved wound healing and tissue regeneration by use of this biosynthetic biomaterial.

Reaction Selectivity[152]

Hydrogels as wound sealants or for drug delivery have been cross-linked using relatively non-specific chemical reactions. These reactions, if allowed to occur *in situ*, may lead to the covalent modification of proteins of surrounding tissue. For example, materials made from poly(ethylene glycol) (PEG) have been formed in the presence of proteins via nucleophilic substitution reactions between activated PEG-carboxylic acids and PEG-nucleophiles.[153] In this case, the activated PEG also reacts with the proteins to be released as therapeutic agents. Therefore, this uncontrolled coupling of the polymer to the protein is undesirable. Other hydrogels have been cross-linked using large doses of γ-radiation, ultraviolet light, or high temperatures, often for 30 minutes or more, which may damage protein drugs[154,155,156,157] or adjacent tissues. More selective reactions using long

wavelength ultraviolet light irradiation and shorter irradiation times have also been described.[158]

The matrices that will be presented in this work consist of proteins grafted with PEG diacrylate by reaction of the terminal PEG-acrylates with protein-thiols. The reaction is rapid at physiological conditions, and reaction between PEG-acrylates and other chemical groups on proteins, notably the proteins' amine terminus and primary amines of lysines, is slow.[152,106,159] The exclusive character of the reaction between acrylates and thiols will be referred to as reaction selectivity.

To verify the reaction selectivity between acrylates and thiols, the model protein albumin was reacted with PEG diacrylate and other electrophiles under various conditions. Part of this chapter will be devoted to these model reactions and their analysis.

MATERIALS AND METHODS

DNA Design

Recombinant DNA techniques were used to obtain protein pentamers [A] and [B]. First, the DNA encoding the monomeric constituents of protein pentamers [A] and [B] was assembled from DNA fragments {a} and {b} (Chart 2). We optimized the DNA sequences of fragments {a} and {b} to match the codon preferences for *E. coli*[160] while taking into account the required restriction enzyme sequences for gene manipulation. In order to obtain both protein pentamer variants [A] and [B], oligonucleotides for {a} and {b} were synthesized with mixed bases at positions 34 and 54 in {a}, and mixed bases at position 16 in {b} (Chart 2). The pairs of DNA fragments {a} and {b} encoding the desired monomeric constituents of recombinant protein pentamers [A] and [B] (bases D,K,K = A,C,C for [A] and bases D,K,K = C,C,C for [B]) were identified by DNA sequence analysis and then ligated at restriction site BsaAI to produce the complete DNA segment {c} (Chart 3).

Chart 4.2: Recombinant Gene Assembly

DNA fragments {a} (four possible variants; coding and anti-coding oligonucleotides)

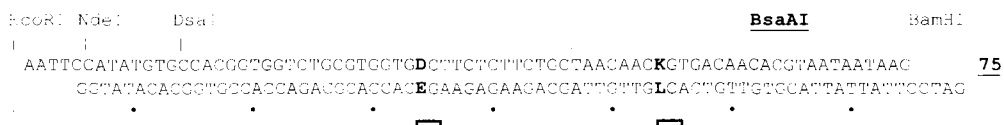

DNA fragments {b} (two possible variants; coding and anti-coding oligonucleotides)

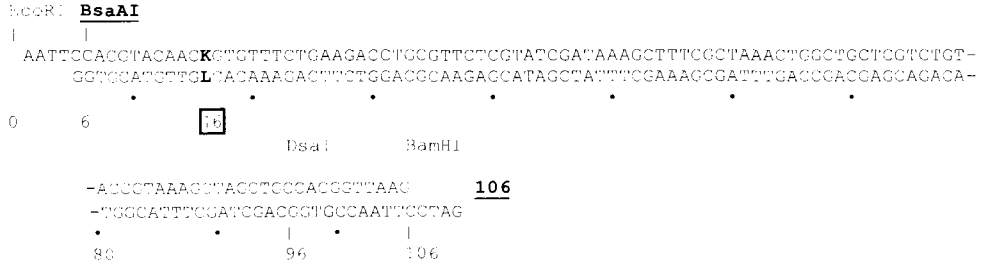

Chart 4.3: DNA Multimerization

Complete DNA segment {c}: {a} and {b} combined

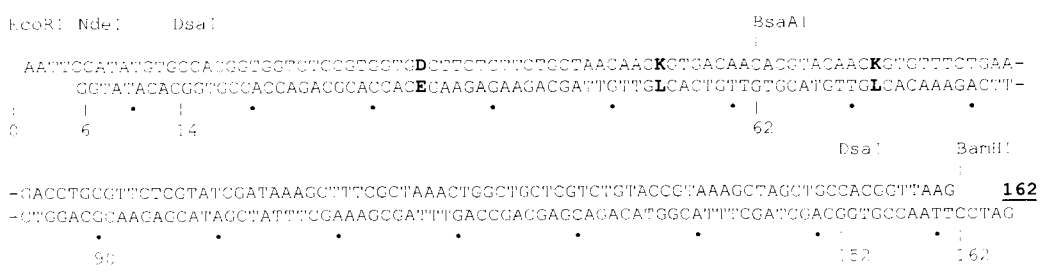

DsaI-digested segment {c} for multimerization

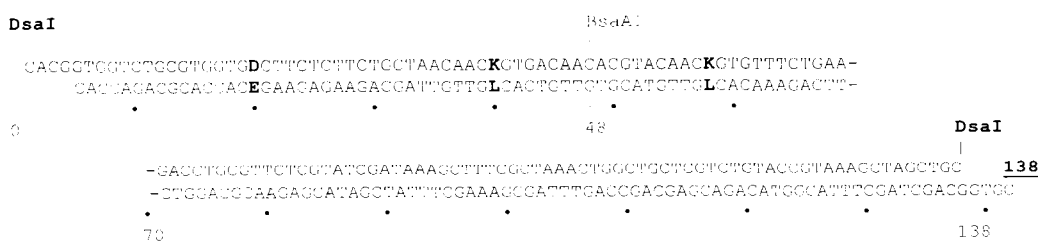

D = mixed bases A/G (if **D** = A → amino acids RGD; if **D** = G → amino acids RGG)
E = matching mixed bases T/C

K = mixed bases G/T (if **K** = C → amino acids NR; if **K** = G → amino acids NG)
L = matching mixed bases G/C

protein pentamer [A]: **D,K,K** = A,C,G; protein pentamer [B]: **D,K,K** = G,G,G

The described design strategy allowed for the efficient assembly of the target DNA and its variant encoding the three simultaneous amino acid substitutions RGD → RGG, NR → NG and, again, NR → NG. The resulting DNA segments {c} were multimerized in correct coding orientation by ligation at the non-palindromic 3' DNA overhangs resulting from DsaI restriction enzyme digestion (Chart 3).[109]

General Notes

Bacterial strains used were *E. coli* strains DH5α-F′ (Life Technologies, Scotland) and JM109 (Promega, USA) for cloning, and BL21(DE3)pLysS (Novagen, USA) for protein expression. In all DNA constructs, appropriate pairs of terminal restriction sites were used: EcoRI and BamHI for simple DNA manipulations with vector pUC18 (Life Technologies, USA) and NdeI and BamHI for gene expression with vector pET14b (Novagen, USA). The restriction enzymes were purchased from Roche Diagnostics GmbH, Germany. Standard molecular biological methods as described elsewhere[161,162] were employed for DNA manipulations, bacterial cultures, agarose gel- and polyacrylamide gel electrophoresis (PAGE), and Western blotting.

Multimerization of DNA and Cloning into pET14b

Coding and anti-coding strands, as supplied (Microsynth GmbH, Switzerland), for DNA fragments {a} and {b} constituting the monomeric target DNA segment {c} (Charts 4.2 and 4.3) were purified by 6% polyacrylamide gel electrophoresis under denaturing conditions (TBE buffer: 89 mM Tris base, 89 mM boric acid, and 2 mM EDTA; with 7M urea). Bands of purified oligonucleotides were cut out of the polyacrylamide gel and eluted over night into DNA elution buffer (0.5 M NH_4OAc), followed by DNA precipitation the next day. For each of oligonucleotides {a} and {b}, 2 μg each of the coding and anti-

coding strands were annealed in 30 µL TE buffer (10 mM Tris, 1 mM EDTA, pH 7.4) by heating to 90 °C and cooling to room temperature overnight. The resulting double-stranded DNA fragments {a} and {b} were phosphorylated with alkaline phosphatase (Roche), ligated into EcoRI,BamHI-cut pUC18 vectors and transformed into DH5α-F'. Plasmid DNA was amplified in 6 mL *E. Coli* cultures followed by isolation via mini preparations (Wizard Plus Minipreps, Promega, USA). Insert-containing pUC18{b} was cut with BsaAI (New England BioLabs Inc., USA) and BamHI. The resulting fragments {b} were ligated into BsaAI- and BamHI-digested pUC18{a} using T4 DNA ligase (New England BioLabs). In this step, fragments {b} and insert-containing vectors pUC18{a} were matched appropriately to form the correct desired DNA segments {c} (Chart 4.3).

To multimerize the DNA segments {c} encoding the monomeric forms of recombinant protein pentamers [A] and [B] (Chart 1), the following steps were performed: Midi preparations (Whizard Plus Midipreps, Promega, USA) of the vectors pUC18{c} were digested with non-palindromic restriction enzyme BstDSI (Hybaid-AGS, Germany), an isoschizomer of DsaI. DsaI-digested segments {c} were separated from host vector pUC18 by 11% polyacrylamide gel electrophoresis in TBE buffer. Bands of 138 base pairs, corresponding to DsaI-digested segments {c}, were cut out from the gel, and the segments eluted into DNA elution buffer overnight followed by precipitation using Pellet Paint™ Co-Precipitant (Novagen) for improved precipitation of small DNA fragments. Ligation, i.e., multimerization, of DsaI-digested segments {c} at 0.3-0.4 µg/µL was allowed to proceed at 16 °C for only 15 min. The ligation products were run on a 1.5% agarose gel to separate the different DNA multimers. Bands of 690 base pairs, corresponding to DNA pentamers of DsaI-digested segments {c}, were cut out, and the DNA extracted using the QiaEx gel extraction kit (Qiagen AG, Switzerland). DNA pentamers were then ligated back into de-phosphorylated BstDSI-cut vector pUC18,

amplified in *E. coli* followed by mini preparation, and cut out with restriction enzymes NdeI and BamHI for ligation into the multiple cloning site of expression vector pET14b, which also encodes the N-terminal thrombin-cleavable hexa-histidine tag, resulting in pET14b[A] and pET14b[B]. All DNA sequences were confirmed by DNA sequencing (Microsynth, Switzerland).

Expression of Recombinant Protein Pentamers [A] and [B]

E. coli strain BL21(DE3)pLysS (Novagen, USA) was transformed with either pET14b[A] or pET14b[B] encoding recombinant protein pentamers [A] and [B], and the resulting BL21(DE3)pLysSpET[A] and BL21(DE3)pLysSpET[B] grew overnight in 2X Yeast-Tryptone broth (10 g/L yeast extract, 16 g/L tryptone, AppliChem, Germany; and 5 g/L NaCl) supplemented with 50 µg/mL ampicillin (AppliChem) and 34 µg/mL chloramphenicol (AppliChem). Shaking-flask cultures of 1 L (same medium and supplements) were inoculated 1:50 from the pre-cultures and grew to an optical absorbance range of 0.6 – 1.0 A measured at 600 nm (OD_{600}), whereupon protein expression was induced by addition of 1 M β–isopropyl thiogalactoside (IPTG, Novagen, Switzerland) to a final concentration of 1 mM. Expression proceeded for 3-4 h, after which cells were harvested by centrifugation (5000 g, 15 min, 4 °C). Expression of recombinant protein pentamers [A] and [B] was monitored by 15% polyacrylamide SDS-PAGE.

Protein Purification

The hexa-histidine tagged target protein, i.e., protein pentamers [A] or [B], was recovered from bacterial cell pellets (3-4 g wet per liter culture) and Ni^{++}-affinity purified (Figure 4.2.a) according to protocols from the pET System Manual.[162] The eluate fractions after Ni^{++}-affinity purification were monitored by 15% polyacrylamide SDS-PAGE for content of target protein. Fractions with target protein were combined and dialysed against

PBS (0.2 g/L KCl , 0.2 g/L KH_2PO_4, 2.16 g/L $Na_2HPO_4 \cdot 7H_2O$, 8 g/L NaCl, pH 7.4) with 8 M urea. Arimedes Biotechnology GmbH, Germany, expressed and purified one 5.5 g batch of recombinant protein pentamer [A] and resuspended it in 100 mM TRIS, pH 6.3, 300 mM imidazole, 4 mM β-mercaptoethanol, and 8 M urea at 7.0 mg/mL. This batch was also dialysed, in fractions, against PBS with 8 M urea to final concentrations of β-mercaptoethanol no greater than 4 nM. The protein concentration after dialysis was estimated by a combination of the Bio-Rad Protein Assay according to Bradford (Bio-Rad Laboratories, USA), and by comparing to known amounts of bovine serum albumin (Bio-Rad) in Coomassie Blue-stained 10% or 15% polyacrylamide gels. Ellman's test for free thiols (Pierce, USA) was performed according to supplier's instructions. Furthermore, protein pentamer [B] was analyzed by matrix-assisted laser desorption ionization (MALDI) mass spectroscopy using the Voyager Elite 122 (Applied Biosystems) and matrix alpha-cyano-4-hydroxycinnamic acid (Aldrich). Finally, Western blots were prepared from 10% polyacrylamide gels containing 1.0 μg recombinant protein pentamers [A] or [B] per lane, using the QIAexpress anti-penta·His antibody (Qiagen) for detection of the hexa- and penta-histidine epitopes found in the recombinant protein pentamers, followed by incubation with a secondary horse-radish peroxidase-conjugated antibody (goat anti-maouse IgG; Sigma). The immunoreactive bands were visualized on X-ray film by enhanced chemiluminescence (ECL) detection (Amersham Pharmacia Biotech Europe GmbH).

Acrylation of Poly(Ethylene Glycol)

Poly(ethylene glycol) α,ω-diacrylate (PEG diacrylate), mol. wt. 6000, was prepared from PEG, mol. wt. 6000 (60 g, 10 mmol, Fluka, Switzerland, M_n = 6000). PEG was dried by azeotropic distillation in 600 mL toluene for 1 hr using a Dean-Stark

trap. After cooling to less than 50 °C under argon, triethylamine (12.3 mL, 4.4 eq., Aldrich, Germany) was added. Addition of acryloyl chloride in two half-portions separated by 10 min (6.74 mL total, 4.0 eq., Aldrich) initiated the reaction. The reaction continued with stirring overnight in the dark at room temperature under argon. The resulting pale yellow solution was filtered through a neutral alumina bed. Sodium carbonate was added to the toluene solution and stirred for 2 hr. The sodium carbonate was removed by filtration, and the toluene was removed by rotary evaporation. The reaction product was re-dissolved in a minimal volume of dichloromethane and precipitated by dropwise addition to diethyl ether in an ice bath. After recovery by filtration, the precipitate was washed with diethyl ether and dried *in vacuo*. The yield was 48.7 g, and ^{1}H NMR spectrometry (200 MHz) in DMSO resulted in the following peaks: 3.5 ppm (264.74 H, PEG), 4.2 ppm (t, 2.51 H, -CH_2-$C\underline{H}_2$-O-CO-CH=CH_2), 5.9 ppm (dd, 1.00 H, CH_2=C$\underline{H}$-COO-), 6.1 ppm, 6.4 ppm (dd, 2.17 H, $C\underline{H}_2$=CH-COO-). Quantitative acrylation was evident from comparison of the peak at 3.5 ppm to the acrylate-associated peak at 5.9 ppm and applying the M_n reported by the supplier. PEG diacrylate, mol. wt. 3400, prepared similarly from PEG, mol. wt. 3400 (Aldrich), was also acrylated quantitatively. Likewise, PEG α-monoacrylate ω-monomethyl ether, mol. wt. 5000, was prepared from PEG monomethyl ether, mol. wt. 5000 (Fluka, Switzerland), following similar protocols for synthesis and purification as for PEG diacrylate, mol. wt. 6000.

Synthesis and Purification of Protein-*graft*-PEGacrylates

In the following, the term "PEGacrylation" refers to the grafting of PEG diacrylate to protein thiols by Michael-type conjugate addition, producing a protein with pendant PEG chains that terminate in acrylate groups. The term "PEGylation" alone refers to the grafting of any functionalized PEG to protein thiols, producing a protein with pendant PEG chains of unspecified terminal functional groups.

PEGacrylation: 10.0 molar equivalents of PEG diacrylate (mol. wt. 3400 or 6000) per protein thiol, pre-dissolved at 250-300 mg/mL PBS with 8 M urea, pH 7.4, reacted with 7 mg/mL recombinant protein pentamers [A] and [B] by Michael-type conjugate addition in PBS with 8 M urea at pH 7.4 for 1 hr after previous reduction of protein disulfide bonds with 2.0 molar equivalents of tris(2-carboxyethyl) phosphine hydrochloride (TCEP·HCl, Pierce, USA; 15 min, 25 °C, shaking) per mole of theoretical disulfide bonds. Reaction progress was monitored by 10% polyacrylamide SDS-PAGE under reducing conditions (Figure 4.3a).

The reaction products, i.e., PEGacrylated recombinant protein pentamers [A] or [B] (presumably protein[A]-*graft*-hexaPEGacrylate or protein[B]-*graft*-hexaPEGacrylate), were purified from excess PEG diacrylate by Ni^{++}-affinity chromatography: Briefly, after raising the pH to 7.9 by addition of 1 N NaOH, the solution of reaction products was applied to beds of His•Bind® resin with sufficient binding capacity for the PEGacrylated target protein. 12-15 consecutive column volumes of wash buffer (17 mM NaH_2PO_4, 183 mM Na_2HPO_4, 286 mM NaCl, adjusted to pH 7.9 with NaOH) removed unreacted PEG, and the PEGacrylated target protein eluted with four consecutive volumes of elution buffer (17 mM NaH_2PO_4, 183 mM Na_2HPO_4, 286 mM NaCl, 1 M imidazole, adjusted to pH 7.9 with NaOH). Again, 10% polyacrylamide SDS-PAGE allowed monitoring of the purification fractions. The wash fractions were freeze dried for verification of complete elution of unreacted PEG diacrylate. Only eluate fractions containing PEGacrylated protein pentamer were dialysed $1:10^5$ in Spectra/Por® dialysis tubing with a molecular weight cut-off of 6-8 kDa (Spectrum Laboratories Inc., USA, MWCO 6-8,000) at 4 °C against ddH_2O containing 0.1% *(v/v)* glacial acetic acid (Aldrich). Finally, the dialysate was lyophilized after addition of ~10% *(m/m)* anhydrous D(+)-glucose (AppliChem) to improve solubility upon re-dissolution. For confirmation of the PEGacrylated recombinant protein pentamers' identities, amino acid analyses were performed on an HP AminoQuant II (Agilent Technologies, Palo Alto, USA). One sample of protein[A]-*graft*-PEGacrylate was

analyzed that originated from protein pentamer [A] expressed by Arimedes Biotechnology GmbH, and four samples of protein[B]-*graft*-PEGacrylate were analyzed that originated from different 1 L protein expressions, but the same clone.

PEG diacrylate, mol. wt. 575 (Aldrich), PEG α-monoacrylate ω-monomethylether, mol. wt. 5000, and PEG α,ω-divinylsulfone, mol. wt. 3400 (Shearwater Polymers Inc., USA), were reacted with 7 mg/mL recombinant protein pentamer [A] by Michael-type conjugate addition under similar conditions and in identical stoichiometric ratios per protein thiol as described for PEG diacrylates, mol. wt. 3400 and 6000.

Verification of Reaction Selectivity

SDS-PAGE was used to demonstrate that model protein albumin remained unmodified by PEG-thiol and PEG-acrylate during hydrogel formation. Bovine serum albumin (BSA, Sigma) was dissolved in 50 mM HEPES buffered saline, pH 7.4, at a concentration of 1.5 mg/mL. To reduce disulfide bonds in albumin before reacting with the PEG derivatives, 10 μL of tris(2-carboxyethyl)phosphine hydrochloride (11.1 mg/mL in DI water, Pierce Chemicals) were added to 500 μL of the albumin solution. The following PEG derivatives were added to aliquots of the albumin solution in specified stoichiometric ratios: PEG-dithiol mol. wt. 3400, PEG-monoacrylate, monoNHS ester mol. wt. 3400 (Shearwater Polymers), or PEG-diacrylate mol. wt. 3400. In addition, acrylic acid (anhydrous, Aldrich) was added to selected albumin solutions in order to quench free thiol groups on PEG-dithiol and prevent thiol exchange with albumin during SDS-PAGE sample preparation. Proteins were analyzed by SDS-PAGE using 10% acrylamide gels. For sample preparation, 10 μL of any given reaction mixture were combined with 6 μL DI water and 4 μL 5x SDS-PAGE running buffer containing 1M dithiothreitol (DTT) unless

otherwise noted. The samples were then boiled for about 3 min. Molecular weight markers (Bio-Rad, Hercules, CA, USA) were 31, 45, 66.2, 97, 116, and 200 kDa.

Heparin-Affinity Chromatography

0.5 g heparin-agarose beads (bead size 50-150 µm, 5-7 mg heparin per milliliter resulting gel; AppliChem A1481, Germany) were pre-swollen in PBS, pH 7.4, for 1 h at room temperature, poured into a chromatography column, and allowed to settle to yield a bed of heparin-agarose gel of approximately 1 mL. 1 mg of protein[A]-*graft*-PEG(6000)acrylate in 1 mL PBS with and without 28.3 mg/mL heparin from porcine intestinal mucosa (MW 16,000 - 18,000, 181 USP units/mg, Sigma H-9399, Germany) was applied to the heparin-agarose gel and allowed to bind for 15 min at room temperature and zero column flow. The column was then drained, and chromatography was performed with seventeen consecutive 1 mL washes of PBS containing increasing amounts of NaCl, starting with the original 137 mM up to 2 M in steps of 110 mM NaCl. The flow-through fractions were collected separately and analyzed by 15% polyacrylamide SDS-PAGE for the presence of protein[A]-*graft*-PEG(6000)acrylate.

Verification of Acrylate Presence

To verify presence of the acrylate termini of both protein[A]-*graft*-PEG(6000)acrylate and protein[A]-*graft*-PEG(3400)acrylate, 80 µL of each PEGacrylated recombinant protein pentamer (1.25 mg/mL in PBS, pH 7.4) were combined with 20 µL 0.3 M triethanolamine, pH 8.0, containing 20.0 molar equivalents per theoretical acrylate group of oligopeptide didansyl-KRDGPDGIWGDDRCG-$CONH_2$ (kindly provided by Dror Seliktar, Institute for Biomedical Engineering, ETH and UNI Zurich, Switzerland). After allowing Michael-type conjugate addition of the peptide thiols to protein-*graft*-

PEGacrylates for 15 min under shaking at 37 °C, a 16 µL sample was quenched with 4 µL DTT-containing SDS-PAGE sample buffer (0.28 M Tris·HCl, 30% *(v/v)* glycerol, 1% *(w/v)* SDS, 0.5M dithiothreitol (DTT), 0.0012% *(w/v)* bromphenol blue; pH 6.8). After heating the sample for 5 min at 95-100 °C, SDS-PAGE was performed using 10% polyacrylamide gels. To visualize unreacted didansyl-oligopeptide as well as dansylated protein-*graft*-PEGacrylate species by virtue of their fluorescence, gels were first placed atop a MacroVue UVis-20 gel viewer (Hoefer Pharmacia Biotech, USA) and photographed through a UV filter with a digital camera. To visualize any protein species by direct staining, the SDS-PAGE gels were subsequently stained in Coomassie Blue G-250 staining solution (0.025% *(w/v)* Coomassie Blue G-250, 10% *(v/v)* acetic acid) and destained in destaining solution (10% *(v/v)* acetic acid, 20% *(v/v)* ethanol).

Gelation by Photopolymerization and Swelling

5%, 7.5%, 10%, 12.5%, and 15% *(w+v)* solutions of PEGacrylated protein pentamers [A] and 10% and 15% *(w+v)* solutions of PEGacrylated protein pentamer [B] in serum-containing DMEM (e.g., to obtain a 10% *(w+v)* solution, 1 mg protein-*graft*-PEG was combined with 10 µL DMEM) containing 0.1 mM eosin Y (Aldrich, Germany), 13.2 µL/mL triethanolamine, and 3.5 µL/mL 1-vinyl-2-pyrrolidinone (Aldrich, USA), were photopolymerized by irradiation at λ = 480 – 520 nm and 75 mW/cm^2 for 15-30 s from a portable Cermax Xenon Fiber Optic Light Source CXE300 (ILC Technology Inc., USA). Swelling of protein[A]-*graft*-PEG(6000) hydrogels was measured by weighing the gels before and after swelling in PBS, pH 7.4, for 16 h.

Rheological Measurements

A Bohlin Instruments CVO 120 High Resolution rheometer (Bohlin Instruments, United Kingdom) was used in combination with a portable Cermax Xenon Fiber Optic Light Source to characterize the light-induced liquid-to-solid transition (photogelation) of protein-*graft*-PEGacrylate solutions in a parallel disc geometry. The light source was installed underneath a glass plate serving as the fixed bottom surface, while a circular parallel plate with radius 10.0 mm was rotating in oscillatory mode atop 30 µL of a 10% *(w+v)* protein[A]-*graft*-PEG(3400)acrylate or –PEG(6000)acrylate solution throughout the measurement, imposing a target shear strain of 0.05 at a frequency of 1 Hz and with an initial shear stress of 1 Pa. The distance between the bottom glass surface and the parallel disc was 95 µm. After allowing the phase angle of the solution to stabilize for 1-2 min, the light source was switched on at designated time = 0 and allowed to irradiate the sample for the entire duration of the rheological measurement. For each protein-*graft*-PEG two measurements were performed on two samples that were prepared identically (n=2), but due to material constraints the measurements have not been repeated independently.

Plasmin Degradation Assay

10% *(w+v)* protein[A]-*graft*-PEG(6000) hydrogels were tested for degradability by plasmin by placing a pre-swollen ~5 mg pieces of protein-*graft*-PEG hydrogel into a 200 µL solution of 2 U/ml plasmin from porcine blood (Sigma P-8644, Germany) in PBS, pH 7.4. Degradation of the gel by plasmin was allowed to proceed for 3 hr at 37 °C. In parallel, pieces of hydrogel, similar in size, were placed in 200 µL PBS, pH 7.4, without plasmin, and incubated at 37 °C for 3 hr.

RESULTS AND DISCUSSION

Multimerization of DNA

As verified by DNA sequencing, the DNA segments {c} (Chart 4.3) encoding the monomeric sequences of recombinant protein pentamers [A] and [B] assembled correctly from matching DNA fragments {a} and {b} (Chart 4.2). The products of the subsequent multimerization of DsaI-digested segments {c} for recombinant protein pentamer [B] can be seen in lane 1 of the agarose gel shown in Figure 4.1.

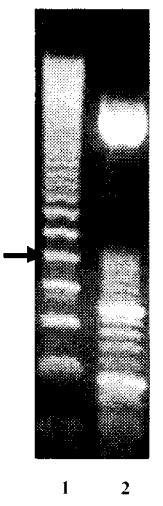

Figure 4.1: 1.5% Agarose Gel Illustrating DNA Multimerization

Lane 1: Products of the multimerization of DsaI-digested DNA segment {c} (138 bp) for recombinant protein pentamer [B]. Multimers $\{c\}_x$ of DsaI-digested DNA segment {c} (Chart 3) can be observed as stained DNA bands that run at multiples of 138 bp, including the un-multimerized segment at 138 bp. The DNA pentamer $\{c\}_5$ (690 bp) encoding recombinant protein pentamer [B] is highlighted with an arrow (→). Lane 2: 50 bp DNA molecular weight ladder.

In particular, multimers $\{c\}_x$ can be observed as DNA bands that run at multiples of 138 bp. The DNA pentamer $\{c\}_5$ (690 bp) encoding recombinant protein pentamer [B] is highlighted with an arrow (→) (Figure 4.1). DNA sequencing of the DNA pentamers $\{c\}_5$ cloned into pET14b confirmed proper gene sequence and orientation.

In summary, using techniques previously established by McGrath, et al.,[109] DsaI-digested segments {c} were multimerized through head to tail polymerization to form the pentameric DNA that encodes protein pentamers [A] and [B]. Codons encoding cysteine residues were present in the monomeric DNA units to introduce equispaced thiols (Chart 4.1, outlined) for subsequent modifications,[163,164,165] such as the PEGacrylation of protein pentamers [A] and [B] described in this work.

Expression and Purification of Recombinant Protein Pentamers [A] and [B]

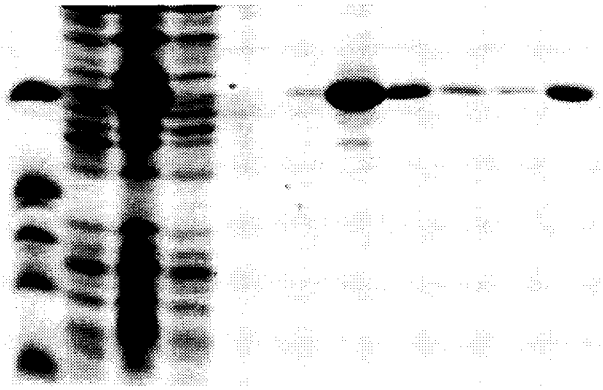

Figure 4.2.a: Bacterial Expression and Purification of Recombinant Protein Pentamer [A]

Coomassie-stained 15% polyacrylamide SDS-PAGE gel documenting the bacterial overexpression and Ni^{++}–affinity purification of recombinant protein pentamer [A]. Lane 1: protein molecular weight marker (3.5, 6.1, 14.4, 16.9, 19.7/20.4, 31 kDa). Lane 2: Soluble bacterial proteins. Lane 3: Insoluble bacterial proteins containing recombinant protein pentamer [A], solubilized with 6 M guanidine HCl; before flow over the Ni^{++}-column. Lane 4: Flow-through after flow over the Ni^{++}-column. Lane 5: Washes. Lanes 6-11: Consecutive eluate fractions containing purified recombinant protein pentamer [A].

As illustrated in the protein purification profile for recombinant protein pentamer [A] (Figure 4.2a), the recombinant protein was expressed successfully (lane 3) using the pET expression system and readily purified (lanes 6 - 11) by Ni^{++}-affinity chromatography (40 mg/L and 10 mg/L, pentamer [A] and [B] respectively, from shaking flask bacterial cultures; 127 mg/L of recombinant protein pentamer [A] from commercial fermentation). The presence of the recombinant protein pentamer band at 31 kDa in lane 3 (Figure 4.2.a), which represents all insoluble bacterial proteins, indicates that recombinant protein pentamer [A] was deposited into bacterial inclusion bodies during protein expression.[1] Expression and purification of recombinant protein pentamer [B] (not shown) was achieved similarly, in agreement with results previously achieved for several artificial periodic

[1] Smaller recombinant protein multimers such as the monomer and dimer, not shown, were not expressed efficiently. This was one of the reasons for focusing exclusively on protein pentamer species in subsequent experiments.

proteins.[166,114,115,112,167,117] Bacterial expression in conjunction with affinity purification was a convenient and straightforward method for producing recombinant protein pentamers [A] and [B].

Characterization of the Recombinant Protein Pentamers

Recombinant protein pentamers [A] (mol. mass 28529) and [B] (mol. mass 27247) both exhibited in SDS-PAGE an apparent molecular mass of about 31 kDa ([B] not shown). MALDI mass spectroscopy of protein pentamer [B] revealed a dominant peak centered at molecular mass 27498.[2] In Western blots, recombinant protein pentamers [A] (Figure 4.2.b) and [B] (not shown) were detectable by immunoreactivity of an anti-penta·His antibody with the protein pentamers' hexa-histidine tags.

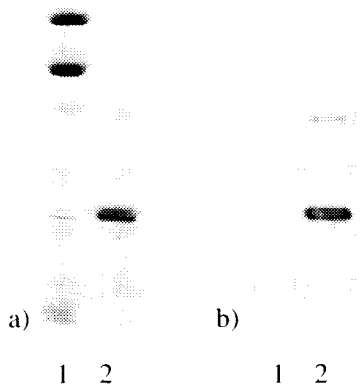

Figure 4.2.b: Western Blot of Recombinant Protein Pentamer [A]

Lane 1 in a): Coomassie-stained protein molecular weight marker (19.7/20.4 kDa *(faint)*, 31.0 kDa *(faint)*, 45.0 kDa, 66.2 kDa).
Lane 2 in a): Coomassie-stained recombinant protein pentamer [A].
Lane 2 in b): Signal in the Western blot of recombinant protein pentamer [A], transferred from the 10% polyacrylamide SDS-PAGE gel shown in a), reacted with anti-penta·His antibody and visualized.

---

[2] MALDI was not performed on protein pentamer [A] because its identity was confirmed by amino acid analysis of protein[A]-*graft*-PEGacrylate (Table 4.1).

Amino acid analysis confirmed the expected amino acid composition of PEGacrylated protein pentamer [A] (Table 4.1), whereas the amino acid composition determined experimentally for PEGacrylated protein pentamer [B] deviated significantly in glutamic acid and proline content, as well as in threonine, serine, isoleucine, valine and lysine content. The numbers of protein pentamer [B]'s other residues agreed with their theoretical abundance.

Table 4.1: Amino Acid Analysis of Protein[A]-*graft*-PEG and Protein[B]-*graft*-PEG

Amino Acid	Experimental values for protein[A]-*graft*-PEG	Theoretical values for protein[A]-*graft*-PEG	Average experimental values for protein[B]-*graft*-PEG ± stnd. error (n=4)	Theoretical values for protein[B]-*graft*-PEG
Asx[i)]	43.6	40	31.9±1.1	35
Glx[i)]	8.6	5	20.5±1.7	5
Ser	25.0	30	16.9±1.2	30
His	11.9	13	9.0±0.4	13
Gly	19.7	19	29.8±1.9	34
Thr	6.3	5	10.3±0.5	5
Ala	30.7	30	26.8±0.7	30
Arg	35.1	36	19.8±0.9	26
Tyr	10.3	10	7.7±0.3	10
Val	8.3	6	13.5±0.8	6
Met	0.0	2	0.7±0.7	2
Phe	10.9	10	10.0±0.2	10
Ile	6.4	5	10.3±0.5	5

Leu	22.1	21	22.6±0.3	21
Lys	13.0	15	13.6±0.2	15
Pro	1.9	1	8.6±0.5	1
Cys[ii]	--	6	--	6
Trp	(not detected)	0	(not detected)	0

Note: i) As a result of acid-based hydrolysis prior to amino acid detection, asparagine and glutamine residues were converted into aspartic acid and glutamic acid, respectively. Therefore, the number of those residues detected reflects the number of original asparagine and aspartic acid residues, or glutamine and glutamic acid residues, in the protein combined. ii) Cysteine residues are not quantifiable by the analysis method used.

Amino acid codes: alanine (Ala), arginine (Arg), asparagine and/or aspartic acid (Asx), cysteine (Cys), glutamic acid and/or glutamine (Glx), glycine (Gly), histidine (His), isoleucine (Ile), leucine (Leu), lysine (Lys), methionine (Met), phenylalanine (Phe), proline (Pro), serine (Ser), threonine (Thr), tryptophan (Trp), tyrosine (Tyr), valine (Val).

In light of the fact that protein pentamer [B]'s encoding DNA was correct and that SDS-PAGE as well as MALDI mass spectroscopy of the purified sample revealed a dominant protein band of the molecular mass expected for protein pentamer [B], a likely explanation for the deviation of the experimental amounts of the amino acids mentioned above is the presence of bacterial impurities, which seem to have altered the numbers of the discrepant amino acids.

Ellman's test for free thiols revealed that unmodified protein pentamers [A] and [B] contained at most 30% free thiols after affinity purification and dialysis against PBS with 8 M urea. Prior to PEGacrylation, recombinant protein pentamers [A] and [B] were insoluble in aqueous buffers with less than 6 M urea. Once precipitated or lyophilized, recombinant protein pentamers [A] and [B] did not re-dissolve in a variety of solvents, neither aqueous (0.1% acetic acid, 50% ethanol, 0.1% SDS) nor organic (acetonitrile, methanol, ethanol, N,N-dimethylformamide, tetrahydrofuran, dimethylsulfoxide), unless 5 mM reducing agent (such as DTT or β–mercaptoethanol) and at least 6 M urea were present.

Synthesis of Protein-*graft*-PEGacrylates

Figure 4.3.a illustrates the Michael-type conjugate addition of recombinant protein pentamer [A]'s six thiols to PEG diacrylate, mol. wt. 6000, as monitored by 10% polyacrylamide SDS-PAGE under reducing conditions. The reaction of PEG diacrylate, mol.wt. 6000, with recombinant protein pentamer [B] was less successful and, in 10% polyacrylamide SDS-PAGE, produced a smear of products from apparent molecular weight 31 kDa (unreacted protein pentamer) to species larger than 200 kDa.

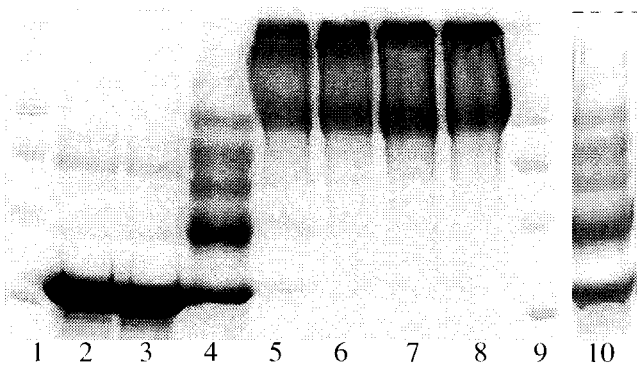

Figure 4.3.a: SDS-PAGE Gel Showing the PEGacrylation of Recombinant Protein Pentamer [A]

Coomassie-stained 10% polyacrylamide SDS-PAGE gel showing the PEGacrylation by Michael-type conjugate addition of recombinant protein pentamer [A]. Lanes 1 and 9: Protein molecular weight marker (31.0, 45.0, 66.2, 97.4 kDa). Lane 2: Recombinant protein pentamer [A]. Lane 3: Recombinant protein pentamer [A] after incubation with TCEP. Lane 4: Intermediate reaction products, after the reaction was quenched by addition of DTT-containing SDS-PAGE sample buffer shortly after combining the reagents. Lanes 5-8: Reaction products after 15, 30, 45, and 60 min. Lane 10: Reaction products after 1.5 hr without previous reduction of disulfide bonds by TCEP.

The difference in reactivity between protein pentamers [A] and [B] may be due to differences in protein structure resulting from the lower net positive charge of protein pentamer [B] as well as its lower total number of charged residues (Table 4.2). Because of its lower net positive charge and lower total number of charged residues, recombinant protein pentamer [B] may be less unfolded than [A], even in the presence of 8 M urea, a chaotropic agent, and, thus, its thiol groups be less accessible for reduction by TCEP and/or reaction with PEG diacrylate than recombinant protein pentamer [A]'s thiols are.

Table 4.2: Charge Analysis of Protein[A]-*graft*-PEG and Protein[B]-*graft*-PEG

	Protein pentamer [A]	Protein pentamer [B]
Theoretical isoelectric point (pI)	10.43	10.11
Total number of negatively charged residues (Asp + Glu)	25	20
Total number of positively charged residues (Arg + Lys)	51	41
Total number of charged residues	76	61
Expected net charge at pH 7.4	+26	+21

reference: ExPASy ProtParam tool[168]

As far as the PEGacrylation of protein pentamer [A] is concerned, Lane 4 of Figure 4.3.a shows that when the reaction was quenched by addition of DTT-containing SDS-PAGE sample buffer seconds after combining the reagents, distinct intermediate reaction products can be observed. These compounds appear to be incompletely PEGacrylated protein pentamers, whereas the final reaction product, expected to be fully PEGacrylated protein[A]-*graft*-hexaPEGacrylate (mol. mass 64.5 kDa), ran in SDS-PAGE at an apparent molecular weight of approximately 100 kDa (Figure 4.3.a, lane 4, top protein band). (The high apparent molecular weight of PEGylated proteins is not surprising, as uncharged PEG chains do not contribute to the proteins' mobility during SDS-PAGE, and even impede migration by steric hindrance.) The PEGacrylation of recombinant protein pentamer did not go to completion unless TCEP was previously used to break disulfide bonds and thus free the protein thiols for reaction with PEG diacrylate (Figure 4.3.a, Lane 10). This is in accordance with the observation from Ellman's assay that after purification and dialysis only about 30% of recombinant protein thiols remained reduced, i.e., capable of conjugate addition to acrylates. TCEP was chosen as a reducing agent, because, in contrast to DTT or β-mercaptoethanol, it does not engage in thiol exchange but is irreversibly consumed in

the process of reducing disulfide-bound thiols. When sufficient TCEP is added, the final reaction product (lanes 5-8), presumably protein[A]-*graft*-hexaPEGacrylate, clearly does not run as one distinct band in 10% polyacrylamide SDS-PAGE. A probable explanation for the occurrence of additional bands is that the DTT present in the SDS-PAGE sample buffer, whose two thiol groups can also react with acrylate groups by conjugate addition, may have crosslinked some protein-*graft*-PEGacrylate molecules, leading to the high-molecular-mass protein band or bands near the very top of the SDS-PAGE separating gel. Thus, these bands likely represent an artifact due to sample preparation. The actual PEGacrylation reaction reaches completion after 15 min (lane 5), as no further change in the reaction products is detectable even after another 45 min (lane 8). It was difficult to verify that the reaction product is fully PEGacrylated protein-*graft*-hexaPEGacrylate or a protein-*graft*-multiPEGacrylate with fewer than six pending PEG acrylate chains. Other predominant products might include protein-*graft*-multiPEGacrylate species with fewer than six pending PEG acrylate chains, as steric hindrance by grafted PEG chains may set a limit to the number of protein thiols that can be PEGacrylated. Nevertheless, proteins PEGacrylated to different degrees may coexist as final products, because the attainable degree of PEGacrylation of a given protein pentamer molecule might even depend on the order in which its six thiols react with PEG diacrylate, or, in fact, on the extent to which some thiols forgo conjugate addition altogether because they engage in intramolecular disulfide bond formation before encountering an acrylate functional group. The exact nature of the (different) protein[A]-*graft*-multiPEGacrylate product species is not so relevant as far as the biological characterization of the eventual protein[A]-*graft*-PEG hydrogels was concerned, as the only two crosslinked matrix components were always protein[A] and PEG.

Figure 4.3.b provides further examples of protein PEGylation reactions by Michael-type conjugate addition of protein thiols to PEG acrylate or vinylsulfone functional groups.

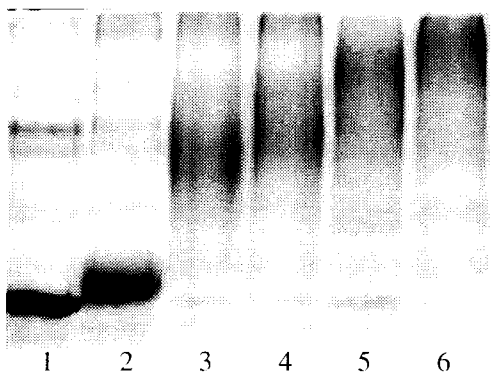

Figure 4.3.b: PEGylation of Protein Pentamer [A] with PEGs of Increasing Molecular Weight

Coomassie-stained 10% polyacrylamide SDS-PAGE gel illustrating the PEGylation of recombinant protein pentamer [A] with a series of PEGs of increasing molecular weight. Lane 1: unreacted protein pentamer [A]. Lane 2: [A] reacted with PEG α,ω-diacrylate, mol. wt. 575. Lane 3: [A] reacted with PEG α,ω-diacrylate, mol. wt. 3400. Lane 4: [A] reacted with PEG α,ω-divinylsulfone, mol. wt. 3400. Lane 5: [A] reacted with PEG α-monoacrylate ω-monomethylether, mol. wt. 5000. Lane 6: [A] reacted with PEG α,ω-diacrylate, mol. wt. 6000.

The 10% polyacrylamide SDS-PAGE gel shown illustrates the increase in molecular weight of recombinant protein pentamer [A] due to PEGylation with a series of PEGs of increasing molecular weight. For instance, while presumed protein[A]-*graft*-hexaPEG(6000)acrylate (mol.wt. 64.5 kDa) and its DTT-crosslinked derivatives ran in SDS-PAGE between ~100 kDa and the top of the separating gel, presumed protein[A]-*graft*-hexaPEG(3400)acrylate (mol.wt. 48.9 kDa) ran at about 60 kDa (lane 3, Figure 4.3.b). Even between presumed protein[A]-*graft*-hexaPEG(6000)acrylate and protein[A]-*graft*-hexaPEG(5000)methylether (mol. wt. 58 kDa; lane 5) a difference in apparent molecular weight can be detected by SDS-PAGE.

Selectivity of Protein PEGylation

One important feature of Michael-type conjugate additions of protein thiols to acrylate functional groups is the high selectivity of this reaction. This is a very desirable feature, because when proteins are modified exclusively via their thiols, primary amine-dependent protein properties and functions may be preserved. Although primary amines of proteins can react with acrylate groups by Michael-type conjugate addition as well, under physiological conditions this reaction is very slow, on the order of hours, whereas thiols react very fast, on the order of minutes.[152,106,159] Because of this highly selective reactivity, Michael-type conjugate addition reactions of protein thiols to suitable conjugated reaction partners are very useful tools for protein modification in general. Additionally, SDS-PAGE was employed as a suitable and straightforward method to monitor protein PEGylation reactions, because the grafting of PEG has a detectable effect on the mobility of proteins in SDS-PAGE.[163]

In the model reactions involving albumin, analysis by SDS-PAGE showed that under physiological conditions almost no reaction was apparent between albumin and PEG-diacrylate, mol. wt. 3400, or between albumin and PEG-dithiol, mol. wt. 3400 (Figure 4.3.c). In particular, Figure 4.3.c.(A) shows that albumin incubated with PEG-diacrylate for 1 hr remained almost entirely unmodified and thus ran virtually identically to native albumin during SDS-PAGE (Figure 4.3c.(A), lane 3 vs. lane 2).

The small smear above the albumin band in Figure 4.3.c.(A), lane 3, may indicate that a small percentage of the protein was modified by PEG-diacrylate. This observation was in stark contrast to the obvious and abundant reaction of PEG-NHS-ester with albumin under physiological conditions (Figure 4.3.c.(A), lane 4), or between PEG-diacrylate and albumin when the albumin was previously reduced and kept under denaturing conditions (Figure 4.3.c.(A), lane 5).

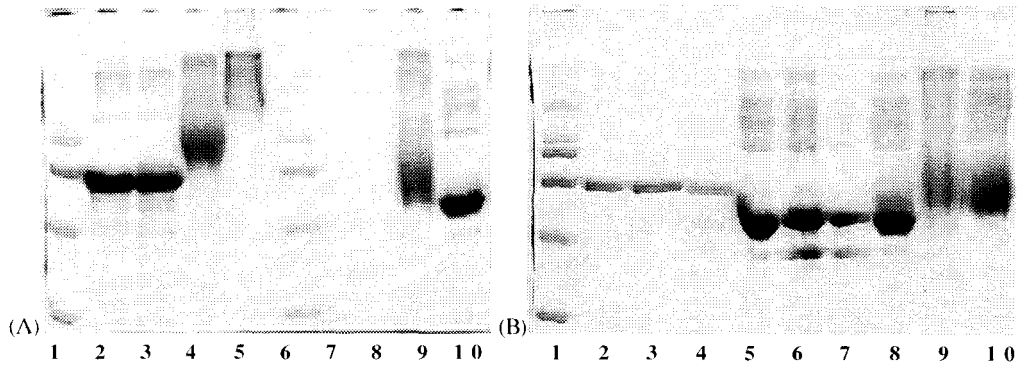

Figure 4.3.c: Reaction Selectivity of Michael-type Conjugate Addition

SDS-PAGE was used to determine the "self-selectivity" of the cross-linking reaction. (A) Lane 1: mol. wt. markers; Lane 2: albumin + running buffer with DTT; Lane 3: albumin + PEG-diacrylate (20 mol PEG/mol albumin) for 1 hr at 37 °C + running buffer with DTT; Lane 4: albumin + PEG-monoacrylate, mono-NHS ester (20 mol PEG/mol albumin) for 1 hr at 37 °C + running buffer with DTT; Lane 5: albumin with 8M urea + reduction with TCEP + PEG-diacrylate (350 mol PEG/mol albumin) for 1 hr at 37 °C + running buffer with DTT; Lane 6: mol. wt. markers; Lane 9: albumin + PEG-dithiol (20 mol PEG/mol albumin) for 1 hr at 37 °C + running buffer without DTT; Lane 10: albumin + running buffer without DTT. It was demonstrated that PEG-diacrylate reacted with albumin only very slowly, if at all (Lane 3), whereas a PEG-NHS-ester reacted rapidly with albumin (Lane 4). Reduction of disulfide bonds in the protein, producing free thiols in the protein, led to rapid reaction of the PEG-diacrylate with the protein (Lane 5). PEG-dithiol initially appeared to react with albumin, presumably by disulfide exchange (Lane 9). However, Figure (B) shows that this was an artifact of sample preparation for gel electrophoresis. (B) Lane 1: mol. wt. markers; Lane 2: albumin + running buffer with DTT; Lane 3: albumin that had been released from a hydrogel made from PEG-tetraacrylate and PEG-dithiol + running buffer with DTT; Lane 4: albumin + acrylic acid (20,000 mol acrylic acid/mol albumin) for 15 min at 37 °C + running buffer with DTT; Lane 5: albumin + running buffer without DTT; Lane 6: albumin + acrylic acid (20,000 mol acrylic acid/mol albumin) for 15 min at 37 °C + running buffer without DTT; Lane 7: albumin + PEG-dithiol (20 mol PEG/mol albumin) for 1 hr at 37 °C + acrylic acid (10,000 mol acrylic acid/mol albumin) for 15 min at 37 °C + running buffer without DTT; Lane 8: albumin + PEG-dithiol for 1 hr at 37 °C + running buffer without DTT; Lane 9: albumin with 8M urea + PEG-dithiol (20 mol PEG/mol albumin) for 1 hr at 37 °C + acrylic acid (10,000 mol acrylic acid/mol albumin) for 15 min at 37 °C + running buffer without DTT; Lane 10: albumin with 8M urea + PEG-dithiol (20 mol PEG/mol albumin) for 1 hr at 37 °C + running buffer without DTT. It was demonstrated that albumin that was released from hydrogels formed from PEG-tetraacrylate and PEG-dithiol was unmodified (Lane 3). Reaction of reduced albumin with acrylic acid did not change the migration of the protein (Lane 4). PEG-dithiol did not react with albumin under physiological conditions, demonstrated by quenching free thiols with acrylic acid before PAGE (Lane 7), which was in contrast with Lane 8 (identical to Lane 9 from Figure (A). The conclusion was that PEG-dithiol does not react with albumin at room temperature, but does react during the boiling step required for SDS-PAGE.

The self-selective chemistry for cross-linking polymers that is described here did not lead to detectable modification of the proteins that were trapped within the cross-linked material. The reaction of the PEG-acrylate with the PEG-dithiol is rapid, but reaction of PEG-acrylate with the free thiol found on bovine serum albumin was not detectable under

cross-linking conditions. It is unknown whether this result is general for other proteins since the single free thiol in albumin is probably relatively inaccessible to the PEG-acrylate due to steric hindrance. Regardless, the number of proteins of interest that would have a free thiol is rather small, and thus this potential side reaction is of little concern.

While the reaction of the acrylate group with amine groups on the protein will occur over a long period of time, we found no evidence that this reaction occurs on the time scale required to cross-link the hydrogel. The lack of reactivity between the PEG derivatives and proteins is not only desirable for the formation of controlled delivery vehicles, but it also implies that the controlled delivery vehicle could be cross-linked in contact with living tissue without modifying proteins found in the tissue.

Purification of Protein-*graft*-PEGacrylates

Returning to protein-*graft*-PEGacrylates, protein pentamer [A]'s and [B]'s Ni^{++}-affinity was not compromised due to the PEGacrylation. Therefore, the removal of unreacted PEG diacrylate from PEGacrylated protein pentamers [A] or [B] was easily accomplished by Ni^{++}-affinity chromatography (Figure 4.4).

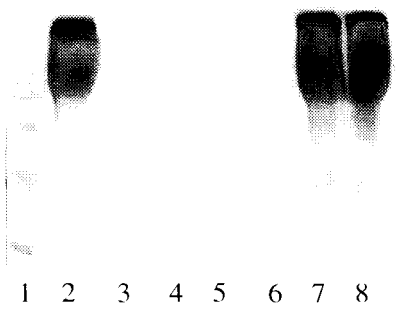

Figure 4.4: Ni^{++}-affinity Purification of Protein[A]-graft-PEGacrylate

10% polyacrylamide SDS-PAGE was used to monitor the purification of protein[A]-*graft*-PEGacrylate by Ni^{++}-affinity chromatography. Coomassie-stained protein[A]-*graft*-PEGacrylate is visible in the sample before purification (lane 2), still containing unreacted excess PEG diacrylate, and in the eluate fractions (lanes 7 and 8).

In two independent Ni^{++}-affinity purifications, the wash fractions (lanes 3 - 6), which had been freeze-dried, contained an amount of PEG diacrylate equal to the expected excess after full PEGylation of protein pentamers [A] or [B]. Furthermore, since large volumes of wash buffer had been used, and PEG is very well soluble in aqueous buffers, the eluate fractions (lanes 7 and 8) were considered to be free of unreacted PEG diacrylate.[3] After dialysis and lyophilization, PEGacrylated protein pentamers [A] or [B] (containing ~10% *(m/m)* D(+)-glucose) were readily soluble up to concentrations of at least 15% *(w+v)* in aqueous buffers as well as in serum-containing media. No spontaneous disulfide bond formation or other solubility problems were encountered with the PEGacrylated pentamers, in agreement with PEG's good solubility and high mobility in water.[128]

---

[3] Also, PEG is unlikely to have any affinity to the Ni^{++}-resin or to the column itself.

Heparin Affinity of Protein[A]-*graft*-PEGacrylate

In the absence of soluble heparin, protein[A]-*graft*-PEG(6000)acrylate was eluted from the heparin-agarose column between salt concentrations of 0.8 - 1.1 M NaCl (Figure 4.5.a).

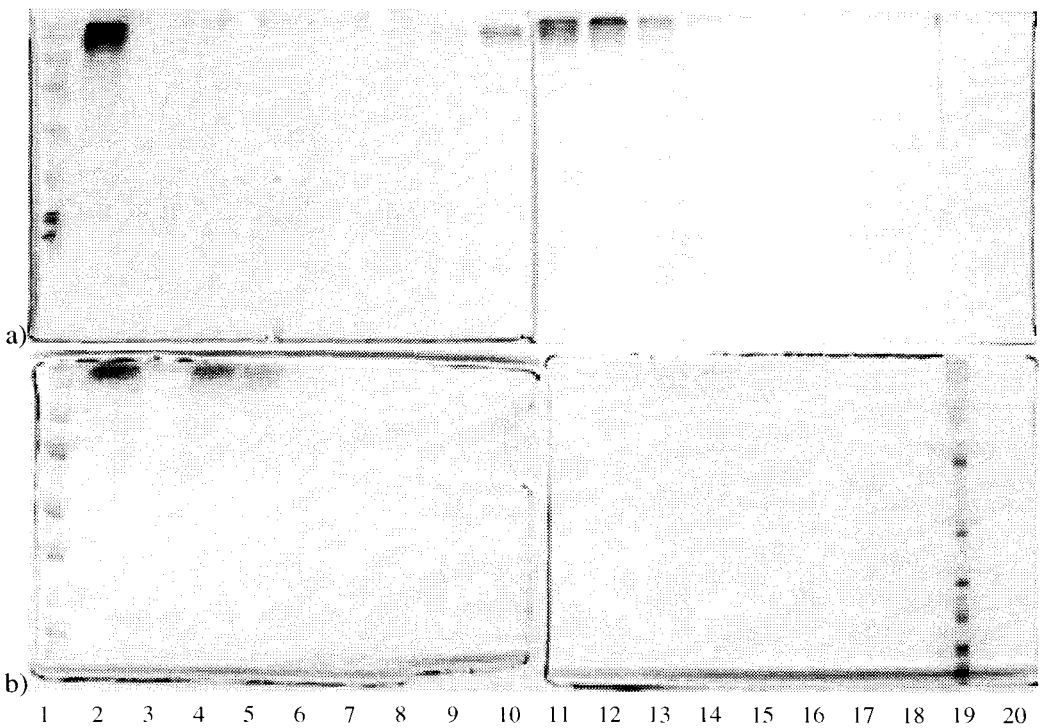

Figure 4.5: Heparin-Agarose Affinity Chromatography With Protein[A]-*graft*-PEGacrylate

20% acrylamide SDS-PAGE gels with 16 µL samples from eluate fractions a) without heparin, b) with the addition of 20 moles of heparin per mole of heparin-binding sites in protein[A]-*graft*-PEGacrylate. Lanes 1: molecular weight marker, 2: sample before chromatography, 3: flow through after initial loading of column with 137 mM NaCl, 4: 137 mM NaCl, 5: 246 mM NaCl, 6: 356 mM NaCl, 7: 466 mM NaCl, 8: 575 mM NaCl, 9: 685 mM NaCl, 10: 794 mM NaCl, 11: 904 mM NaCl, 12: 1014 mM NaCl, 13: 1123 mM NaCl, 14: 1228 mM NaCl, 15: 1342 mM NaCl, 16: 1452 mM NaCl, 17: 1562 mM NaCl, 18: 1671 mM NaCl, 19: a) 1781 mM NaCl, b) mol. weight marker, 20: a) 1890 mM NaCl, b) 1781 mM NaCl. Note in a) the separation into protein[A]-*graft*-PEG acrylates of increasing molecular weight with increasing NaCl concentration of the eluate fractions.

Elution at such high salt concentrations is evidence for the strong affinity of recombinant protein pentamer [A] for heparin, indicating that the heparin binding site was not sterically

hindered by pendant PEG chains. The competing presence of 28.3 mg/mL soluble heparin, corresponding to 20 moles of heparin per mole of heparin-binding sites in the protein pentamer, almost completely inhibited binding of protein[A]-*graft*-PEG(6000)acrylate to the column at 137 mM NaCl (Figure 4.5.b). Protein[A]-*graft*-PEG(6000)acrylate was then eluted entirely from the heparin-agarose column with the next wash of 250 mM NaCl (lane 5). These results confirm the affinity of recombinant protein pentamer [A]'s heparin binding site for heparin.

Confirmation of Acrylate Presence

Fluorescently labeled thiol containing compounds can be used to probe and quantify acrylate functional groups in acrylate containing systems. Here, the didansyl-containing oligopeptide didansyl-KRDGPDGIWGDDRCG-$CONH_2$ reacted readily with PEGacrylated and purified recombinant protein pentamer [A] by Michael-type conjugate addition, as evident from the fluorescence associated with the PEGylated protein pentamer after the 15 min reaction (Figure 4.6). This implies that PEGacrylated protein pentamer [A] and, accordingly, protein pentamer [B] do indeed acquire and retain reactive acrylate termini due to their PEGacrylation.

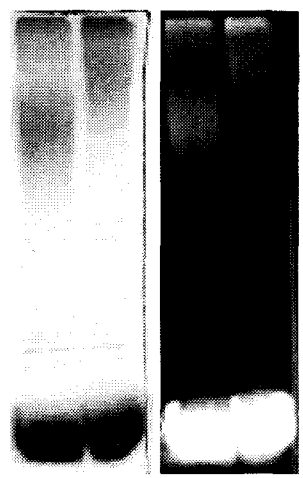

Figure 4.6: Acrylate Presence

Identical Coomassie-stained (left) and UV-exposed (right) 10% polyacrylamide SDS-PAGE gel confirming terminal acrylate viability of protein[A]-*graft*-PEG(3400)acrylate (lane 1) and protein[A]-*graft*-PEG(6000)acrylate (lane 2). Fluorescence associated with the PEGylated protein pentamers is evidence for viable acrylates, which are important for crosslinking of the constructs. Note the fluorescent acrylate probe alone, near the bottom.

Gelation by Photopolymerization and Characterization of Protein-*graft*-PEG Hydrogels

Lyophilized protein[A]-*graft*-PEG(3400)acrylate and protein[A]-*graft*-PEG(6000)acrylate completely redissolved after 1 hr at 4 °C and gelled upon photoinitiation at all concentrations between 5% and 15% *(w+v)* PEGacrylated protein (Figure 4.7).

A) B)

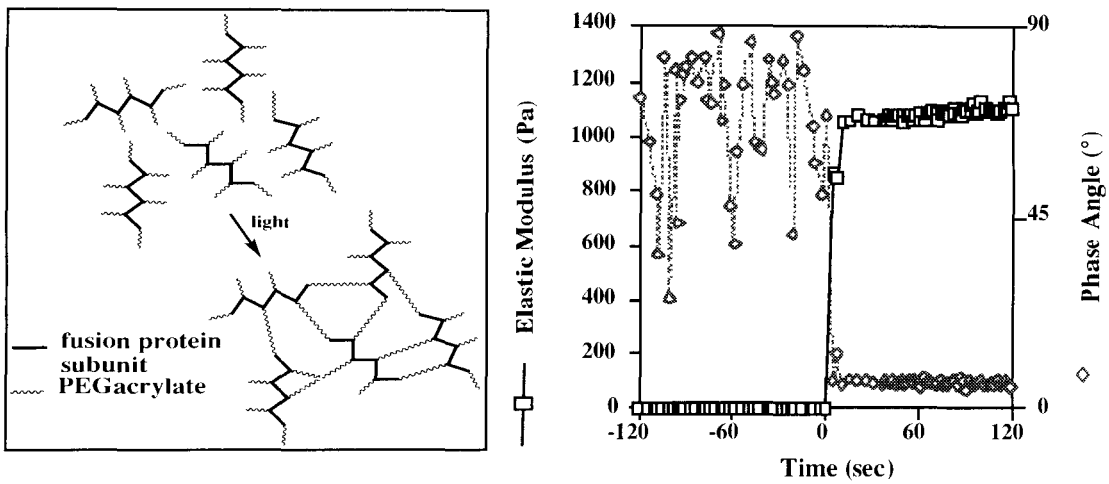

Figure 4.7: Gelation of Protein[A]-*graft*-PEGacrylate

A) Schematic of light-induced gelation of protein[A]-*graft*-PEGacrylate. Note that more than two or three acrylate termini (as shown) can polymerize to crosslink the PEGacrylated protein pentamers.
B) Rheological characterization of light-induced gelation of a 10% *(w+v)* protein[A]-*graft*-PEG(6000)acrylate solution. □ Elastic modulus, G′, (Pa); ◇ Phase angle, δ, (°).

In contrast, at all concentrations that were tested, purified and lyophilized protein[B]-*graft*-PEG(6000)acrylate did not completely redissolve nor gel during irradiation. Recombinant protein [B]'s poor extent of PEGylation as well as its lower net positive charge compared to protein[A]-*graft*-PEG(6000)acrylate explain the poor solubility of protein[B]-*graft*-PEG(6000)acrylate at such high concentrations as up to 15 % *(w/v)*. The poor solubility of protein[B]-*graft*-PEG(6000)acrylate and, consequently, the low concentration of crosslinkable acrylate groups in solution explain the lack of crosslinkability.

The density of crosslinkable acrylate groups in solutions of protein[A]-*graft*-PEG(3400)acrylate as well as –PEG(6000)acrylate were at or above the minimum concentration necessary for gelation. Since concentrations of protein[A]-*graft*-PEG(6000)acrylate less than 10% *(w+v)* produced gels that were of poor mechanical strength, all subsequent experiments were done at a concentration of 10% *(w+v)* PEGacrylated protein. The 10% *(w+v)* hydrogels were homogeneous, firm to the touch of a pipette tip, perfectly transparent, and swelled by up to 200% of their initial mass in PBS, pH 7.4, over 16 h. Rheological characterization of the gelation, shown for protein[A]-*graft*-PEG(6000)acrylate in Figure 4.7, reveals that photoinitiated gelation occurred on the order of a few seconds. Gelation is evident from the crossover of the phase angle, δ, and the elastic modulus (or "storage modulus"), G′, and, in particular, from the rapid leveling of the phase angle to nearly 0, typical for a solid. The phase change from liquid to solid due to gelation is also evident from the rapid increase in the elastic modulus to about 1.2 kPa upon photoinitiation. This corresponds to a Young's modulus ($E_{PEG6000}$) of approximately 3.5 kPa. (Note: $E = 2(1 + \mu)G'$, where μ is Poisson's ratio, assumed to be the ideal value, 0.5, a reasonable assumption for cross-linked gels). Surprisingly, the range of Young's Modulus $E_{PEG6000}$ measured for protein[A]-*graft*-PEG(6000) gels was higher (2.9 – 3.5 kPa) than the measured range of $E_{PEG3400}$ for protein[A]-*graft*-PEG(3400) gels (2.4 – 3.1 kPa), although a higher crosslink density, firmer consistency, and therefore larger $E_{PEG3400}$, was expected for the latter. It may be that the longer tether between the reactive acrylate and the protein backbone allows for more effective polymerization after photoinitiation.

The visible light-induced gelation of protein-*graft*-PEGacrylate solutions occurred at a sufficiently rapid rate under the low intensity of visible light that was utilized, so gelation *in situ* should be feasible in surgical contexts. Moreover, the reaction results in

little heat generation when the acrylate functional groups polymerize at low concentrations (~8.5 mM theoretical acrylates in the case of 10% *(w+v)* solutions of fully PEGacrylated protein[A]-*graft*-PEG(6000), and ~11.3 mM theoretical acrylates in 10% *(w+v)* solutions of fully PEGacrylated protein[A]-*graft*-PEG(3400)).

Plasmin Degradability

Protein[A]-*graft*-PEG(6000) hydrogels incubated with 2 U/ml human plasmin in PBS, pH 7.4, were degraded completely after 3 hrs, whereas pre-swollen hydrogels incubated in PBS without plasmin did not change in size even after 5 days. This shows that one or both of the plasmin degradation sites (↑) in recombinant protein pentamer [A] (Chart 1) are accessible and can be cleaved by human plasmin, even when they are part of a highly crosslinked protein-*graft*-PEG network. The particular human fibrinogen sequence in protein[A]-*graft*-PEG hydrogels preserved its enzymatic degradability although it was fused with other protein fragments, was produced in a bacterial expression host, did not exist in its native three-dimensional shape and environment, and was part of a partially synthetic matrix with poly(ethylene glycol).

CONCLUSION

Initial design objectives were met by the "selective" grafting of PEG diacrylate to recombinant protein pentamer [A] to obtain protein[A]-*graft*-PEG(3400)acrylate and –PEG(6000)acrylate. These compounds were subsequently gelled successfully by photopolymerization to obtain protein[A]-*graft*-PEG hydrogels, which were transparent (allowing future microscopic analysis of three-dimensional cell cultures), had promising mechanical strength to support ingrowth of cells toward applications in tissue regeneration, and which were plasmin degradable. Especially bulk plasmin degradability was an

important indication that the design objective of an enzymatically degradable matrix had been fulfilled, in which cells might specifically degrade the material in synchrony with cellular migration. The results presented in Chapter 5 further illustrate the successful implementation of relevant biological features into these artificial matrices and the promise of tissue repair and wound healing that these novel materials represent.

CHAPTER 5

INTERACTIONS OF hFFs WITH RECOMBINANT PROTEIN PENTAMERS AND PROTEIN[A]-*graft*-PEG HYDROGELS

INTRODUCTION

hFF-Fibrin Clusters as a Model for Tissue Regeneration

Cell migration from the periphery into the core of an implanted matrix and simultaneous resorption of the matrix are desirable features of a material intended for tissue repair and regeneration. To test protein[A]-*graft*-PEG hydrogels *in vitro* regarding this intended role, it was necessary to juxtapose the matrices to native tissue or a model of living tissue. The intention was to see if cellular invasion would occur from the tissue into the artificial hydrogels. Fibroblasts were chosen as a model cell type in light of their ease of handling in tissue culture as well as their important role in wound healing. *In vivo*, fibroblasts near the site of an injury are among the first cells to invade and reorganize the fibrin clot that initially forms in a wound.

To avoid using tissue explants and to evaluate the behavior of a single cell type, a relatively easy encapsulation system was developed by Pratt *et al.*, 2001,[126] to test fibroblast migration into a material of interest. hFFs were first embedded in fibrin at high concentration, and the resulting hFF-fibrin clusters then embedded in self-forming hydrogels (see details in Chapter 2). In Pratt *et al.*'s system, hFFs migrated out of and away from the region of high local cell concentration into the unpopulated and proteolytically degradable surrounding material, driven by fibroblasts' innate mobility and cell-associated protease activity.

Inspired by the elegance and ease of this assay to model tissue regeneration, Pratt *et al.*'s "fibrin drop assay" was also used in this work to evaluate cells' interaction with protein-*graft*-PEG hydrogels under various culture conditions.

MATERIALS AND METHODS

General Notes

Well established techniques[147] were used for cultures of neonatal human foreskin fibroblast (hFFs, Clonetics(Cambrex) via BioWhittaker Europe, Belgium) of passage numbers up to 14. Unless otherwise noted, hFFs were cultured in Dulbecco's Modified Eagle Medium (DMEM, with 1000 mg/L glucose, 110 mg/L sodium pyruvate, 862 mg/L L-alanyl-L-glutamine) supplemented with 10% *(v/v)* heat-inactivated fetal bovine serum and 1X antibiotic-antimycotic (all Life Technologies, Scotland).

Nickel-Affinity Surface Coating and Cell Adhesion Experiments

By placing 100 µL of the appropriate coating solution (PBS, pH 7.9, with 8 M urea) per well, protein pentamers [A] or [B] adsorbed to Ni-NTA HisSorb 96-well plates (Qiagen) from solutions of the following concentrations: 0, 12.4, 24.8, 31, 37.2, 43.4, 49.6, and 62 µg/mL for protein [A] and 0, 10.8, 21.6, 27, 32.4, 37.8, 43.2, and 54 µg/mL for protein [B]. Binding of protein to the Ni^{++}-coated well surfaces occurred over night at room temperature under gentle shaking. After rinsing twice with PBS containing 8 M urea to remove unbound protein, and twice with PBS to remove the urea, the 96-wells were blocked with bovine serum albumin (Fraction V, Sigma A-9418, Switzerland) (3% *m/v* albumin in PBS, 100 µL/well, 2 hrs, 37 °C). After rinsing twice with PBS to remove any non-adsorbed albumin, 10000 hFFs were seeded per 96-well in serum-free cell culture medium and incubated at 37 °C, 5% CO_2, ~80% relative humidity for 1 hr. Cultures were terminated, and cells fixed, by gradual and careful exchange of the culture medium with formalin solution (10%, neutral buffered, Sigma). After 15 min of fixing, adherent hFFs were stained with Crystal Violet Stain (4.8 mg/mL Crystal Violet (Merck, Germany) and

1.6 mg/mL NaCl in 33% ethanol, 1.12% formaldehyde) for 5-10 min, thoroughly rinsed with deionized H_2O, and air-dried prior to microscopic analysis. Microscopy and image processing were performed using a Zeiss inverted confocal light microscope (Axiovert 135, Zeiss, Germany) in conjunction with a Hamamatsu Color Chilled 3CCD Camera (Hamamatsu, Japan) and LeicaQWin image processing software (Leica Imaging Systems Ltd., 1997). Matrox Inspector 3.0 software (Matrox Electronic Systems Ltd., Dorval, Canada) was used to count the hFFs.

Ni-NTA HisSorb 96-wells were coated with protein pentamer [A], from a solution of 0.6 mg/mL, for competitive inhibition studies with soluble adhesion ligand, oligopeptide GRGDSP (soluble RGD, Calbiochem, USA), and for inhibition studies with heparin (from porcine intestinal mucosa, MW 16,000 - 18,000, 181 USP units/mg, Sigma H-9399, Germany). Serum-containing cell culture media with soluble RGD were prepared at concentrations of 0, 0.3, 3, 15, 30, 58, 110, 150, 190, 230, 270, and 300 μM soluble RGD. Similarly, cell culture media with heparin were prepared at concentrations of 0, 3, 6, 30, 60, 600, 6000, and 60000 nM heparin by consecutive dilution.

For all sets of data, at least two independent experiments, carried out in duplicate or triplicate, were performed and analyzed.

Embedding and Culture of hFF-Fibrin Clusters Inside Protein-*graft*-PEG Hydrogels

Near-confluent cultures of hFFs were trypsinized (Trypsin-EDTA: 0.5 g/L trypsin, 0.2 g/L EDTA, Life Technologies), centrifuged (700 g, 3 min, room temp.), and resuspended in 2% *(m/v)* fibrinogen from human plasma (Fluka, Switzerland) in sterile PBS to a concentration of 30000 hFFs/μL. To induce gelation of the hFF-fibrinogen suspension, thrombin (Sigma T-6884, Switzerland) and Ca^{++} were added to final concentrations of 2 NIH units/mL and 2.5 mM, respectively, and rapidly mixed with the

cell suspension. Prior to gelation, 2 µL droplets containing approximately 60000 hFFs each were quickly transferred to Sigmacote®-coated (Sigma, USA) microscope slides, on which gelation of the hFF-fibrin clusters was allowed to reach completion in a humidified atmosphere at 37 °C for 20 min. The hFF-fibrin clusters were embedded inside 30 µL protein-*graft*-PEG hydrogels by placing up to four of the clusters into a 30 µl volume of 10% *(w+v)* protein-*graft*-PEGacrylate solution on the bottom of a 12-well tissue culture plate.[14,15,169] Crosslinking of the protein-*graft*-PEGacrylate around the hFF-fibrin clusters was induced *in situ* by exposure to the portable light source through the culture well lid. The hFF-fibrin clusters, thus embedded inside the protein-*graft*-PEG hydrogels, were then cultured in the 12-well tissue culture plates after covering each gel with 1.5 mL serum-containing DMEM. For inhibition studies wth heparin, or heparin and soluble, linear RGD peptide, cell culture media with heparin from porcine intestinal mucosa (MW 16,000-18,000, 181 USP units/mg, Sigma H-9399, Germany) were prepared at concentrations of 0, 10, 100, and 500 µg/mL heparin by consecutive dilution. For inhibition studies with additional soluble, linear peptide GRGDSP (solRGD, Novabiochem), cell culture media with solRGD and heparin were prepared at concentrations of 0, 10, 100, and 500 µg/mL heparin and constant 500 µM solRGD each. During inhibition studies, the respective inhibitor concentrations were maintained for four days by daily exchanges of the cell culture medium with freshly prepared medium at the original inhibitor concentrations. Starting on day 5, however, the culture was continued with serum-containing DMEM alone. For competitive inhibition studies with cyclic RGD peptide, cell culture media with soluble cyclo(Arg-Gly-Asp-D-Phe-Val) peptide (cyclic RGDFV, Calbiochem, USA) were prepared at concentrations of 0, 7.2, 28.7, and 143.4 µM peptide by consecutive dilution, followed by pH adjustment with 1 N NaOH (negligible volumes). For inhibition studies

with aprotinin, a serine-protease inhibitor, cell culture media with bovine lung aprotinin (Calbiochem, USA) were prepared at concentrations of 0, 5, 20, and 50 μg/mL aprotinin. During inhibition studies, the respective inhibitor concentrations were maintained by daily exchanges of the old cell culture medium with freshly prepared medium at the original inhibitor concentrations.

To measure the cell outgrowth from hFF-fibrin clusters into the surrounding protein-*graft*-PEG hydrogels, the clusters were imaged and recorded with their center plane in focus. To quantify the penetration depth of the outgrowth, the area of the original hFF-fibrin cluster was measured in the center plane, as was the area of the hFF outgrowth, defined by the tips of the hFF branches in the center plane of focus. These two areas were approximated as circular areas, and their theoretical radii subtracted from each other to give an average hFF outgrowth length. To quantify the number of outgrowing hFF branches (hFF outgrowths), the perimeter of a cell cluster was measured in its center plane, and the number of hFF branches emerging from this perimeter were counted. Dividing one by the other gave the number of hFF outgrowths per 100 μm perimeter length.

For all sets of data, at least two independent experiments, carried out in duplicate or triplicate, were performed and analyzed.

RESULTS AND DISCUSSION

Cell Adhesive Properties of Recombinant Protein Pentamers [A] and [B]

Figure 5.1 reveals that hFFs adhered to surface-immobilized protein pentamer [A] in a concentration dependent manner. Microscopy (Figure 5.1.A) further revealed an obvious enhancement in the degree of hFF spreading with increasing coating concentration of protein pentamer [A]. In contrast, hFF adhesion to surface-immobilized protein pentamer [B] remained at background levels at all coating concentrations (Figure 5.1.B).

These results suggest that the RGD motifs in recombinant protein pentamer [A] have specific integrin-binding capability and, thus, mediate the observed cellular adhesion and spreading. Recombinant protein pentamer [B], in which the RGD motif was changed to RGG, does not support specific hFF adhesion, as expected for this loss-of-function mutation.

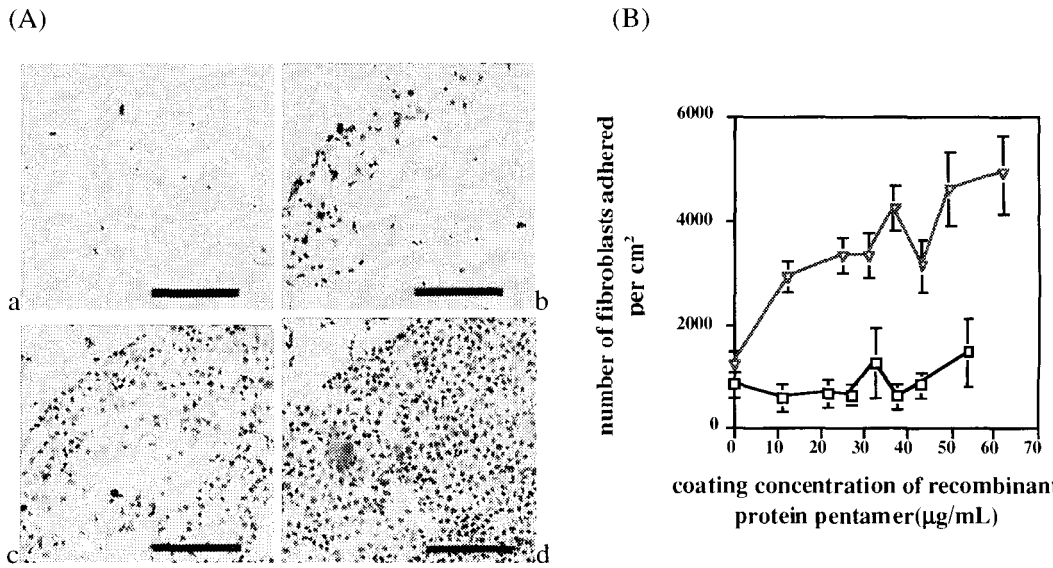

Figure 5.1: hFF Adhesion to Protein Pentamers

(A) hFF adhesion after 1 h to surface-immobilized protein pentamer [A] on circular Ni^{++}-patterns in serum-containing medium. Coating concentrations: a) 0 µg/mL, b) 5 µg/mL, c) 20 µg/mL, d) 40 µg/mL protein pentamer [A]. (Scale bar = 500 µm) Note the enhanced cell spreading with increasing coating concentration.

(B) Human fibroblast adhesion to surface-immobilized protein pentamers. ∇ Number of fibroblasts adhered to surfaces with recombinant protein pentamer [A]. □ Number of fibroblasts adhered to surfaces with recombinant protein pentamer [B]. Both in serum-free cell-culture medium.

When soluble, linear GRGDSP peptide (soluble RGD) was added to the culture medium of wells coated with recombinant protein pentamer [A] and blocked with BSA, hFF adhesion to surface-immobilized protein pentamer [A] was competitively inhibited with a half-inhibition concentration (IC_{50}) of about 85 µM soluble RGD (Figure 5.2). This

observation is further evidence for the specific biological activity of recombinant protein pentamer [A]'s RGD-motif as a ligand for cellular integrin receptors.

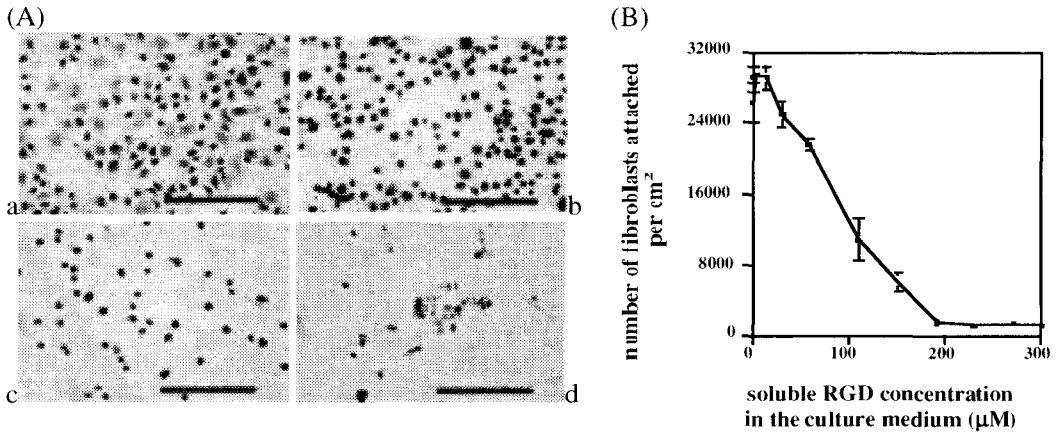

Figure 5.2: Competitive Inhibition of hFF Adhesion to Recombinant Rrotein Pentamer [A]

(A) Competitive inhibition of hFF adhesion to surface-immobilized protein pentamer [A] by solRGD in serum-containing medium. a) 0 μM, b) 75 μM, c) 150 μM, d) 300 μM sol RGD. (Scale bar = 200 μm) (B) Competitive inhibition of hFF adhesion to recombinant protein pentamer [A] as a function of soluble RGD concentration in serum-containing medium. Number of fibroblasts attached per cm^2 surface area coated with 0.6 mg/mL recombinant protein pentamer [A].

When heparin was added to the culture medium of wells coated with recombinant protein pentamer [A] and blocked with BSA, hFF adhesion to surface-immobilized protein pentamer [A] was inhibited with an IC_{50} of about 3 nM heparin, and hFF attachment was suppressed to background levels at 30-60 nM heparin (Figure 5.3).

Thus it could be that, in accordance with protein pentamer [A]'s strong affinity for heparin, which was shown by heparin-affinity chromatography as described above, heparin (MW 16,000 – 18,000) bound to the surface-immobilized protein pentamers' heparin-binding sites, and sterically hindered access of cell-surface integrins to the protein pentamers' RGD adhesion sites, as integrin binding would otherwise have enabled cell adhesion to the surface. It could also be that, in the conformation in which the RGD in the protein pentamer [A] is presented, both integrin receptor binding and binding of cell-surface heparan sulfate proteoglycans are required simultaneously for effective cell adhesion; our data cannot distinguish between the two possibilities.

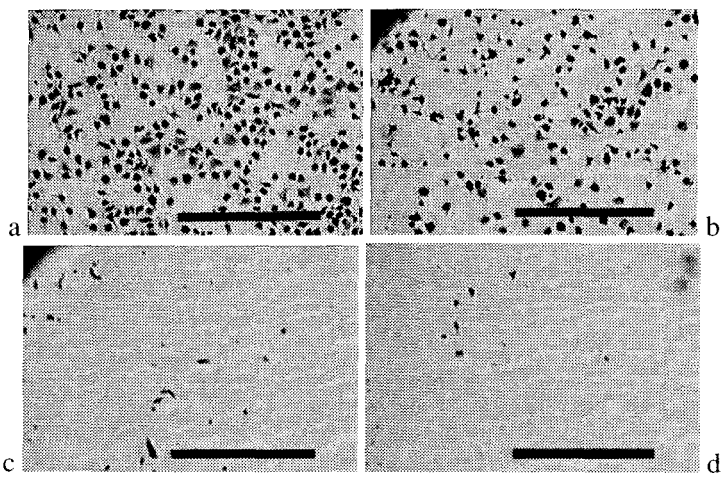

Figure 5.3: Adhesion Inhibition by Heparin

Inhibition of hFF adhesion to surface-immobilized protein pentamer [A] by heparin in serum-containing medium. a) 0 nM, b) 3 nM, c) 30 nM, d) 60 nM heparin. (Scale bar = 500 μm)

hFF Outgrowth Into Hydrogel Matrix

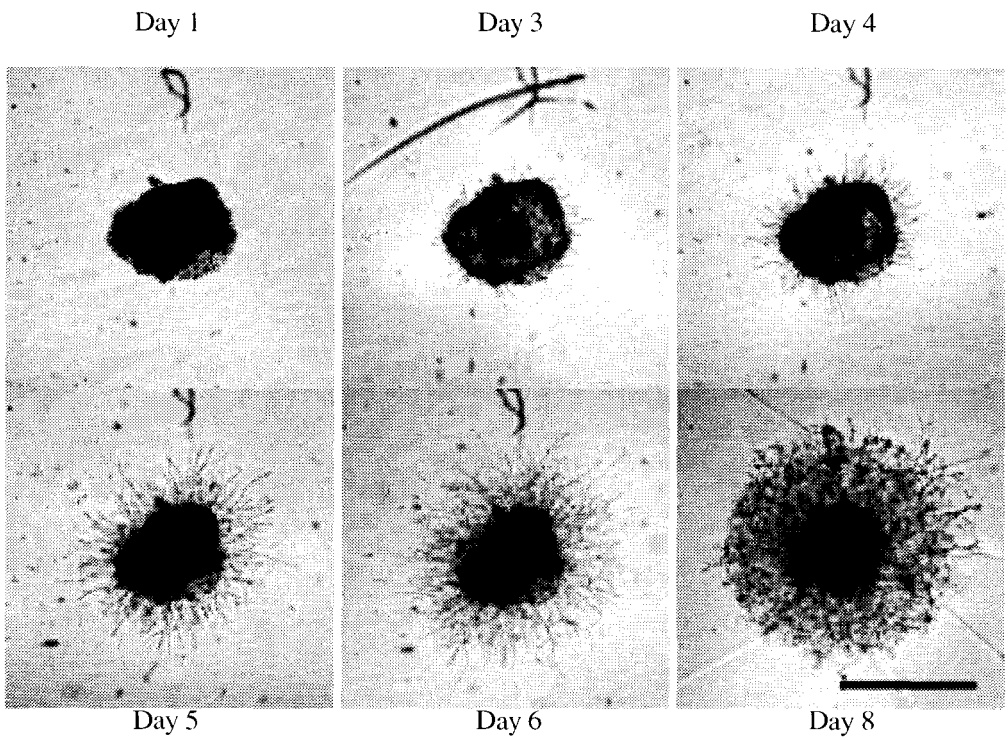

Figure 5.5: Three-Dimensional hFF Outgrowth
Three-dimensional hFF migration and apparent proliferation in a protein[A]-*graft*-PEG(6000) hydrogel. Culture days 1, 3, 4, 5, 6, 8. (Scale bar = 750 μm)

Figure 5.5 illustrates that hFFs embedded in fibrin on day 1, started to migrate three-dimensionally into the surrounding protein-*graft*-PEG hydrogel matrix after two days (day 3). The hFFs assumed an extended and branched morphology as they migrated into the gel materials, and this outgrowth occurred in both protein[A]-*graft*-PEG(3400) and –PEG(6000) hydrogels (Figure 5.6). The highly branched nature of the hFF outgrowths suggests a proliferative mode of matrix penetration, i.e., simultaneous migration and proliferation, because to account for the abundance of cells, too many cells would have had to follow from the fibrin bed if no proliferation had occurred along with branching and further outgrowth.

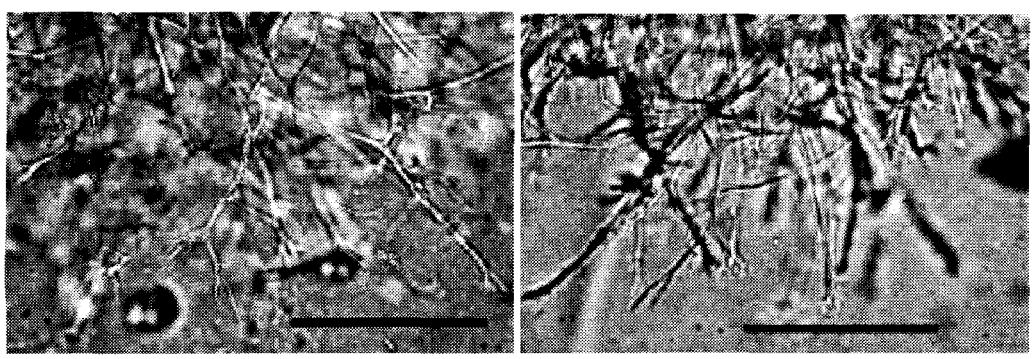

Figure 5.6: hFF Morphology and Proliferative Penetration Inside Protein-*graft*-PEG Hydrogels

Three-dimensional hFF morphology in protein[A]-*graft*-PEG(3400) and -PEG(6000) hydrogels on culture day 8. The highly branched nature of the hFF outgrowths suggests that the cells engaged in a proliferative mode of penetration, i.e., simultaneous migration and proliferation. (Scale bar = 100 μm)

When individual hFFs were separated from their fibrin bed during placement into the protein-*graft*-PEG solution prior to gelation, these individual cells also started to migrate through the hydrogel matrix (Figure 5.7) and connect with neighboring cells in their proximity (Figure 5.8).

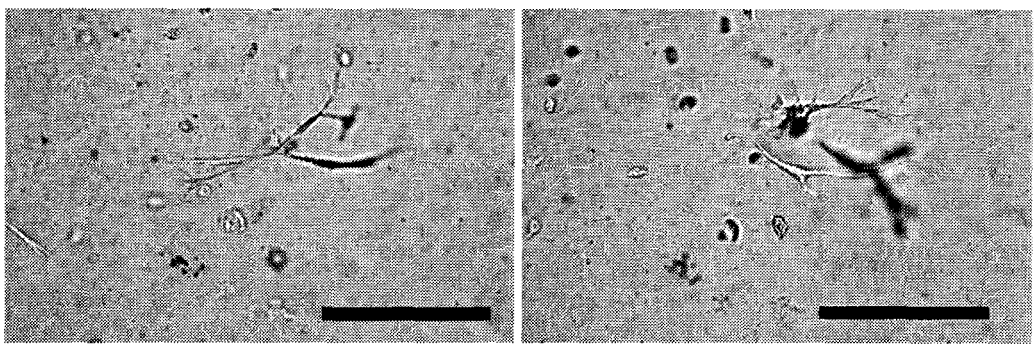

Figure 5.7: Three-Dimensional Migration of Individual Cells

Individual hFFs migrating three-dimensionally in a protein[A]-*graft*-PEG(6000) hydrogel, as seen in identical internal hydrogel sections shown on culture days 6 and 7. However, as can be seen, not many cells survived when separated from the fibrin bed, or each other, during placement into protein-*graft*-PEG hydrogels. (Scale bar = 100 μm)

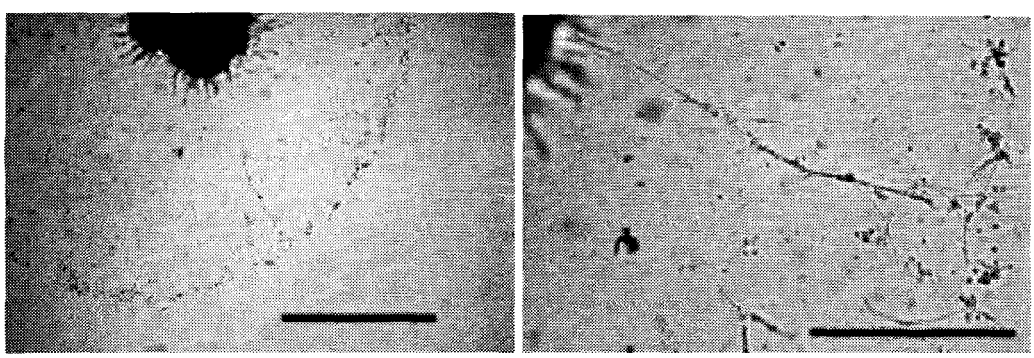

Figure 5.8: hFFs Forming Three-Dimensional Intercellular Connections

hFFs initially separated from the fibrin bed re-connected with cells in the hFF-fibrin cluster or other individual cells (culture day 5). (Scale bars = 1mm, 200 μm)

hFF outgrowth from the fibrin bed as well as apparent proliferation (Figure 5.9), proceeded for 5-7 days, after which the combined effects of potential bulk hydrolysis of the hydrogel (at the acrylate esters), proteolysis, and the increasing inward tension caused by the hFFs led to the concentric collapse of the cellular outgrowth (Figure 5.5, day 8).

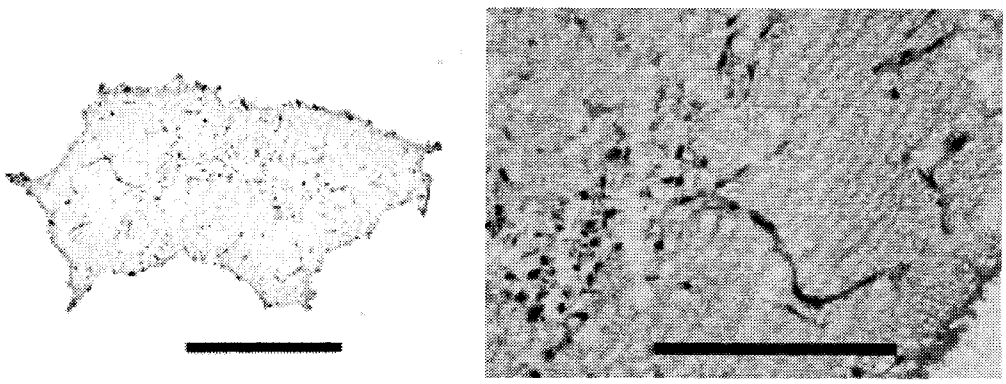

Figure 5.9: Apparent Cell Divisions Inside Protein-*graft*-PEG Hydrogels

Entire histological section of a hFF-fibrin cluster (left) and partial close-up (right) with surrounding protein-*graft*-PEG hydrogel showing apparent cell divisions at high magnification. Note the high density of the protein-*graft*-PEG hydrogel that hFFs were invading. (Scale bars = 500 μm, 200 μm)

The inward tension exerted by the hFFs was so strong that in some cases sections of the hydrogels near edges of cellular outgrowth started to fold back upon themselves (images not show). Note, for instance, the folds and furrows visible on the hydrogel surface on day 8 (Figure 5.5) as the cell outgrowth collapses. After days 10-14, when the hydrogels had been completely degraded by bulk hydrolysis and/or proteolysis, the hFFs formed perfect spheres of cells (Figure 5.10.a), which were larger than the original hFF-fibrin clusters, further supporting the conclusion that hFFs did indeed proliferate in the system. hFFs survived near the surface of the spherical cluster for at least ten more days, as evident from hFF migration from the sphere's surface to the underlying tissue culture plastic (Figure 5.10.b).

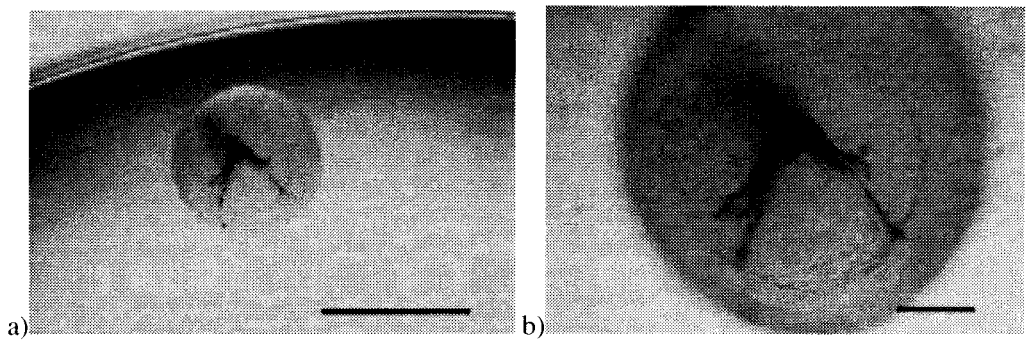

Figure 5.10: Dense hFF Sphere Formation

hFF-sphere (left) and partial close-up (right) after degradation of the surrounding protein-*graft*-PEG hydrogel on cluture day 17. hFF spheres consisted of necrotic areas near the center and viable cells near the surface as evident from hFFs that migrated from the sphere's surface onto the underlying TCPS. (Scale bars = 1 mm, 200 µm)

Comparison of the outgrowth from hFF-fibrin clusters into surrounding protein[A]-*graft*-PEG(3400) and –PEG(6000) gels (Figure 5.11) underlines the importance of mechanical strength for sustainable cell outgrowth. Protein[A]-*graft*-PEG(3400) gels most likely have a higher crosslink density than –PEG(6000) gels (with ~11.3 mM vs. ~8.5 mM theoretical acrylate groups, respectively), even though their Young moduli, $E_{PEG3400}$ = 2.4 – 3.1 kPa and $E_{PEG6000}$ = 2.9 – 3.5 kPa, do not seem to differ greatly. Nevertheless, hydrolytic and/or proteolytic bulk degradation led to a faster loss of mechanical properties and a sooner collapse of cell outgrowth in protein[A]-*graft*-PEG(6000) hydrogels than in –PEG(3400) hydrogels. Initial outgrowth of hFFs

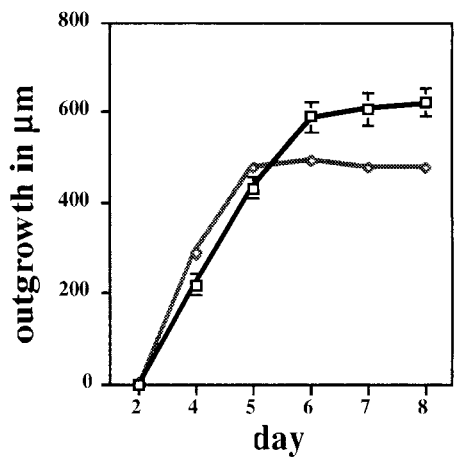

Figure 5.11: hFF Outgrowth in Protein[A]-*graft*-PEG(3400) and -PEG(6000) Hydrogels

□ hFF outgrowth (in µm) in protein[A]-*graft*-PEG(3400) hydrogels, ◇ hFF outgrowth (in µm) in protein[A]-*graft*-PEG(6000) hydrogels.

was only slightly faster in the protein[A]-*graft*-PEG(6000) gels, possibly because their lower crosslink density permitted faster enzymatic degradation by advancing hFFs and, therefore, enabled faster cell migration.

Inhibition of Three-Dimensional hFF Outgrowth by Heparin and solRGD (linear) in Protein-*graft*-PEG Hydrogels.

When only heparin was added to cultures of hFFs inside protein-*graft*-PEG hydrogels, complete inhibition of three-dimensional outgrowth occurred at a concentration of 500 μg/mL heparin, while virtually uninhibited outgrowth was still observed at 100 μg/mL heparin (Figure 5.12 and Figure 5.13.A.c). In contrast, in the presence of 300 μg/mL solRGD peptide, significant inhibition ($p \leq 0.021$) of hFF outgrowth by heparin already occurred at 10 μg/mL heparin (Figure 5.12 and Figure 5.13.B.b).

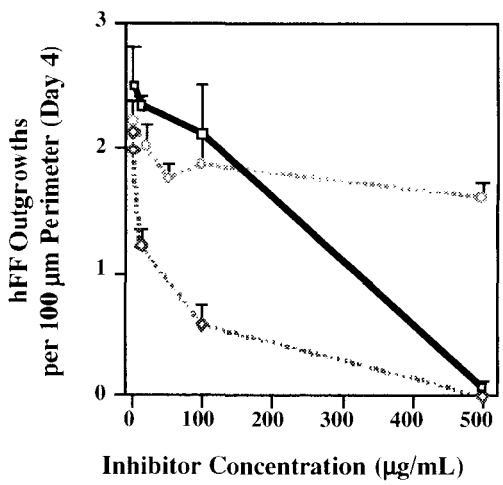

Figure 5.12: Inhibition of hFF Outgrowth

Inhibition of three-dimensional hFF outgrowth by solRGD peptide [circle], heparin alone [square], and heparin plus constant 300 μg/mL solRGD peptide [diamond].

In cultures where complete inhibition of hFF outgrowth by heparin or heparin plus solRGD peptide had occurred, the hFF clusters contracted dramatically, leaving a void volume that had initially been filled by the original hFF-fibrin clusters (Figure 5.13.A.d and 5.13.B.c,d).

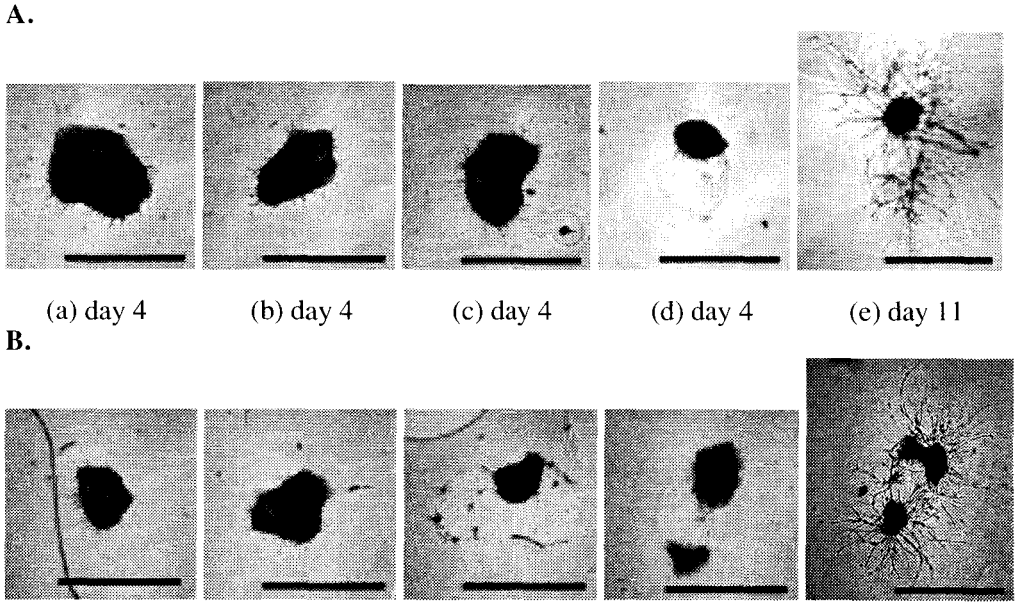

Figure 5.13: Inhibition of hFF Outgrowth by Heparin and solRGD Peptide

Inhibition by heparin and solRGD peptide of outgrowth from hFF-fibrin clusters into surrounding protein-*graft*-PEG hydrogels, shown on day 4. A: a) 0 μg/mL, b) 10 μg/mL, c) 100 μg/mL, d) 500 μg/mL heparin alone.
B: all with 300 μg/mL solRGD and a) 0 μg/mL, b) 10 μg/mL, c) 100 μg/mL, d) 500 μg/mL heparin. A and B: e) same cluster as d), after six more days of culture without inhibitors

By day eleven, i.e., after six days of culture in the absence of inhibitors heparin and solRGD peptide, abundant outgrowth occurred even from hFF clusters whose outgrowth had been completely inhibited until day 4 (Figure 5.13, day 11). This proves that inhibition of outgrowth and contraction of the hFF clusters was not due to toxicity and cell death. Instead, at 500 μg/mL heparin, so much heparin was binding to the heparin-binding sites in the hydrogel matrix that all cellular adhesion to the matrix was blocked, and cell-cell adhesions became so dominant for lack of adhesion to the surrounding hydrogel that the hFF clusters contracted so dramatically. At high concentrations, therefore, heparin alone not only seems to block cell-surface proteoglycan binding to the hydrogel matrix, but also seems to mask, or sterically hinder access by cell-surface integrins to, the RGD sites present in the hydrogel matrix. When 300 μg/ml solRGD peptide are present in the

system, much lower concentrations of heparin are necessary to achieve inhibition of hFF outgrowth, because solRGD competitively inhibits integrin-mediated cell attachment to the hydrogel matrix. However, solRGD alone does not completely inhibit hFF outgrowth up to concentrations of 500 µg/ml (850 µM) solRGD. The cooperative effect of heparin seems to be necessary to mask a sufficient number of integrin-binding sites in the matrix in addition to blocking proteoglycan-mediated cell adhesion. Although it was previously shown that only 143.4 µM of a cyclic RGD peptide (cyclo RGDFV), which blocks integrin-binding much more strongly [170], [171], completely inhibited three-dimensional hFF outgrowth in identical protein-*graft*-PEG hydrogels, it is not surprizing that linear solRGD did not fully inhibit outgrowth even at 850 µM, considering that the concentration of RGD motifs in a 10% (*w*+*v*) protein-*graft*-PEG hydrogel is about 4000 µM (after 200% swelling). While the presence of solRGD evidently augmented the inhibitory effect of heparin on hFF outgrowth in protein-*graft*-PEG hydrogels, masking or sterical hindrance by heparin was necessary to render solRGD sufficiently inhibitory at all. By varying the concentrations of, both, heparin and solRGD, it might be possible to find concentrations of solRGD peptide that are competitively inhibitory to hFF outgrowth at only minimal concentrations of heparin. However, small concentration of heparin bound to heparin-binding sites in the hydrogel matrix might initially promote cell attachment and outgrowth, as heparin can immobilize cell-secreted growth factors and extracellular matrix proteins in the hydrogel which might provide additional adhesion sites and trophic stimuli favorable to cell migration, matrix penetration and, thus, three-dimensional outgrowth.

Competitive Inhibition of hFF Outgrowth by Cyclic RGDFV Peptide

When cyclic RGDFV was added to the cell culture medium, cyclic RGDFV-concentration dependent inhibition of cell outgrowth from hFF-fibrin clusters into the surrounding protein-*graft*-PEG matrix was observed (Figure 5.14).

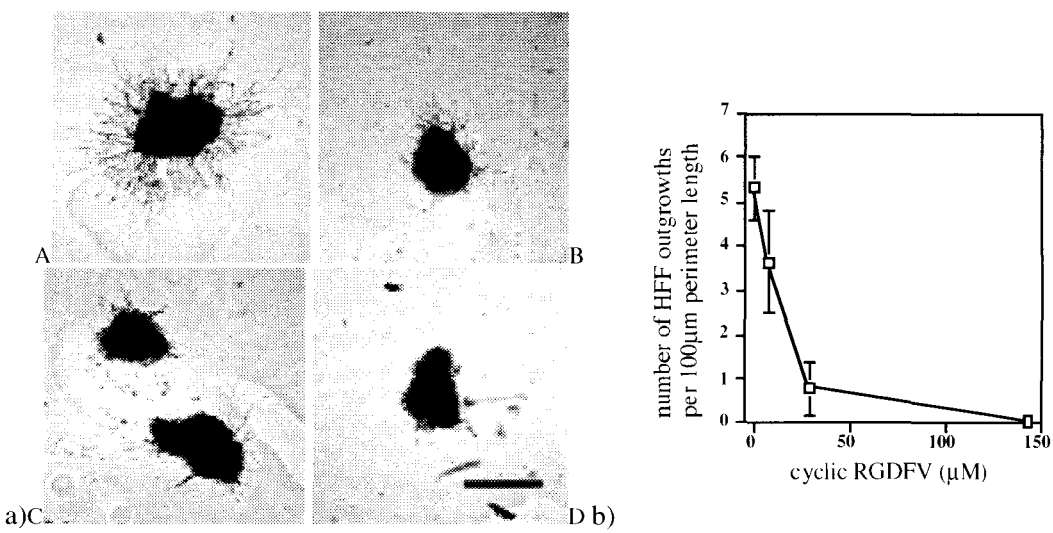

Figure 5.14: Inhibition of hFF Outgrowth by Cyclic RGDFV.

a) Representative images of outgrowth from hFF-fibrin clusters into protein[A]-*graft*-PEG hydrogels on day 5 in the presence of A) 0 µM, B) 7.2 µM, C) 28.7 µM, D) 143.4 µM cyclic RGDFV in serum-containing media. (Scale bar = 500 µm)
b) Amount of hFF outgrowth as a function of cyclic RGDFV concentration measured in terms of cell outgrowths per 100 µm perimeter length of the original hFF-fibrin cluster.

Both the abundance of hFF outgrowth as well as hFF penetration depth into the surrounding protein-*graft*-PEG hydrogel was dramatically decreased with an IC_{50} of about 20 µM cyclic RGDFV, and outgrowth was completely suppressed at maximally 143 µM cyclic RGDFV (Figure 5.14.b). Analogous to competitive inhibition of cell adhesion to surface-immobilized protein pentamer [A] (Figure 5.2) with soluble RGD peptide, cyclic RGDFV potently blocks cell-surface expressed integrins[170-171] and thus, even in three-dimensional culture, competitively prevented their binding to RGD sites in the protein-

graft-PEG matrix. This suggests that in the case of uninhibited outgrowth within protein-*graft*-PEG hydrogels, RGD-mediated integrin binding was indeed a relevant and, in fact, necessary mode of hFF attachment to the protein-*graft*-PEG hydrogels, as had been intended by the original material design by the incorporation of RGD adhesion sites into the protein-*graft*-PEG matrix. Binding of cell-surface proteoglycans to the heparin-binding sites in the matrix might also have contributed to hFF attachment and migration, but without RGD-mediated integrin binding, proteoglycan-based binding was not sufficient to sustain hFF outgrowth in the protein-*graft*-PEG hydrogels.

Inhibition of hFF Outgrowth by Aprotinin, a Serine-Protease Inhibitor

When bovine lung aprotinin was added to the cell culture medium, aprotinin-concentration dependent inhibition of cell outgrowth from hFF-fibrin clusters into the surrounding protein-*graft*-PEG matrix was observed (Figure 5.15.a,b).

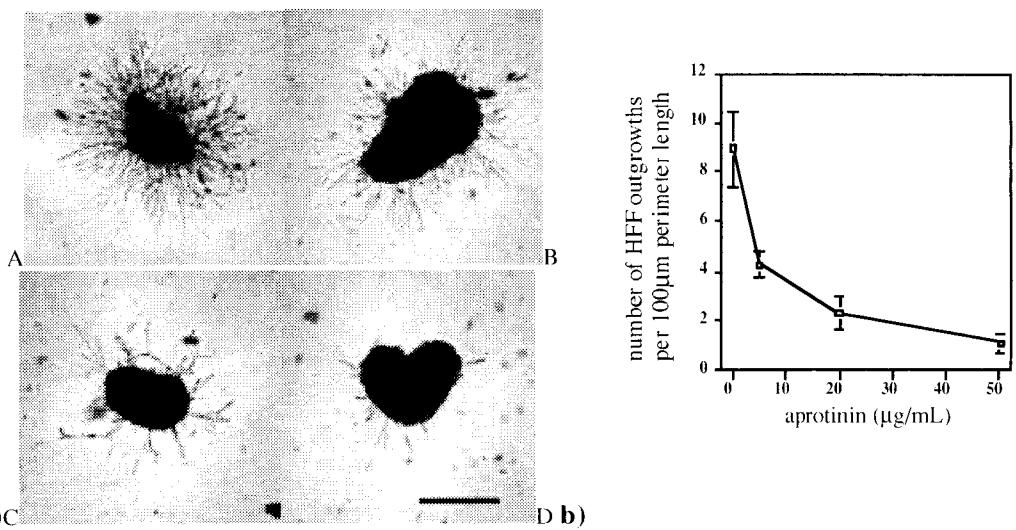

Figure 5.15: Inhibition of hFF Outgrowth by Aprotinin

a) Representative images of outgrowth from hFF-fibrin clusters into protein[A]-*graft*-PEG hydrogels on day 6 in the presence of A) 0 µg/mL, B) 5 µg/mL, C) 20 µg/mL, D) 50 µg/mL aprotinin in serum-containing media. (Scale bar = 500 µm)

b) Amount of hFF outgrowth as a function of aprotinin concentration measured in terms of cell outgrowths per 100 µm perimeter length of the original hFF-fibrin cluster.

At concentrations up to 20 μM aprotinin, primarily the abundance of hFF outgrowth was dramatically reduced, but at 50 μM aprotinin also the average penetration depth of the few existing hFF outgrowths was reduced. These results show that cell-derived serine-protease activity (such as activation of plasminogen and induction of fibrinolysis) is the relevant mode of matrix penetration of the protein-*graft*-PEG hydrogels.

To verify further that the plasmin degradation sites in protein[A]-*graft*-PEG hydrogels were the only cleavage sites responsible for cell-associated proteolysis during cell migration, it would have been useful to have protein[B]-*graft*-PEG hydrogels containing the point-mutated plasmin degradation sites in the protein backbone. However, the relative insolubility of protein[B]-*graft*-PEGacrylate, designed to demonstrate this, illustrated that it was not possible to remove the plasmin substrate sites and alter the RGD sites without causing associated physicochemical changes in the protein and gel character. Due to the anticipated mechanical and charge differences between protein[B]- and protein[A]-*graft*-PEG hydrogels, a different microstructure and generally different cellular behavior would have to be expected. The inhibition studies with cyclic RGD and aprotinin, therefore, serve as alternative, and perhaps more meaningful, negative controls for cell adhesivity and serine-protease degradability of protein[A]-*graft*-PEG hydrogels, respectively, without the complexities of differences in the physical properties of the gels due to sequence alterations.

CONCLUSION

Cell survival, spreading, migration, and proliferation in three dimensions require sufficient mechanical support as well as specific sites for cellular attachment and proteolytic remodeling. The present materials provide these features, based on an artificial protein backbone and covalent crosslinking via PEG-tethered acrylate groups for polymerization.

The fact that hFFs survived, spread, and migrated through these materials in a manner that depended on RGD ligation and plasminogen activation demonstrates this. The cell adhesion sites and plasmin substrate sites are provided within the protein backbone of the protein-graft-PEGacrylate precursor, as well as sites for attachment of the PEG acrylate to that backbone. Photoinitiated polymerization of the acrylates at the termini of the dangling PEG chains provides for covalent gelation. A heparin-binding domain was further incorporated into this construct, for use in future studies.[89,90] These materials may be useful in wound healing and tissue regeneration, situations in which cell migration from a periphery into the core of an implanted matrix is desirable. In such cases, degradation should occur in exact temporal synchrony with cell outgrowth and be localized to the site and direction of cellular outgrowth. Therefore, degradation should be cell-associated and cell-controlled, avoiding any bulk degradation which would cause the general loss of the very matrix that the cells need for attachment and overall mechanical support. The hFF migration and apparent proliferation observed inside the protein-*graft*-PEG hydrogels, and the inhibition of these cellular functions by the serine protease inhibitor aprotinin, provides clear evidence that the biosynthetic matrix presented was specifically degradable in a localized manner by cell-associated proteolysis, as it was originally designed to be by incorporation of two plasmin degradation sites from human fibrinogen. It would thus appear that the design objectives for a biosynthetic extracellular matrix have been achieved by artificial protein-*graft*-PEG hydrogels: The matrix was cell adhesive, degradable by specific cell-derived enzymatic activity, and had sufficient mechanical strength to support cellular outgrowth for at least 7-9 days *in vitro*, which is a relevant time scale for many healing processes. The immunologic properties of the matrix remain to be tested, but considering that human sequences were selected in construction of the hydrogels' protein component, and in light of the well-established immunocompatibility of PEG,[128] the challenge of immunoacceptability may not be daunting.

CHAPTER 6

EFFECT OF HEPARIN ON CHICK NEURITE OUTGROWTH ON PROTEIN-*graft*-PEG HYDROGELS

INTRODUCTION

The ultimate goal of the protein-*graft*-PEG hydrogel material described in Chapters 4 and 5 was to be used as a matrix for nerve regeneration. The general material requirements that were demonstrated by the hFF-fibrin cluster model system, namely appropriate mechanical strength, integrin- and proteoglycan-mediated cellular adhesivity and cell-associated degradability in spatial and temporal synchrony with cellular outgrowth, also need to be fulfilled by a material that is intended to support neurite outgrowth inside a nerve guide tube. However, while it was possible to achieve hFF outgrowth with a minimal set of matrix components that enabled integrin- and cell-surface proteoglycan binding to the matrix, Chapter 2 illustrated that nerve cells are more complicated and require additional signals for outgrowth or even mere attachment. While the permanent presence of the RGD motif in the protein[A]-*graft*-PEG gels provides binding sites for many integrin receptors, some of which are ubiquitously expressed, including in the peripheral nervous system,[24] the heparin-binding site in the hydrogel's protein backbone makes it possible to immobilize additional adhesion- and/or trophic factors. As was briefly mentioned in Chapter 5, this can be achieved by taking advantage of the matrix's affinity for heparin, as heparin can serve as a "bridge" for the immobilization of additional biological factor(s). This binding scheme, involving heparin as a linker or "heparin bridge" between two heparin-binding sites, is illustrated in Figure 6.1.

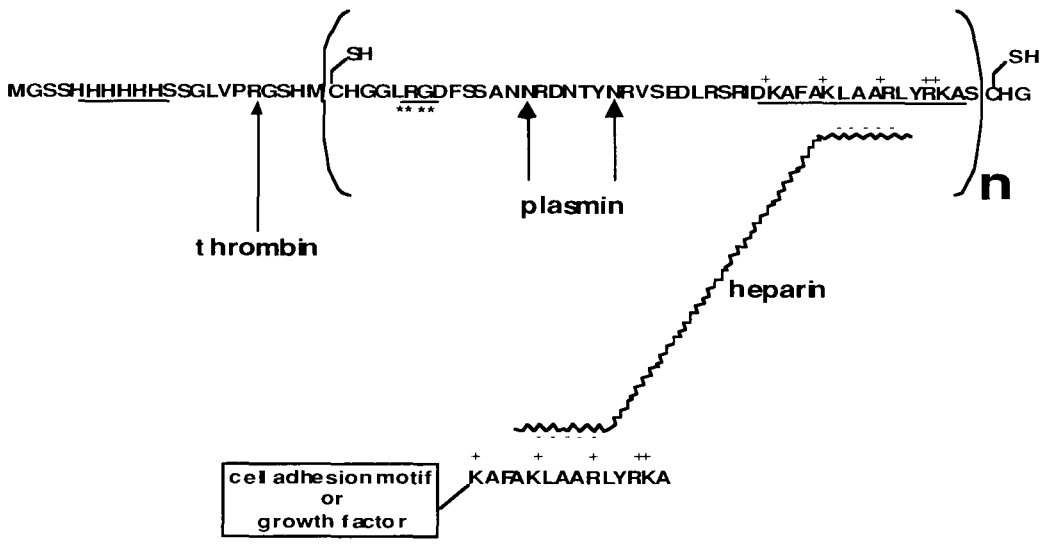

Figure 6.1: "Heparin Bridge" Immobilization Scheme

Cell adhesion molecule or growth factor bound by a "heparin bridge" to the pentameric protein core of protein-*graft*-PEG hydrogels (n = 5). HHHHHH is the protein's thrombin-cleavable hexa-histidine tag used for Ni^{++}-affinity purification; RGD is the fibrinogen-based integrin-binding site; and KAFAKLAARLYRKA is an ATIII-based heparin-binding site. Also shown are the protein pentamer's thrombin and plasmin cleavage sites as well as the protein construct's thiol functional groups that were used for grafting PEG diacrylate. Finally, - - - indicates the highly negative charge of heparin, and + marks the positive charge of amino acids that are part of the protein pentamer's heparin-binding site.

In addition to heparin's intended role as an immobilization agent for exogenous heparin-binding factors, even without any further additions immobilized heparin is expected to have growth-promoting effects in an artificial matrix, as cells secrete extracellular matrix components and growth factors that require immobilization by heparin or other glycosaminoglycans in order not to diffuse away. In fact, results with the protein-*graft*-PEG system presented in this chapter indicate that matrix-bound heparin alone was necessary to elicit surface outgrowth of neurites on the hydrogels, while additional factors such as the hep.bind.-YIGSR peptide had no further beneficial effect.

Before elaborating on the heparin-dependent two-dimensional neurite outgrowth on protein-*graft*-PEG hydrogels, this chapter will describe and analyse the many unsuccessful attempts to elicit three-dimensional neurite outgrowth inside protein-*graft*-PEG matrices

using various medium formulations and additions, different neuronal cell types, and even different ways of embedding or juxtaposing neuronal cells to photopolymerized hydrogels.

BACKGROUND

DRG Assay

In adult vertebrates, dorsal root ganglia (DGRs) lie within the vertebral column immediately adjacent to the spinal cord. In day 8 chick embryos, DRGs can be dissected easily because of their relatively large size (d ~ 500 μm), incomplete nerve fiber development, and because all embryonic tissues, including adjacent bone, are still very soft and penetrable. DRG neurons relay information from skin, muscles, and joints of the limbs and trunk to the spinal cord. They are sensory cells that belong to the class of pseudo-unipolar neurons, whose axons have a central and a peripheral branch.[129] NGF strongly promotes neurite outgrowth from DGRs onto, or within, permissive substrates such as laminin, or fibrin, respectively. Such NGF-induced neurite outgrowth served as an assay and model system in the context of this study. In particular, the physiological similarities between embryonic nerve development and adult nerve regeneration after injury render embryonic neurons especially useful to test a material for its neuroinductive, neuroconductive, and degradative qualities, all essential features toward improvement of functional nerve regeneration.

PC12 Cells

The PC12 cell line was derived from a transplantable rat adrenal pheochromocytoma.[172] PC12 cells represent a single cell clonal line which responds reversibly to nerve growth factor (NGF). By one week's exposure to NGF, PC12 cells cease to multiply and begin to extend branching varicose processes similar to those

produced by sympathetic neurons in primary cell culture. By several weeks of exposure to NGF, the PC12 processes reach 500-1000 μm in length under suitable culture conditions. Removal of NGF is followed by degeneration of processes within 24 hr and by resumption of cell multiplication within 72 hr.[173] NGF prevents the death and stimulates the neuronal differentiation of PC12 cells in serum-free medium.[174]

Because of their ease of handling and inducible neuron-like behavior, PC12 cells were used to test the neuroinductive, neuroconductive, and degradative qualities of protein-*graft*-PEG hydrogels. In particular, the hope was that PC12 cells in the presence of NGF would attach to, degrade, and extend neuritic processes inside protein-*graft*-PEG hydrogels, thereby verifying the material's intended functions in a neuronal context.

MATERIALS AND METHODS

Peptide Synthesis

Peptides α-dansyl-LN-KAF(βA)KLAARLYRKA-N-DPGYIGSR-$CONH_2$ (hep.bind.-YIGSR, mol. mass 3027.5 Da) and α-dansyl-LN-KAF(βA)KLAARLYRKA-G-RGD-SPASS-$CONH_2$ (hep.bind.-RGD, mol. mass 2882.3 Da) were made with a "Pioneer" peptide synthesizer (Applied Biosystems, USA) by automated solid phase peptide synthesis using 0.4 g peptide amide resin (NovaSyn TGR, Novabiochem-Calbiochem AG, Switzerland) per peptide. Synthesis occurred by standard 9-fluorenyl-methyloxycarbonyl (Fmoc) chemistry,[119] using solvents from Applied Biosystems (Warrington, England) and all other reagents from Novabiochem-Calbiochem. After synthesis, the peptide resin was washed with MeOH and dried in a vacuum overnight. Peptides were cleaved from the resin and deprotected for 4 hrs by shaking the resin in 10 mL of a solution containing 8.8 mL trifluoroacetic acid (TFA, Fluka, Switzerland), 0.5 mL phenol (Aldrich), 0.2 mL triisopropylsilane (Aldrich), and 0.5 mL water. The resin was removed by vacuum

filtration through fritted glass funnels and washed with 5 resin volumes of TFA. Precipitation of the peptides occurred when the filtration flow-through was added drop-wise to chilled diethyl ether (~400 mL). The white precipitate was recovered by vacuum filtration (0.2 µm pore-sized PTFE membrane filters, Gelman Sciences) and washed with three ~50 mL portions of diethyl ether. The final filtrate was dried in a vacuum chamber overnight and then sealed under argon for temporary storage at –20 °C.

Peptides were purified by preparative C_{18} chromatography (Prep Nova-Pak 19 x 300 mm column; Waters, USA) using a BioCAD 700E chromatograph (PerSeptive Biosystems). Separation of peptides from impurities was achieved by applying a gradient of acetonitrile in 0.1% TFA. The resulting eluate fractions were freeze-dried and analyzed by matrix-assisted laser desorption ionization-time of flight (MALDI-TOF) mass spectroscopy using the "Voyager Elite 122" spectrograph (Applied Biosystems, USA) and, as MALDI matrix, alpha-cyano-4-hydroxycinnamic acid (Aldrich). Before storage at –20 °C, verified and identical peptide fractions were combined, dried in a vacuum chamber overnight and finally sealed under argon for storage.

Heparin-Affinity Chromatography with Heparin-Binding Adhesion Peptide

0.5 g heparin-agarose beads (bead size 50-150 µm, 5-7 mg heparin per milliliter gel; AppliChem A1481, Germany) were pre-swollen in PBS (0.2 g/L KCl, 0.2 g/L KH_2PO_4, 2.16 g/L $Na_2HPO_4 \cdot 7H_2O$, 8 g/L NaCl, pH 7.4) for 1 h at room temperature, poured into a chromatography column, and allowed to settle to yield a bed of heparin-agarose gel of approximately 1 mL. 0.75 mg of hep.bind.-YIGSR in 1 mL PBS with and without 9.13 mg/mL heparin from porcine intestinal mucosa (MW 16,000-18,000, 181 USP units/mg, Sigma H-9399, Germany) was applied to the heparin-agarose gel and allowed to bind for 15 min at room temperature and zero column flow. The column was then drained, and chromatography was performed with seventeen consecutive 1 mL

washes of PBS containing increasing amounts of NaCl, starting with the original 137 mM of PBS up to 2 M in steps of 110 mM NaCl. The flow-through fractions were collected separately and analysed by 20% polyacrylamide SDS-PAGE for the presence of hep.bind.-YIGSR peptide.

Rheological Characterization of Protein-*graft*-PEG(6000) Hydrogels Containing Heparin

A Bohlin Instruments CVO 120 High Resolution rheometer (Bohlin Instruments, United Kingdom) was used in combination with a portable Cermax Xenon Fiber Optic Light Source to obtain dynamic rheological measurements of protein-*graft*-PEG hydrogels formed *in situ* in a circular parallel plate geometry. The light source was installed underneath a glass plate serving as the fixed bottom surface, while a circular parallel plate with radius 10.0 mm was rotating in oscillatory mode atop 30 µL of a 10% *(m+v)* protein[A]-*graft*-PEG(6000)acrylate solution throughout the measurement, imposing a target shear strain of 0.05 at a frequency of 1 Hz and with an initial shear stress of 1 Pa. The solutions further contained 2.83 mg/mL heparin or no heparin. The distance between the bottom glass surface and the circular parallel plate was 95 µm. After allowing the phase angle of the solution to stabilise for 1-2 min, the light source was switched on at designated time = 0 and allowed to irradiate the sample for the entire duration of the rheological measurement. For the two conditions (i.e., with and without heparin) two measurements each were performed on two samples that were prepared identically (n=2), but due to material constraints the measurements have not been repeated independently.

Preparation of Neural Culture Medium (NCM)

Unless otherwise stated, the composition of the medium for culture experiments with whole mouse or chick dorsal root ganglia (DRGs), dissociated chick DRG cells, and PC12 cells was as follows:

	100 mL	Neurobasal™ Medium[175] (Gibco 21103-031)
added:	1 ml	N2 Supplement[176] (100X) (Gibco 17502-014)
	100 mg	Albumin From Bovine Serum (Sigma A-9418)
	1 mL	ABAM (Gibco 15240-062)
	500 µL	0.1% Fibronectin Solution (Sigma F-1141)
	250 µl	L-Glutamic Acid (2mg/mL) (Gibco 12419-016)
	1 mL	Glutamax I (100X) (Gibco 35050-020)
	500 µL	Nerve Growth Factor (7S-NGF) From Mouse Submaxillary Glands (20 µg/mL) (Sigma N-0513)

further additions:	Mouse Laminin (from frozen aliquots of 1 mg/mL, Sigma L-2020)
(as indicated)	Bovine Aprotinin (from 2 mg/mL in PBS; Calbiochem, USA)
	Plasmin (from frozen aliquots of 0.3 mg/mL, Sigma P-8644)

Note: N-2 Supplement (100X) contains the following components:

Bovine Insulin (500 µg/mL)
Human Transferrin (holo) (10 mg/mL)
Progesterone (0.63 µg/mL)
Putrescine (1611 µg/mL)
Selenite (0.52 µg/mL)

Neither Neurobasal™ Medium nor N-2 Supplement contain any cell adhesion proteins such as fibronectin, laminin, collagen, or fibrinogen.

The medium was prepared by dissolving the albumin in the Neurobasal™ Medium and then adding all additional components except NGF. NGF was added after sterile-filtering the medium (0.22 µm pore-sized cellulose acetate sterile filter unit, Corning).

Serum-containing RPMI 1640 medium consisted of the following components (by volume percent):

	85%	RPMI 1640 with GlutaMax II (Gibco 82400-029)
	10%	Heat-Activated Horse Serum (Gibco 26050-088)
	5%	Foetal Bovine Serum (Gibco 10106-169)
added:	1%	ABAM (100X) (Gibco 15240-062)

Dissection of Chick Dorsal Root Ganglia (DRGs)

Day 8 chick embryos (or day 9 chick embryos, when stated) were taken from Lewis Brown chicken eggs. DRGs were dissected according to standard protocols described elsewhere[147] and then kept in a small petri dish with NCM at 37 °C for up to 30 min until further processing.

Dissection of Mouse DRGs

Mouse DRGs were dissected from neonatal (P0) mice (1:1 hybrids of strain C57BL/6:FVB, kindly provided by Hasan Mohajeri of the Brain Research Institute, University of Zurich) and then briefly stored in NCM according to the same protocol that was followed for embryonic chick DRGs.

Embedding and Culture of Whole DRGs Inside Protein-*graft*-PEG Hydrogels

Mouse or chick DRGs were embedded inside 30 µL protein-*graft*-PEG(3400) or –PEG(6000) hydrogels by placing up to four DRGs directly into a 30 µl volume of initiator-containing 10% *(m+v)* protein-*graft*-PEGacrylate solution on the bottom of a 12-well tissue-culture plate. Photopolymerization of the protein-*graft*-PEGacrylate around the DRGs was induced *in situ* according to the same method used for hFF-fibrin clusters (Chapter 5). The DRGs, thus embedded inside the protein-*graft*-PEG hydrogels, were then cultured in the 12-well tissue-culture plates after covering each gel with 1.5 mL NCM.

Independent additions to the 10% *(m+v)* protein-*graft*-PEG(6000)acrylate solutions prior to gelation included the following:

- 2, 20, and 200 µg laminin per mL protein-*graft*-PEG hydrogel before swelling → with the intent to entrap laminin and thereby provide native neural adhesion sites within the matrix; this was intended as a positive control for neurite outgrowth in the protein-*graft*-PEG material.
- 2.83 mg/mL heparin (16-18 kDa) and 20 µg/mL laminin → with the intent to immobilize laminin, which has heparin-binding sites,[32,47,48] by immobilization via the heparin-binding scheme illustrated in Figure 6.1.
- 2 µg/mL human plasminogen (Boeringer Mannheim/Roche) with and without 5 µg/mL bovine lung aprotinin → Plasminogen was added with the intent to eliminate low plasminogen concentrations as a limiting factor for proteolytic matrix degradation. Aprotinin was added to ensure that plasmin diffusion would not lead to bulk degradation of the matrix.
- 0.5% *(v/v)* embryonic chick extract → to provide other (growth) factors –in addition to those contained in the NCM– that contribute to neurite outgrowth from embryonic chick DRGs. However, an undefined addition such as chick embryo extract also entailed the risk of introducing factors inhibitory to neurite extension.
- (i) no additions, (ii) 0.28 mg/mL heparin (16–18 kDa) and 0.05 mg/mL hep.bind.-YIGSR, (iii) 1.42 mg/mL heparin and 0.25 mg/mL hep.bind.-YIGSR, (iv) 2.83 mg/mL heparin and 0.5 mg/mL hep.bind.-YIGSR, (v) 28.3 mg/mL heparin and 5 mg/mL hep.bind.-YIGSR → with the intent to immobilize additional neuronal adhesion sites within the matrix using the heparin-binding scheme. Note that 2.83 mg/mL heparin corresponded to an amount equal to 1 molecule of heparin per 62 heparin-binding sites in the unswollen protein-*graft*-PEG(3400) hydrogels. Adhesion peptides

and heparin were added in equimolar amounts to ensure, in theory, binding of all adhesion peptides by heparin. The paired additions of heparin and hep.bind.-*YIGSR* will be referred to in terms of "number of heparin and number of hep.bind.-YIGSR molecules per number of heparin-binding sites," i.e., "0, 1 per 500, 1 per 100, 1 per 50, 1 per 5." Presumably due to the instantaneous and strong affinity of hep.bind.-YIGSR for heparin when these two additions were present, a white precipitate became visible at concentrations greater than, and sometimes equal to, "1 per 50." Nevertheless, such suspensions were used after good mixing, and precipitates often disappeared after the addition of further constituents.

- (i) no additions, (ii) 0.208 mg/mL heparin (5 kDa, kindly provided by Pharmacia Upjohn, USA) and 0.126 mg/mL hep.bind.-YIGSR peptide, (iii) 0.833 mg/mL heparin (5 kDa) and 0.505 mg/mL hep.bind.-YIGSR peptide, or (iv) 1.04 mg/mL heparin (5 kDa) and 0.631 mg/mL hep.bind.-YIGSR peptide (corresponding to (i) 0, (ii) "1 per 200," (iii) "1 per 50," and (iv) "1 per 40" heparin and hep.bind.-YIGSR molecules per heparin-binding sites in the gel before swelling) → the use of heparin with smaller molecular mass assured better solubility of the heparin in the presence of hep.bind.-YIGSR peptide, so more of both could be incorporated in the hydrogels, i.e., up to 1 heparin and hep.bind.-YIGSR molecule per 40 heparin-binding sites in the gel. Also, smaller heparin molecules were less likely –should that have been a problem at all– to bind to the hydrogel matrix and block or mask other signals in the hydrogel matrix, i.e., integrin-binding RGD sites or plasmin degradation sites.

Other variations in the attempt to elicit three-dimensional neurite outgrowth from chick DRGs embedded in protein-*graft*-PEG(6000) hydrogels included the following:

- using day 9, instead of day 8, chick embryonic DRGs → Day 9 DRGs were expected to be more robust and to contain cells more differentiated toward their neuronal fate. The hope was that even in an unusual environment such as protein-*graft*-PEG hydrogels, neurite extensions could be achieved from more differentiated neurons.

- using 8% (*m*+*v*) protein-*graft*-PEG(6000) hydrogels → to test whether hydrogels that are less dense and less crosslinked might allow better proteolytic penetration and, therefore, facilitate neurite outgrowth. However, this also potentially makes possible non-proteolytic penetration of the matrix, i.e., if penetration was merely through channels and defects in the gel, which are more abundant the less dense the matrix is.
- using modified DMEM/F12 medium (Gibco 41331-026) with:

  1% (*v*/*v*) insulin – transferrin – selenium supplement (100X) (Gibco 51300-044)

  1% (*v*/*v*) ABAM (100X) (Gibco 15240-062)

  0.5% (*v*/*v*) chick embryo extract, 60Å ultrafiltrate (Gibco 16460-057)

→ to provide an alternative to NCM so as to exclude the possibility that NCM was deficient or scarce in some essential component, which relatively "rich" modified DMEM/F12 was less likely to be. However, once again, an undefined addition such as chick embryo extract also entailed the risk of introducing factors inhibitory to neurite extension.

DRGs were also embedded in 10% (*m*+*v*) protein-*graft*-PEG(3400) gels under various conditions with the hope to provide DRGs with a more densely crosslinked matrix that would assure better mechanical support, in case the lower mechanical strength or lesser degree of crosslinking of protein-*graft*-PEG(6000) hydrogels should have been insufficient in supporting three-dimensional neurite outgrowth. Independent additions to the 10% (*m*+*v*) protein-*graft*-PEG(3400)acrylate solutions prior to gelation included the following:

- 2, 20, and 200 µg laminin per mL protein-*graft*-PEG hydrogel before swelling → with the intent to entrap laminin and thereby provide native neural adhesion sites as in A.
- 2.83 mg/mL heparin (16-18 kDa) and 20 µg/mL laminin → with the intent to immobilize laminin, which has heparin-binding sites,[32,47,48] by immobilization via the heparin-binding scheme as in B.

- 2.83 mg/mL heparin (16-18 kDa) and 0.5 mg/mL hep.bind.-YIGSR → with the intent to immobilize additional binding sites within the matrix using the heparin-binding scheme as in E. Note that these amounts correspond to 1 heparin and 1 hep.bind.-YIGSR molecule per 62 heparin-binding sites in the gel before swelling.

Embedding and Culture of DRG-Fibrin Clusters Inside Protein-*graft*-PEG Hydrogels

2-4 µL droplets of 2% *(m/v)* fibrinogen from human plasma (Fluka, Switzerland) in sterile PBS containing 2 NIH units/mL thrombin (Sigma T-6884, Switzerland) and 2.5 mM Ca^{++} were quickly placed onto Sigmacote®-coated (Sigma, USA) microscope slides. Using dissection tweezers, individual DRGs were rapidly transferred into these 2-4 µL droplets of fibrinogen solution. Fibrinogen crosslinking occurred around the DRGs after incubation in a humidified atmosphere at 37 °C for 20 min. The DRG-fibrin clusters were embedded inside 30 µL protein-*graft*-PEG(3400) and –PEG(6000) hydrogels by placing up to three clusters into a 30 µl volume of 10% *(m+v)* protein-*graft*-PEGacrylate solution on the bottom of a 12-well tissue-culture plate. Crosslinking of the protein-*graft*-PEGacrylate around the DRG-fibrin clusters was induced *in situ* by exposure to the portable light source through the culture-well lid. The DRG-fibrin clusters, thus embedded inside the protein-*graft*-PEG hydrogels, were then cultured in the 12-well tissue-culture plates after covering each gel with 1.5 mL NCM.

Embedding and Culture of Dissociated DRG Cell-Fibrin Clusters Inside Protein-*graft*-PEG Hydrogels

DRGs were dissociated by incubation at 37 °C with trypsin-EDTA for 5 min followed by gentle trituration with a 1 mL plastic pipette tip. The dissociated DRG cells

were centrifuged (700 g, 3 min, room temp.) and resuspended in 2% *(m/v)* fibrinogen from human plasma (Fluka, Switzerland) in sterile PBS to a concentration of ~6000 DRG cells/μL. To induce gelation of the DRG cell-fibrinogen suspension, thrombin (Sigma T-6884, Switzerland) and Ca^{++} were added to final concentrations of 2 NIH units/mL and 2.5 mM, respectively, and rapidly mixed with the cell suspension. Prior to gelation, 2 μL droplets containing approximately 12000 DRG cells each were quickly transferred to Sigmacote®-coated (Sigma, USA) microscope slides, on which gelation of the DRG cell-fibrin clusters was allowed to reach completion in a humidified atmosphere at 37 °C for 20 min. The DRG cell-fibrin clusters were embedded inside 30 μL protein-*graft*-PEG hydrogels by placing up to four of the clusters into a 30 μl volume of 10% *(m+v)* protein-*graft*-PEGacrylate solution on the bottom of a 12-well tissue-culture plate. Crosslinking of the protein-*graft*-PEGacrylate around the hFF-fibrin clusters was induced *in situ* by exposure to the portable light source through the culture well lid. The dissociated DRG cell-fibrin clusters, thus embedded inside the protein-*graft*-PEG hydrogels, were then cultured in the 12-well tissue-culture plates after covering each gel with 1.5 mL NCM. The protein-*graft*-PEG hydrogels contained (i) 1.42 mg/mL heparin and 0.25 mg/mL hep.bind.-YIGSR peptide, or (ii) 2.83 mg/mL heparin and 0.5 mg/mL hep.bind.-YIGSR peptide.

Embedding and Culture of PC12 Cell-Fibrin Clusters Inside Protein-*graft*-PEG Hydrogels

PC12 cells (American Type Culture collection, ATCC Number CRL-1721, USA), pre-cultured in serum-containing RPMI 1640 medium, were centrifuged (700 g, 3 min, room temp.) and resuspended in 2% *(m/v)* fibrinogen from human plasma (Fluka,

Switzerland) in sterile PBS to a concentration of 30000 PC12 cells/μL. Embedding in 2 μL fibrin droplets was achieved according to the same method used to embed dissociated DRG cells. PC12 cell-fibrin clusters were then embedded similarly inside 30 μL protein-*graft*-PEG hydrogels. Independent culture conditions for PC12 cell-fibrin clusters in protein-*graft*-PEG(6000) hydrogels included (A) NCM with 0, 50, and 200 ng/mL NGF, no other additions; (B) hydrogels with 2 and 20 μg/mL laminin, NCM with 100 ng/mL NCM.

Culture of DRGs on Laminin-Coated Surfaces with Subsequent *In Situ* Formation of Protein-*graft*-PEG Hydrogels in Contact with DRGs

Tissue-culture polystyrene (TCPS) 12-well plates were coated with 20 μg/mL laminin solutions in TBS by incubating 0.5-1 mL per tissue-culture well for 30 min at 37 °C. The coating solution was removed, the wells rinsed with TBS once, and freshly dissected chick DRGs cultured on the laminin-coated surfaces in NCM. After one day, when neuritic extensions of up to 300 μm had grown, the NCM was removed. 10% (*m*+*v*) protein-*graft*-PEG(3400)acrylate or –PEG(6000)acrylate solutions with the usual initiator system were placed around the DRGs, covering the entire bottom of the tissure-culture well and leaving the DRGs immersed to about half its height. Crosslinking of the protein-*graft*-PEGacrylate around the DRGs was induced *in situ* by exposure to the portable light source through the culture well lid. The DRGs, thus half-embedded inside the protein-*graft*-PEG hydrogels, and their neuritic extensions blanketed with hydrogel, were then cultured in the 12-well tissue-culture plates after covering each gel with 1.5 mL NCM.

Culture of DRGs on Protein-*graft*-PEG Hydrogels

Chick DRGs were half-embedded on the surface of 30 μL protein-*graft*-PEG(3400) or –PEG(6000) hydrogels by placing up to four DRGs directly onto a 30 μl volume of initiator-containing 10% *(m+v)* protein-*graft*-PEGacrylate solution on the bottom of a 12-well tissue-culture plate. Photopolymerization of the protein-*graft*-PEGacrylate underneath the DRGs was induced *in situ* according to the same method as for gels around hFF-fibrin clusters, Chapter 5. The DRGs, thus embedded on the surface of protein-*graft*-PEG hydrogels, were then cultured in the 12-well tissue-culture plates after covering each gel with 1.5 mL NCM.

Table 6.1: Culture Conditions for DRGs Half-Embedded in Protein-*graft*-PEG(3400) Hydrogels

BELOW: THEORETICAL NUMBER OF THE IMMOBILIZED MOLECULES, ON THE RIGHT, PER HEPARIN-BINDING SITES IN THE MATRIX	heparin (16-18 kDa)	hep.bind.-YIGSR ("YIG")	hep.bind.-RGD ("RGD")
0	0[a]	0[a]	0[a]
1 hep. + YIG per 620	0.28 mg/mL[b]	0.05 mg/mL[b]	0
1 hep. + YIG per 124	1.42 mg/mL[c]	0.25 mg/mL[c]	0
1 hep. + YIG per 62	2.83 mg/mL[d]	0.5 mg/mL[d]	0
1 hep. + RGD per 62	2.83 mg/mL[e]	0	0.48 mg/mL[e]
1 hep. only per 62	2.83 mg/mL[f]	0	0

Independent additions to the 10% *(m+v)* protein-*graft*-PEG(3400)acrylate solutions prior to gelation included (a) no additions, (b) 0.28 mg/mL heparin and 0.05 mg/mL hep.bind.-YIGSR, (c) 1.42 mg/mL heparin and 0.25 mg/mL hep.bind.-YIGSR (d) 2.83

mg/mL heparin and 0.5 mg/mL hep.bind.-YIGSR, (e) 2.83 mg/mL heparin and 0.48 mg/mL hep.bind.-RGD, or (f) 2.83 mg/mL heparin only. 2.83 mg/mL heparin corresponded to an amount equal to 1 molecule of heparin per 62 heparin-binding sites in the unswollen protein-*graft*-PEG(3400) hydrogels. Adhesion peptides and heparin were added in equimolar amounts to ensure, in theory, binding of all adhesion peptides by heparin.

Independent additions to the 10% *(m+v)* protein-*graft*-PEG(6000)acrylate solutions prior to gelation included (g) no additions, (h) 0.28 mg/mL heparin and 0.05 mg/mL hep.bind.-YIGSR (i) 2.83 mg/mL heparin and 0.5 mg/mL hep.bind.-YIGSR. Here, 2.83 mg/mL heparin corresponded to an amount equal to 1 molecule of heparin per 50 heparin-binding sites in the unswollen protein-*graft*-PEG(6000) hydrogels. Again, adhesion peptides and heparin were always added in equimolar amounts to ensure binding of all adhesion peptides by heparin.

Table 6.2: Culture Conditions of DRGs Half-Embedded in Protein-*graft*-PEG(6000) Hydrogels

BELOW: THEORETICAL NUMBER OF THE IMMOBILIZED MOLECULES, ON THE RIGHT, PER HEPARIN-BINDING SITES IN THE MATRIX	**heparin (16-18 kDa)**	**hep.bind.-YIGSR ("YIG")**
0	0[g]	0[g]
1 hep. + YIG per 500	0.28 mg/mL[h]	0.05 mg/mL[h]
1 hep. + YIG per 50	2.83 mg/mL[i]	0.5 mg/mL[i]

To measure the neurite outgrowth from DRGs onto the protein-*graft*-PEG hydrogels, after three days in culture the DRGs were imaged and recorded with the plane of neurite outgrowth in focus. Microscopy and image processing were performed using a

Zeiss inverted confocal light microscope (Axiovert 135, Zeiss, Germany) in conjunction with a Hamamatsu Color Chilled 3CCD Camera (Hamamatsu, Japan) and LeicaQWin image processing software (Leica Imaging Systems Ltd., 1997). To quantify the neurite outgrowth, the area of the original DRG was measured, as was the area of neurite outgrowth, defined by the tips of neurites in the plane of outgrowth. These two areas were approximated as circular areas, and their theoretical radii subtracted from each other to give an average length of neurite outgrowth.

For the comparison of conditions (d), (e) and (f), only one set of 4, 8, and 8 DRGs, respectively, was analysed. For all other sets of data, at least two independent experiments, carried out in triplicate or higher number of DRGs, were performed and analysed. In parallel with all DRG cultures on protein-*graft*-PEG hydrogels, DRGs were cultured on laminin-coated TCPS to ensure DRG viability.

Verification of Chick Neurite Outgrowth by Immunostaining with Anti-Growth-Associated Protein-43 (GAP-43) Monoclonal Antibody

Outgrowth on protein-*graft*-PEG hydrogels was stopped and DRGs fixed by replacement of NCM with formalin solution (10%, neutral buffered, Sigma). To avoid a fluorescent background due to antibody entrapment in the hydrogel matrix, the hydrogels were hydrolysed by adding 1 M NaOH and incubating at room temperature for 5 min. After removal of the hydrogel lysate, the DRGs were permeabilized with 0.1% TritonX solution (Sigma) for 5 min, followed by rinsing with TBS, pH 7.4, three times. Non-specific adsorption of antibodies to the DRGs and tissue-culture well surfaces was prevented by blocking with a 3% (*m*/*v*) bovine serum albumin (BSA) solution (Sigma), and the DRGs were then incubated for 1 h at 37 °C with a 1X working solution of anti-GAP-43 monoclonal antibody (Sigma, G-9264) in TBS, also containing 3% (*m*/*v*) BSA. After three rinses with antibody-free TBS containing 3% (*m*/*v*) BSA, the DRGs were

incubated with a 1X working solution of FITC-labeled, Fab-specific anti-Mouse IgG antibody (Sigma, F-5262) in TBS with 3% (*m*/*v*) BSA for 1 h at 37 °C. Again, after three rinses with antibody-free TBS containing 3% (*m*/*v*) BSA, the immunostained DRGs were visualized by observing emission between 510-540 nm (Zeiss, Germany) under excitation at 483 nm. As a positive control for GAP-43 staining, DRGs cultured on laminin-coated TCPS were similarly immunostained with anti-GAP-43 monoclonal antibody followed by FITC-labeled, Fab-specific anti-Mouse IgG antibody.

RESULTS AND DISCUSSION

Heparin Affinity of hep.bind.-YIGSR Peptide

In the absence of soluble heparin, the hep.bind.-YIGSR peptide eluted from the heparin-agarose column between salt concentrations of 0.7-1.1 M NaCl (Figure 6.2 a,b). Elution at such high salt concentrations suggests a strong affinity of hep.bind.-YIGSR for the agarose-bound heparin. In the presence of 9.13 mg/mL soluble heparin, corresponding to 2 moles of heparin per mole of hep.bind.-YIGSR peptide, elution of hep.bind.-YIGSR occurred between salt concentrations of 0.5-1.1 M NaCl (Figure 6.2 c,d). This shift suggests that soluble heparin competitively compromised binding of the heparin-agarose to the hep.bind.-YIGSR peptide, causing the peptide to be eluted at a lower range of salt concentrations than in the absence of soluble heparin. Together, these results confirm the strong and specific affinity of hep.bind.-YIGSR peptide for heparin. Hydrophobic interactions or other non-specific binding of hep.bind.-YIGSR to the heparin-agarose resin can be excluded because of the reduction in binding when soluble heparin was added. However, more heparin should have been added to obtain better competitive inhibition, and to better illustrate the specific interaction of the heparin-binding peptide with the agarose-bound heparin in the column.

Figure 6.2 a,b; c,d: Heparin-Agarose Affinity Chromatography With hep.bind.-YIGSR Peptide

20% acrylamide SDS-PAGE gels with 16 µL samples from eluate fractions a,b) without heparin, c,d) with the addition of 2 moles of heparin per mole of hep.bind.-YIGSR peptide. Lane 1: molecular weight marker, 2: flow through after initial loading of column with 137 mM NaCl, 3: 137 mM NaCl, 4: 246 mM NaCl, 5: 356 mM NaCl, 6: 466 mM NaCl, 7: 575 mM NaCl, 8: 685 mM NaCl, 9: 794 mM NaCl, 10: 904 mM NaCl, 11: 1014 mM NaCl, 12: 1123 mM NaCl, 13: 1228 mM NaCl, 14: 1342 mM NaCl, 15: 1452 mM NaCl, 16: 1562 mM NaCl, 17: 1671 mM NaCl, 18: 1781 mM NaCl, 19: 1890 mM NaCl, 20: molecular weight marker.

Together with results described in Chapter 4, which showed the strong and specific affinity of protein-*graft*-PEGacrylate for heparin, the affinity of designed heparin-binding peptides, e.g., hep.bind.-YIGSR, for heparin supported the feasibility of the immobilization scheme for additional adhesion sites within protein-*graft*-PEG hydrogels using heparin as a linker (see Figure 6.1). However, to show that heparin-binding peptides hep.bind.-YIGSR and hep.bind.-RGD really remained bound to the hydrogels even when peptide- and largely heparin-free medium came in contact with the gels during

culture, binding and release studies remain to be performed. This should be straightforward by measuring the presence and release of fluorescence from the hydrogels due to the heparin-binding peptides' N-terminal dansyl groups.

Increase of the Mechanical Strength of Protein-*graft*-PEG Hydrogels Due to Heparin

Rheological characterization of protein-*graft*-PEG(6000) hydrogels with and without 2.83 mg/mL heparin revealed that gels containing heparin have greater mechanical strength. After photo-crosslinking, protein-*graft*-PEG hydrogels that contained heparin reached elastic moduli (or "storage moduli"), G′, up to 1.7 kPa (Figure 6.3), which corresponds to a Young's modulus ($E_{\text{with heparin}}$) of approximately 5.1 kPa.

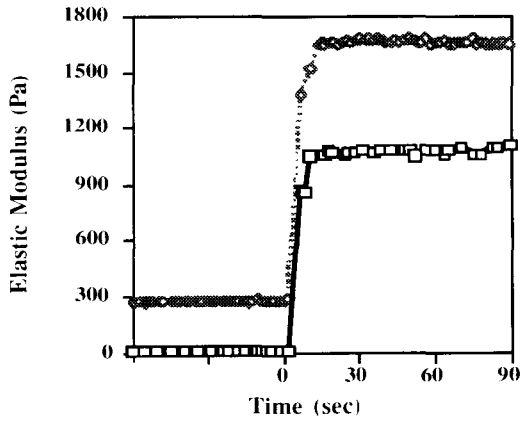

Figure 6.3: Physical Intermolecular Crosslinking by Heparin

Elastic moduli, G′, of protein-*graft*-PEG(6000) hydrogels with [diamond] and without [square] 2.84 mg/mL heparin. Photo-initiation of gelation was started at designated time = 0.

(Note: $E = 2(1 + \mu)G'$, where μ is Poisson's ratio, assumed to be the ideal value, 0.5, a reasonable assumption for cross-linked gels). The range of Young's Modulus $E_{\text{without heparin}}$

measured in parallel for protein-*graft*-PEG(6000) gels without heparin was only 2.9 – 3.7 kPa, in close agreement with the values reported in Chapter 4.

The greater mechanical strength of protein-*graft*-PEG hydrogels can be explained by heparin's ability to contribute to the crosslinking by electrostatic interaction with more than one heparin-binding site in the hydrogel's protein backbone. Because of this physical crosslinking effect, even protein-*graft*-PEGacrylate solutions containing heparin already exhibited appreciable elasticity ($G'_{\text{with heparin}}$ = 280 kPa; Figure 6.3), as opposed to pre-gel solutions without heparin ($G'_{\text{without heparin}} \approx 0$).

Fibroblast or Glial Cell Outgrowth, but Lack of Neurite Outgrowth, from Whole DRGs Inside Protein-*graft*-PEG Hydrogels

In contrast to the human fibroblast outgrowth observed in protein-*graft*-PEG hydrogels (Chapter 5), no three-dimensional neurite outgrowth from embryonic chick DRGs could be elicited in protein-*graft*-PEG hydrogels under any of the conditions A – L described in the *Materials and Methods* section of this chapter (Figure 6.4). Even the most promising conditions involving the presence of laminin in the hydrogels (conditions A and B) did not lead to neurite outgrowth. Apparently, even the presence of laminin and fibronectin (the latter usually provided in the medium) was not sufficient to promote three-dimensional neurite extension, as these proteins may not have been sufficiently adsorbed or immobilized to the matrix to serve as cellular adhesion sites. In a non-immobilized state, laminin and fibronectin might even have inhibited neural adhesion, namely by occupying cellular receptors without providing the mechanical support of an underlying surface or matrix.

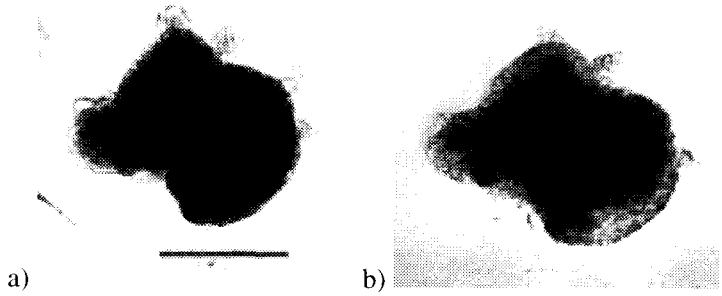

Figure 6.4: Lack of Three-Dimensional Neurite Outgrowth from Embryonal Chick DRGs

DRG in a protein-*graft*-PEG(6000) hydrogel with 200 µg/mL laminin. a) day 1, b) day 4. (Scale bar = 300 µm)

Nevertheless, in occasional instances, chick fibroblast or glial cell outgrowth from the DRGs was observed (Figures 6.5, 6.6, 6.7), but never with the same abundance as outgrowth from hFF-fibrin clusters in Chapter 5. Notably, this outgrowth only occurred when heparin was present in the hydrogels. This suggests that even for the occasionally observed three-dimensional chick fibroblast or glial outgrowth, and especially for chick neurite outgrowth, additional factors or a modification of hydrogel properties were necessary, namely different or beyond those of plain protein-*graft*-PEG gels. The additional feature that heparin appears to have provided could either be better mechanical strength or a means for retaining in the hydrogel additional adhesion and/or trophic factors.

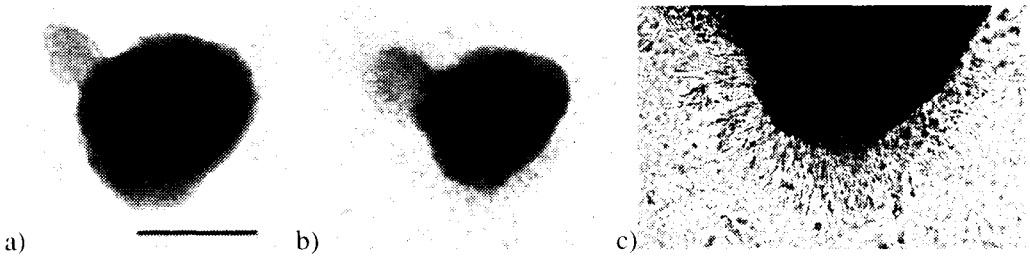

Figure 6.5: Occasional Three-Dimensional Fibroblast or Glial Cell Outgrowth from Embryonal Chick DRGs

DRG in a protein-*graft*-PEG(3400) hydrogel with 2.83 mg/mL heparin (16-18 kDa) and 0.5 mg/mL hep.bind.-YIGSR peptide in the gel before gelation. a) day 1, b) day 5, c) day 5, magnified view (1.6x). (Scale bar = 300 µm)

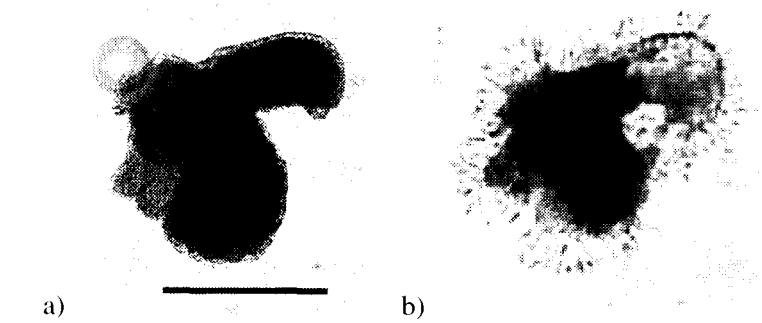

Figure 6.6: Late Three-Dimensional Fibroblast or Glial Cell Outgrowth from Embryonal Chick DRGs

DRG in a protein-*graft*-PEG(6000) hydrogel with 2.83 mg/mL heparin (16-18 kDa) and 0.5 mg/mL hep.bind.-YIGSR peptide in the gel before gelation. a) day 1, b) day 8. (Scale bar = 300 μm)

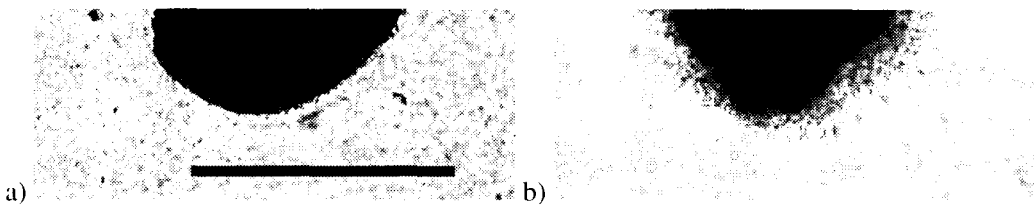

Figure 6.7: Three-Dimensional Fibroblast or Glial Cell Outgrowth from Embryonal Chick DRGs at Low Gel Density

DRG in a 8% (*m*+*v*))protein-*graft*-PEG(6000) hydrogel with 2.83 mg/mL heparin (16-18 kDa) and 0.5 mg/mL hep.bind.-YIGSR peptide in the gel before gelation. a) day 1, b) day 5. (Scale bar = 400 μm)

Assuming, based on the latter hypothesis, that under Condition B (gels supplemented with heparin and laminin) laminin was immobilized in the matrix by heparin-bridging as invisioned in Figure 6.1, it remains unclear why three-dimensional neurite outgrowth did not even occur then. Likewise, the addition of embryonic chick extract had no conducive effect (Condition D), nor the use of a richer growth medium than NCM (Condition I), nor the use of day 9 embryonic chick DRGs (Condition G).

Lack of Neurite Outgrowth from P0 Mouse DRGs in Protein-*graft*-PEG Hydrogels

To exclude the possibility that non-mammalian neurons (such as those of chick DRGs) could not efficiently penetrate or attach to a matrix based on mammalian adhesion-

and plasmin degradation sites, neonatal mouse DRGs were embedded in protein-*graft*-PEG hydrogels.

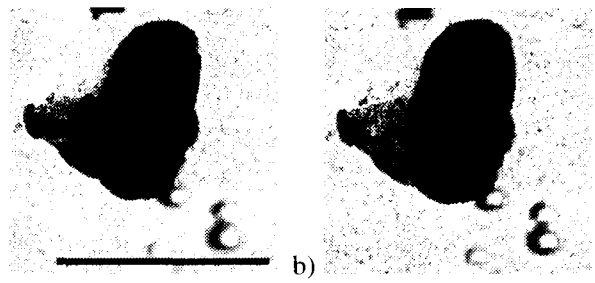

Figure 6.8 a: Lack of Three-Dimensional Neurite Outgrowth from P0 Mouse DRGs

Mouse DRG in a protein-*graft*-PEG(3400) hydrogel with 2.83 mg/mL heparin (16-18 kDa) and 0.5 mg/mL hep.bind.-YIGSR peptide in the gel before gelation. a) day 1, b) day 3. (Scale bar = 500 µm)

However, no three-dimensional neurite extension occurred in these systems, either (Figure 6.8), although the DRG neurons did remain viable in contact with the hydrogel material, as evident from normal neurite outgrowth on the surface of the material (Figure 6.9). Inter-species differences with regard to chick- versus mouse plasmin's ability to digest the material are thus unlikely as a sole reason for the failure of neurons to extend neurites in protein-*graft*-PEG hydrogels.

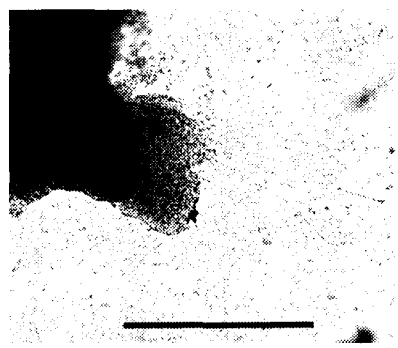

Figure 6.9: Surface Neurite Outgrowth from P0 Mouse DRGs

Mouse DRG surface-embedded on a protein-*graft*-PEG(3400) hydrogel with 2.83 mg/mL heparin (16-18 kDa) and
0.5 mg/mL hep.bind.-YIGSR peptide in the gel before gelation, on culture day 2. Healthy neurite outgrowth proved the viability of the DRG neurons. (Scale bar = 300 µm)

Further studies would be necessary to verify that chick plasmin can specifically degrade protein-*graft*-PEG hydrogels, but chick DRG neurites generally are capable of penetrating human fibrin via plasmin-mediated fibrinolysis.[177,91] Nevertheless, the lack of human fibrin degradation by embedded chick DRGs under conditions described in the next section suggests that some impairment of fibrinolysis -perhaps plasmin activation- might have played a role in preventing DRG neurite outgrowth.

Lack of Outgrowth from DRG-Fibrin Clusters Inside Protein-*graft*-PEG Hydrogels

When chick DRGs were first embedded in fibrin, and these clusters then cultured in protein-*graft*-PEG hydrogels, the hope was to elicit neurite outgrowth into the surrounding fibrin first, followed by a continuing outgrowth into the protein-*graft*-PEG material. However, as shown in Figure 6.10, neurite outgrowth did not occur at all. Moreover, no fibrinolysis was observed either, suggesting that plasmin activation or activity might have been impaired.

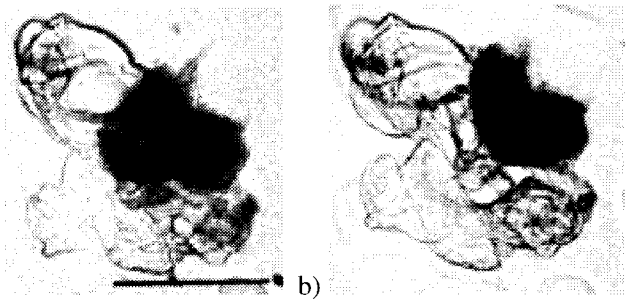

Figure 6.10: Lack of Three-Dimensional Neurite Outgrowth from Embryonal Chick DRG-Fibrin Clusters

DRG, partially embedded in a 0.2% (*m/v*) fibrin gel, in a protein-*graft*-PEG(6000) hydrogel with 2.83 mg/mL heparin (16-18 kDa) and 0.5 mg/mL hep.bind.-YIGSR peptide in the protein-PEG gel before gelation. a) day 1, b) day 5. (Scale bar ≈ 600 μm)

These observations raise the possibility that diffusion of certain relevant nutrients or growth factors through the 10% (*m+v*) protein-*graft*-PEG material was limited due to small

pore size and absence of defects. In that case, even 8% (*m*+*v*) protein-*graft*-PEG hydrogels (Figure 6.7) must have been too densely crosslinked, as no neurite outgrowth was observed, either. The fact that fibroblast or glial outgrowth still occurred at a later point is not inconsistent with this argument. Fibroblasts and glial cells may not require the same growth factors and likely remain viable longer than neurons, until partial hydrogel degradation allows better nutrient flow and facilitated proteolytic penetration.

Lack of Neurite Outgrowth from Dissociated DRG Cell-Fibrin Clusters Inside Protein-*graft*-PEG Hydrogels

Not surprisingly in light of the previous section, dissociated DRG neurons also did not extend, nor apparently survive for long, in fibrin clusters surrounded by protein-*graft*-PEG hydrogels (Figure 6.11).

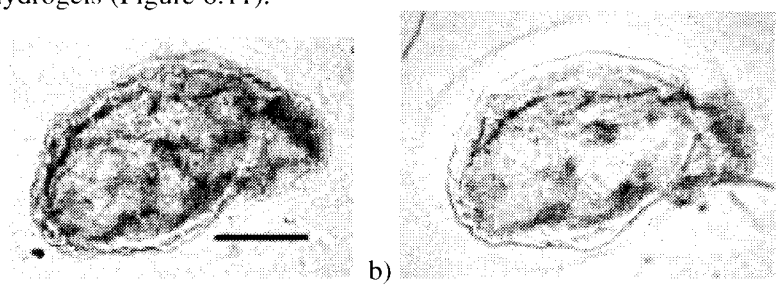

a) b)

Figure 6.11: Lack of Three-Dimensional Neurite Outgrowth from Embryonal Chick DRG Cell-Fibrin Clusters

Dissociated DRG Cells, embedded in a 0.2% (*m*/*v*) fibrin gel, in a protein-*graft*-PEG(6000) hydrogel with 2.83 mg/mL heparin (16-18 kDa) and 0.5 mg/mL hep.bind.-YIGSR peptide in the protein-PEG gel before gelation. a) day 1, b) day 3. (Scale bar ≈ 300 µm; both images shown at the same magnification)

While widespread cell death was obvious inside the DRG cell-fibrin clusters, some fibroblasts and/or glial cells did survive and even started to spread (Figure 6.12). Also, proteolytic enzymes were released that lead to the total degradation of the surrounding protein-*graft*-PEG matrix by day 7, but not the fibrin bed. Degradation of the surrounding protein-*graft*-PEG matrix was already visible on day 3 (Figure 6.11.b, above).

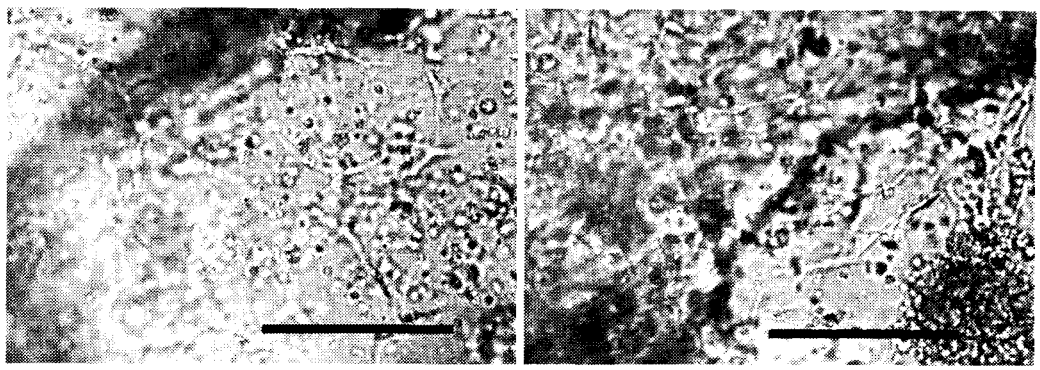

Figure 6.12: Fibroblast or Glial Cell Spreading Inside Embryonal Chick DRG Cell-Fibrin Clusters

Dissociated DRG Cells, embedded in a 0.2% (*m/v*) fibrin gel, surrounded by protein-*graft*-PEG(6000) hydrogel with 2.83 mg/mL heparin (16-18 kDa) and 0.5 mg/mL hep.bind.-YIGSR peptide in the protein-PEG gel before gelation, on culture day 7. (Scale bars = 100 µm; both images shown at the same magnification)

Lack of Neurite Extension by PC12 Cells Embedded in Fibrin and Placed Inside Protein-*graft*-PEG Hydrogels

Similar to dissociated DRG cell-fibrin clusters embedded in protein-*graft*-PEG hydrogels, there was also no outgrowth of neuritic extensions from, or within, PC12 cell-fibrin clusters (Figure 6.13).

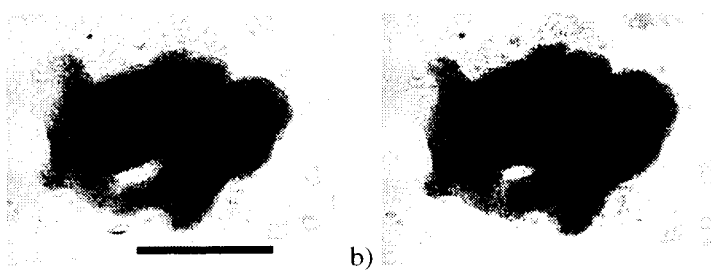

Figure 6.13: Lack of Neurite Outgrowth from PC12-Fibrin Clusters Inside Protein-*graft*-PEG Hydrogels

PC12 cells, embedded in a 0.2% (*m/v*) fibrin gel, surrounded by a protein-*graft*-PEG(6000) hydrogel with 100ng/mL NGF. a) day 1, b) day 5. (Scale bar = 300 µm)

It was not tested whether PC12 cells extend neuritic processes when embedded in fibrin that is not surrounded by potentially diffusion-limiting protein-*graft*-PEG material, but in most previous studies (see *BACKGROUND* on *PC12 Cells*) PC12 cells only extended

neurites when firmly attached to coated TCPS surfaces. Therefore, PC12 cell-fibrin clusters might not have been a good three-dimensional model system to begin with.

Arrest of Neurite Outgrowth after *In Situ* Formation of Protein-*graft*-PEG Hydrogels

To test whether neurites, which had already started to extend and which continued to be guided by an underlying laminin surface (much like nerve regeneration along a basal lamina or columns of Schwann cells), would penetrate a suddenly imposed protein-*graft*-PEG matrix, protein-*graft*-PEG hydrogel was formed on top of neurites extending on a laminin-coated tissue-culture surface. As shown below (Figure 6.14), the neurite outgrowth was arrested after hydrogel formation, and cell death probably ensued soon after, because the entire DRG no longer remained attached to the laminin-covered surface (Figure 6.14 c). This observation raises the possibility that hydrogel formation in contact with DRG neurons causes neuronal cell death, which in turn triggers subsequent apoptosis, at least of neurons, in the entire DRG. Nutrient diffusion could not have been limiting in this system.

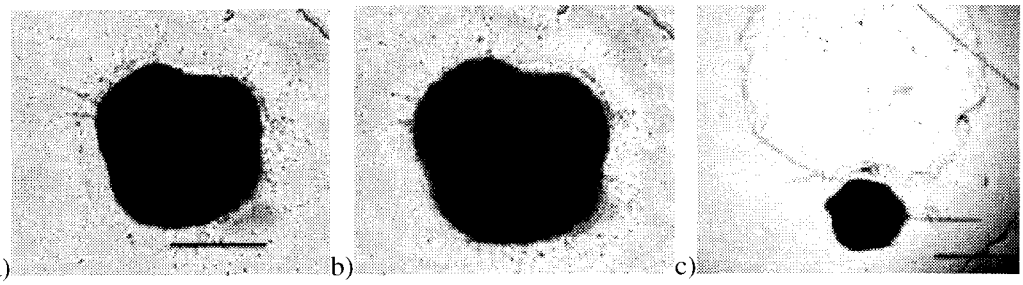

Figure 6.14: Arrest of Neurite Outgrowth After Hydrogel Formation in Contact with Chick Embryonic DRGs

DRG cultured on laminin-coated TCPS for one day, followed by protein-*graft*-PEG(3400) hydrogel formation (no additions) around the DRG, thus covering the neurites that had extended on the TCPS. a) On the day of gel formation, b) after 1 day (slightly magnified), and after 5 days of culture in NCM. (Scale bars = 300 μm and 600 μm)

Surface Neurite Outgrowth upon Protein-*graft*-PEG Hydrogels

Neurite-like extensions grew from surface-embedded embryonic chick DRGs on protein-*graft*-PEG hydrogels under various culture conditions (Figure 6.15.a,b). To verify that these extensions were axonal extensions expected of pseudo-unipolar sensory neurons present in DRGs,[129] immunohistochemistry was performed. The extensions immuno-stained positive for growth-associated protein-43, GAP-43, a neural-specific, intracellular phosphoprotein, also known as B-50, F1, pp46, p57 and neuromodulin, that is found exclusively in the peripheral and central nervous systems.[178] GAP-43 is a major protein of axonal growth cones[179] and in certain presynaptic terminals, but it is absent from dendritic growth cones.[180]

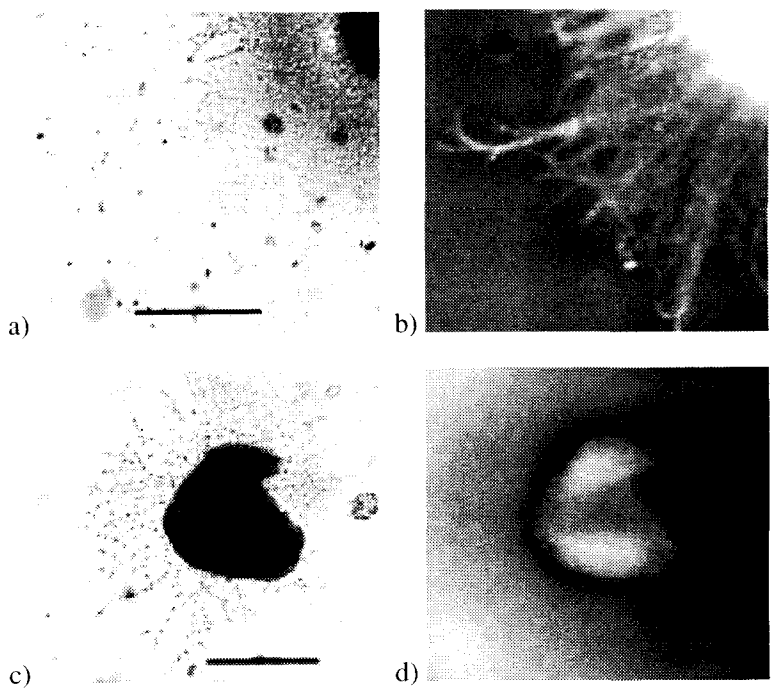

Figure 6.15: Anti-GAP-43 Immunostaining of Axonal (a and b) and Non-Axonal (c and d) Outgrowth

a) DRG, surface-embedded on a protein-*graft*-PEG hydrogel, with 2.83 mg/mL heparin (16-18 kDa) and 0.5 mg/mL hep.bind.-YIGSR peptide in the gel before gelation, on culture day 4. c) DRG fully embedded, but near the gel's top surface, in a protein-*graft*-PEG hydrogel with 2.83 mg/mL heparin (16-18 kDa) and 0.5 mg/mL hep.bind.-YIGSR peptide in the gel before gelation, on culture day 4. (Scale bars = 300 μm)

The positive stain for GAP-43 associated with the neurite-like extensions from chick DRGs (Figure 6.15.b) indicates that these extensions were indeed axonal extension from pseudo-unipolar sensory neurons present in DRGs.[129] When monoclonal anti-GAP-43 and secondary antibody were used to stain cellular outgrowth from DRGs under conditions that did not produce neurite-like extensions (Figure 6.15.c), only a weak fluorescent signal resulted that was associated with the body of the original DRG (Figure 6.15.d), indicating that, indeed, no axonal outgrowth had occurred. (In this case, the DRG had sunk too deeply into the protein-*graft*-PEGacrylate solution before gelation, so apparently only fibroblasts managed to emerge from the DRG onto the hydrogel surface.) Immunostains of chick DRGs cultured on laminin-coated TCPS served as positive controls for the presence and staining of GAP-43. As expected, only the neuritic extensions from the DRG stained positive (Figure 6.16.b), while neuronal support cells that had also migrated along with the neuritic extensions (Figure 6.16.a) did not stain positive for GAP-43 (Figure 6.16.b).

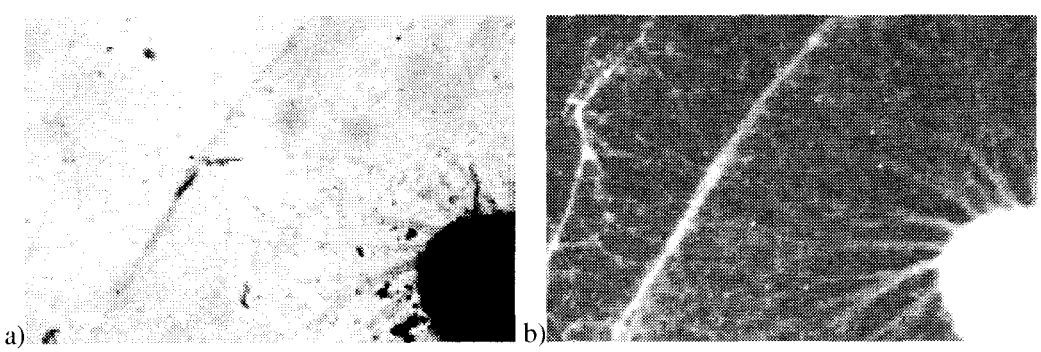

Figure 6.16: Anti-GAP-43 Immunostaining of Axonal Outgrowth Upon Laminin-Coated TCPS

DRG cultured on a laminin-coated surface for six days; fixed with formalin and immunostained against GAP-43. Note neuronal support cells in a) that did not stain positive for GAP-43.

Heparin-Dependence of Neurite Outgrowth upon Protein-*graft*-PEG Hydrogels

Based on Figure 6.17.a, surface neurite outgrowth seemingly required both heparin and hep.bind.-YIGSR to be bound to 10% *(m+v)* protein-*graft*-PEG(3400) hydrogel matrices. However, when incorporating heparin alone, surprisingly the same levels of

surface neurite outgrowth occurred as with hep.bind.-YIGSR. This clearly suggests that in this system the necessary factor in promoting neurite outgrowth was heparin, not the laminin-based hep.bind.-YIGSR peptide. The hep.bind.-YIGSR peptide, if biofunctional at all, even seemed to have a mildly inhibitory effect on neurite extension. This inhibitory effect could be due to competitive inhibition of neural adhesion by soluble YIGSR peptide that was not properly immobilized in the matrix via heparin. Alternatively, the inhibitory effect on neurite outgrowth could be due to an excessive concentration of hep.bind.-YIGSR peptide in the matrix. At excessive ligand concentrations, cell migration and neurite outgrowth can be inhibited, because cells and growth cones actually bind too strongly to their substrate.[181,182]

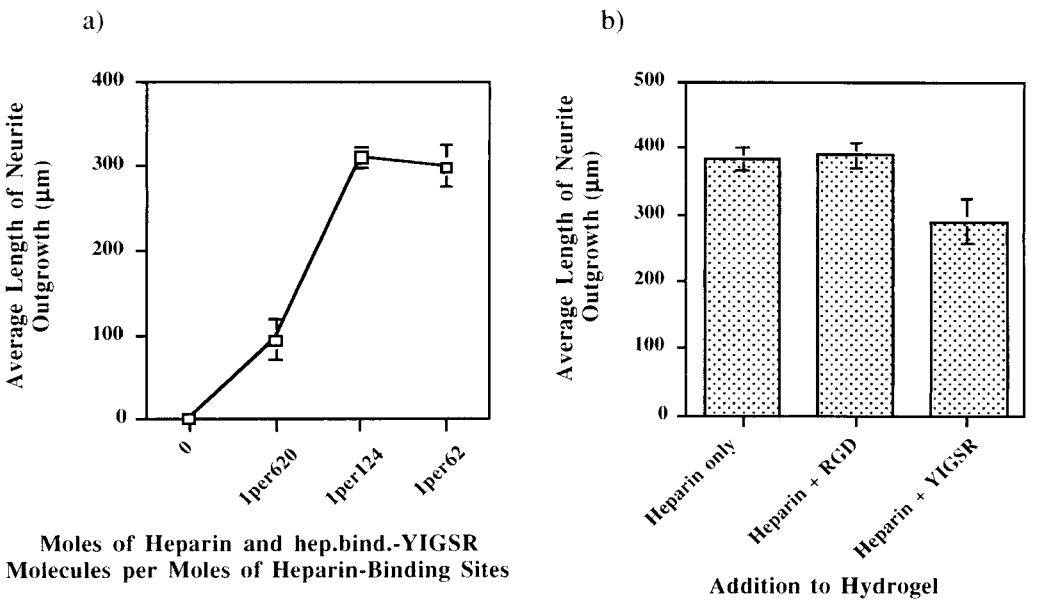

Figure 6.17: Heparin-Dependence of Axonal Outgrowth On the Surface of Protein-*graft*-PEG Hydrogels

a) Neurite outgrowth, after three days of culture, on protein-*graft*-PEG(3400) hydrogels as a function of heparin and hep.bind.-YIGSR concentration expressed in terms of heparin and hep.bind.-YIGSR molecules per number of heparin-binding sites in the hy drogels. The relevant factor in promoting the observed neurite outgrowth was heparin, not the hep.bind.-YIGSR peptide. b) Length of neurite outgrowth after three days with different additions to protein-*graft*-PEG(3400) hydrogels prior to gelation. Addition of heparin alone apears to be the relevant factor that enabled axonal outgrowth on hydrogels. (Added were 2.83 mg/mL heparin and equimolar amounts of hep.bind.-peptides, as indicated.)

Resolution of this issue hinges upon the results of anticipated release studies of hep.bind.-YIGSR peptide from protein-*graft*-PEG hydrogels. A combination of factors could explain why the addition of heparin to the protein-*graft*-PEG hydrogels promoted neurite extension. Bare protein-*graft*-PEG hydrogels only allow minimal or no protein adsorption due to their high PEG content, which is a constituent known to prevent protein adhesion in hydrogels and in surface-tethered forms.[128] (Recall the PEG-based, and therefore cell- and protein-adhesion resistant surfaces of Chapter 2.) Therefore, a protein-*graft*-PEG hydrogel constitutes a matrix containing only RGD adhesion sites, unless additional adhesion molecules and neuronal growth factors are actively immobilized by design, or are directly deposited by outgrowing neurons themselves. The addition and binding of heparin to the protein-*graft*-PEG matrix (see Chapter 4) provided binding sites for the exogenous hep.bind.-YIGSR adhesion peptide and, perhaps more importantly, for extracellular matrix components and growth factors secreted by cells present in DRGs. Although the hep.bind.-YIGSR peptide was either not successfully, or excessively, immobilized to matrix-bound heparin or was not functional for structural and/or accessibility reasons, matrix-bound heparin likely bound cell-secreted molecules to the hydrogel matrix, thus enabling outgrowth on a material that is otherwise non-adhesive, deficient, or for other reasons not supportive of axonal outgrowth.

In addition to heparin's role in immobilizing adhesion and growth factors in the hydrogel matrix, the rheological results with protein-*graft*-PEG(6000) hydrogels showed that heparin enhances the mechanical strength of the matrix presumably by virtue of its physical interactions with more than one heparin-binding site in the hydrogel. Hydrogels that exhibit better mechanical integrity are also likely to better support neurite extension, as cell attachment and deposition of extracellular matrix on a weak and flexible substrate are difficult.

Dependence of Neurite Outgrowth on Crosslink Density of Protein-*graft*-PEG Hydrogels

Although the mechanical properties of 10% (*m*+*v*) protein-*graft*-PEG(3400) and -PEG(6000) hydrogels did not seem to differ significantly (Chapter 4), Figure 7 shows a pronounced difference in the length of neurite outgrowth on protein-*graft*-PEG(3400) versus -PEG(6000) gels.

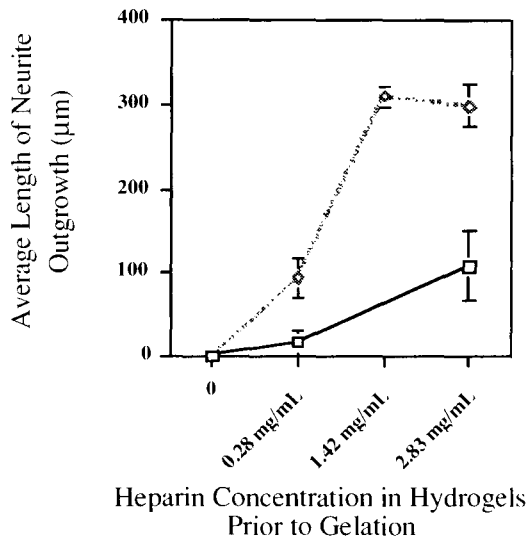

Figure 6.17: Effect of Hydrogel Crosslink Density on DRG Neurite Outgrowth

Difference in length of DRG neurite outgrowth on protein-*graft*-PEG(3400) [diamond] versus -PEG(6000) [square] hydrogels after three days of culture.

A likely explanation for the effect of PEG chain length on neurite outgrowth is that protein-*graft*-PEG(3400) hydrogels are expected to be more highly crosslinked, considering a theoretical acrylate concentration of ~11.3 mM at the time of crosslinking compared to only ~8.5 mM theoretical acrylates in the case of 10% (*m*+*v*) protein-*graft*-PEG(6000) gels. It appears that the difference in crosslink density and, therefore, subtle differences in network architecture facilitated better cell adhesion and/or extracellular matrix deposition on protein-*graft*-PEG(3400) gels than on protein-*graft*-PEG(6000) gels. Better and more abundant

matrix deposition onto protein-*graft*-PEG(3400) gels may also have resulted from the higher overall concentration of heparin binding sites, i.e., theoretically ~9.4 mM in PEG(3400) gels versus ~7.1 mM in PEG(6000) gels.

CONCLUSION

Three-dimensional neurite outgrowth could not be elicited within protein-*graft*-PEG hydrogels under the culture conditions and with the neural cell types that were tested. However, surface neurite outgrowth upon protein-*graft*-PEG matrices occurred under certain conditions.

When small amounts of heparin were added to protein-*graft*-PEG hydrogels (up to 1 molecule of heparin per 50 heparin-binding sites in the hydrogel), surprisingly the heparin promoted neurite outgrowth from chick DRGs and, thus, served as a tissue engineering tool toward better implant materials. In particular, the results in this chapter suggest that heparin bound to the hydrogel matrix by virtue of the ATIII-based heparin-binding site that the hydrogels contain. Heparin molecules that are thus immobilized in the matrix affected the physical properties and, arguably, the molecular structure of the protein-*graft*-PEG hydrogels. Furthermore, while other glycosaminoglycans (e.g., chondroitin sulfate)[55,54] directly inhibit neurite outgrowth, heparin can facilitate neurite outgrowth by binding relevant neuronal adhesion molecules, including laminin and fibronectin[183,184] as well as a number of heparin-binding growth factors. Therefore, when protein-*graft*-PEG hydrogels bind heparin, heparin in turn can serve as an anchor for such extracellular matrix proteins and/or growth factors which might otherwise diffuse away from the hydrogel.

In summary, on protein-*graft*-PEG hydrogels, surface outgrowth of axons from DRG neurons depended on heparin-content in the hydrogels. While further examination of the effect of heparin is under way, apparently heparin not only improves the mechanical properties of protein-*graft*-PEG hydrogels and thereby enables better neurite outgrowth,

but heparin may also serve as an anchor for neural adhesion and trophic factors relevant in neuronal attachment, survival, and outgrowth.

FUTURE WORK

In order to effect three-dimensional neurite outgrowth, it is necessary to know what exact conditions in two dimensions enable surface neurite outgrowth, while processes do not extend three-dimensionally. The possibility that enclosure in a gel and the resulting spatial arrest prevent outgrowth is one possible circumstance. A way to identify active inhibitory factors or mere limitations on outgrowth due to poor neuron-associated plasminolytic activity, and to lift possible diffusional limits on essential neuroactive molecules, is to assess neurite outgrowth inside porous protein-*graft*-PEG gels. For this, methods would have to be designed to pattern protein-*graft*-PEG gels three-dimensionally.

Furthermore, cellular staining techniques should be employed to assess the survival of neurons inside versus on protein-*graft*-PEG gels; and the presence, survival, and role of supporting cells in fully embedded versus surface-embedded DRGs should be further characterized. Supporting cells should be identified and their possible role at the front of two-dimensional neurite outgrowth be analysed, keeping in mind that supporting cells might well be the key to neurite outgrowth even in materials that favorably interact with neurons directly.

CHAPTER 7

SUMMARY, CONCLUSIONS, AND OUTLOOK

MATERIAL DEVELOPMENT

The key achievement in the work presented in this doctoral thesis was the creation of a novel and versatile class of biosynthetic materials: protein-*graft*-PEG hydrogels. During the development of this material, future variants of which can contain virtually unlimited biological functionality based on its protein component, several challenges had to be addressed that arose from the processing of proteins toward the goal of rendering them within a hydrogel matrix.

Protein Solubility and Oxidation State

For *in situ* applications in tissue repair, the protein-based precursor of protein-*graft*-PEG hydrogels had to exist in a water-soluble form. However, due to electrostatic, hydrophobic and covalent interactions proteins –including small oligopeptides– often coalesce and precipitate, making chemical modification of proteins difficult. In contrast to some native water-soluble proteins, this problem is even more pronounced in recombinant proteins that are not optimized for solubility or folded appropriately after recovery from their expression host. Even more problematic are cysteine-rich proteins, which may exist in a reduced form inside bacterial expression hosts, but are very prone to disulfide bonding during downstream processing.

These difficulties were solved in the case of protein-*graft*-PEG hydrogels by synthesizing PEGylated protein precursors whose thiols were used, and thus prevented from intermolecular disulfide bonding, as designated PEGylation sites. PEGylation, in turn, ensured good water solubility based on high-molecular-weight PEG's excellent solubility, high mobility, and large exclusion volume in water.[128] Transforming proteins

by PEGylation into hydrogel precursors is a powerful and necessary tool especially when incorporating hydrophobic protein constructs in a hydrogel matrix.

Before the PEGylation of protein pentamers, a crucial step toward obtaining protein-*graft*-PEG hydrogels was the reduction of protein thiols by TCEP, avoiding the use of thiol-containing reducing agents such as β-mercaptoethanol or DTT, which engage in mere thiol exchange and require repeated dialysed for –often incomplete– removal. The invaluable advantage of choosing TCEP as a reducing agent was that it liberates thiols, but is irreversibly consumed itself without introducing unwanted additional thiols into the system. The thiols that were reduced by TCEP are thus available instantly for further reaction without interference by the reducing agent itself.

Modification of Proteins by Michael-Type Conjugate Addition

Many protein modification schemes have either directly targeted, or inadvertently involved, protein primary amines (i.e., a protein's amine-terminus or amines found in lysine residues).[165,185] As elaborated in Chapter 4, this was successfully avoided in the PEGylation of protein pentamers [A] and [B], and their amine-related functions thus retained, by PEGylating via a Michael-type conjugate addition that consisted in the selective addition of protein thiols to PEG acrylate groups. To employ this Michael-type conjugate addition in order to PEGylate <u>any</u> protein or protein fragment of interest, protein thiols can be added by recombinant incorporation of cysteine residues in the protein.

Purification by Ni^{++}-Affinity Chromatography

Separation of protein-*graft*-PEGacrylate product from unreacted PEGdiacrylate after Michael-Type conjugate addition was necessary, because an excess of PEGdiacrylate was used during the PEGacrylation of protein pentamers to ensure complete PEGacrylation. Usually, separations of PEG from PEGylated product represent

formidable difficulties, but in the case of protein-*graft*-PEGacrylate the hexa-histidine tag, which had already served in the purification of protein pentamers from bacterial lysate and in their immobilization on Nickel-coated tissue culture wells, also enabled purification of the PEGacrylated protein. The hexa-histidine tag, therefore, proved to be an extremely fortunate addition to protein pentamers [A] and [B].

In situ Photogelation

The photochemistry used for the crosslinking of protein-*graft*-PEGacrylate involved non-toxic initiators, generated little heat, and –even when performed in direct contact with actual or model tissue– caused no apparent cell death, e.g., by radical transfer to cellular membrane proteins. Furthermore, crosslinking only required initiation with visible light at low intensity, and complete gelation of protein-*graft*-PEGacrylate solutions occurred at a sufficiently rapid rate. Therefore, crosslinking *in situ* should be feasible in surgical contexts even when time limitations are of major concern.

In summary, this research has defined and optimized a set of tools for designing and expressing recombinant proteins with intermittent, thiol-containing cysteines; for selective PEGacrylation of these thiols via Michael-type conjugate addition; for purification of the PEGacrylated proteins by Ni^{++}-affinity chromatography; and for the rapid, *in situ* formation of protein-*graft*-PEG hydrogels by photocrosslinking.

The successful creation of prototypic protein[A]-*graft*-PEG hydrogels promises that many other protein domains can be combined and rendered in a similar hydrogel form toward the repair of specific target tissues or toward applications beyond tissue repair such as biosensors, "self-cleaning" (proteolytically active) contact lenses, or other implantable devices.

MATERIAL PROPERTIES

Physical Properties

Protein-*graft*-PEG hydrogels fulfill the majority of physical requirements postulated in Chapter 2 for a matrix intended for implantation and tissue repair:

5. Protein-*graft*-PEG hydrogels represent a homogeneous, highly crosslinked matrix whose mechanical strength was sufficient to support cell attachment and migration. While non-covalent crosslinking schemes are conceivable (e.g., based on hydrophobic interactions or ionic linkers), in protein-*graft*-PEG hydrogels covalent photocrosslinking was the key feature that enabled rapid formation and ensured sufficient mechanical strength of this highly hydrated system containing flexible PEG chains grafted onto a protein core.
6. Aqueous solutions of protein-*graft*-PEGacrylate can be coated or injected into a medical device (such as a nerve guidance channel) or pasted directly onto the site of an injury (such as the severed nerve endings after peripheral nerve transection) and then be transformed to a solid state under physiological conditions. Liquid-to-solid transformation of a material *in situ* is desirable in applications of the material as a scaffold for tissue regeneration, because the matrix will conform perfectly to the micromorphology of adjacent tissues, avoiding spaces and gaps that might fill with unwanted ECM molecules or scar tissue. Also, liquid-to-solid transformation and perfect morphological conformity of the matrix enable its use as a resorbable sealant (e.g., for the nerve guide openings).
7. Protein-*graft*-PEG hydrogels were transparent and, therefore, allowed microscopic analysis of three-dimensional cell cultures. The high water content of PEG matrices and their homogeneous sub-micron architecture may account for this feature.

Biofunctional Features

Even more important in a material intended for implantation and tissue repair are its biological characteristics and functions:

8. To impart biological function to the protein-*graft*-PEG hydrogels, minimal functional protein elements were assembled by recombinant DNA techniques and the target protein bacterially expressed. Thus, the protein constituent of the matrix as well as PEG, the synthetic polymer precursor, are artificial. By avoiding animal- and human donor-derived materials, the complexities and risks associated with non-autologous tissue products were avoided.
9. Protein-*graft*-PEG hydrogels' principal constituent, protein-*graft*-hexaPEGacrylate, as well as the hydrogels' degradation products appeared to be non-toxic in contact with model tissue, hFF-fibrin clusters, as well as embryonic chick DRGs. However, it remains to be tested whether the matrices' degradation products are systemically non-toxic and non-immunogenic *in vivo*. To minimize the potential for immunogenicity, the core protein sequence was based on human protein sequences, and poly(ethylene glycol) was chosen as the bulk constituent because of its well-established immunocompatibility.[128]
10. Integrin-mediated hFF attachment and three-dimensional cell migration inside the protein-*graft*-PEG matrices was achieved by incorporating the RGD motif as a permanent element of the matrix. Immobilization of heparin led to surface neurite outgrowth on protein-*graft*-PEG matrices. Most likely, neuroactive adhesion- and/or trophic factors from the culture medium, or substances secreted by cells, bound to the heparin and, thus, stimulated neurite extension onto the otherwise non-permissive matrix.

11. Protein-*graft*-PEG matrices were degradable by plasmin *in vitro*, and by cell-associated enzymatic activity *in vivo*, both by virtue of plasmin-degradation sites that were part of the matrices by design.

MATERIAL IMPROVEMENTS AND FUTURE APPLICATIONS

Material Improvements

To avoid photochemical crosslinking of protein-*graft*-PEGacrylate, which involves light-induced radical polymerization, a small dithiol-containing crosslinking agent such as PEG dithiol, HS-PEG-SH, might prove feasible to form a hydrogel network with protein-*graft*-PEGacrylate *in situ*. The hope is that both thiols react with terminal acrylates of different protein-*graft*-PEGacrylate molecules and thus link them. Many such Michael-type conjugate additions would lead to a crosslinked network under the same benign conditions under which photocrosslinking was performed, albeit probably slower, but without the occurrence of any radical species.

Another potential material deficiency of the protein-*graft*-PEG hydrogels might be bulk hydrolytic degradation (at the acrylate esters), although relative to enzymatic degradation, hydrolysis is probably insignificant under physiological conditions. Should it nevertheless be desirable to preclude potential bulk hydrolysis of the protein-*graft*-PEG hydrogels, core proteins could be PEGylated by Michael-type conjugate addition to PEG divinylsulfone,[159] whose functional end groups are much less prone to hydrolysis, so that the resulting hydrogels would be degradable by enzymatic processes only. However, photocrosslinking as described in Chapter 4 does not work with vinylsulfone-terminated protein-*graft*-PEG. Therefore, possible alternative photochemical schemes would have to be identified, or protein-*graft*-PEGvinylsulfones would have to be crosslinked by HS-PEG-SH, for example, at the expense of crosslinking speed. PEG divinylsulfone-based

hydrogels, crosslinked by multithiol-containing oligopeptides, are currently under investigation by Hubbell *et al.*

Arguably the most serious deficiency of protein-*graft*-PEG hydrogels is the difficulty of micropatterning, which is desirable in some scaffolds for the engineering of artificial organs, and which some researchers consider necessary for better and faster functional regeneration of severed peripheral nerves.[4] Proposing ways to produce patterned protein-*graft*-PEG hydrogels is beyond the scope of this doctoral thesis. Likewise, in the context of nerve regeneration, it was not one of the design goals for protein-*graft*-PEG matrices to contain inherent structural clues that facilitate proper path finding and correct nerve cable connections when the regenerating axons reach the distal nerve stump. The hope is that even unguided distal stump invasion and eventual target re-innervation, combined with axonal plasticity in the periphery and in the brain, will eventually lead to satisfactory functional recovery.

Biological Considerations

Although no three-dimensional neurite outgrowth was observed in protein[A]-*graft*-PEG hydrogels, the fact that hFFs invaded this biosynthetic material was still promising of its potential as a matrix to promote nerve regeneration. If hFFs infiltrated the material, the right combinantion of adhesive and neuroinductive signals might enable neurite ingrowth into future variants of protein[A]-*graft*-PEG hydrogels. One way of modifying present protein[A]-*graft*-PEG hydrogels is by using the heparin-bridging scheme to present additional adhesion- and/or growth factors. Studies are in progress to get a clearer understanding and better control over heparin-mediated immobilization of additional factors in the material.

Another way of creating an environment conducive to nerve regeneration is to pre-seed protein-*graft*-PEG hydrogels with suitable autologous support cells, in particular

Schwann cells, that secrete relevant ECM adhesion molecules and growth factors, and that promote neurite extension directly by engaging neurites in intercellular adhesions. Alternatively, stem cells that develop into such support cells should be considered as a way to avoid sacrificing a patient's functional and mature nervous tissue. Protein-*graft*-PEG hydrogels might prove to be useful matrices for the delivery of stem cells that differentiate in response to local stimuli at the site of implantation.

As far as the material design is concerned, as long as uncertainty remains about the usefulness (and choice) of minimal neuroactive oligopeptides (Figure 6.17) which might or might not actually be immobilized in the hydrogels via heparin, additional neuroactive domains could however be incorporated into the protein backbone of protein-*graft*-PEG hydrogels in hopes of promoting neurite outgrowth three-dimensionally.

As an alternative to immobilization of neuroactive signals via a "heparin bridge," neuroadhesive domains could be coupled to a heparin analogue. Such a *heparin analogue-coupled neuroactive factor* would in theory bind directly to the heparin-binding sites of protein-*graft*-PEG hydrogels, and could thus be immobilized inside the hydrogels without the need for a "heparin bridge." This would constitute a more direct immobilization scheme than the one chosen in this study (Figure 6.1), and it would avoid the need for one of the original design's two binding interactions. In fact, if a proven immobilization scheme can be established, adhesion sites in the backbone become dispensable, as any signal of choice could be delivered by coupling it to a heparin analogue followed by direct binding to exclusively heparin-binding protein-*graft*-PEG hydrogels. Future studies will show whether incorporation of adhesion signals into the backbone or whether the more flexible scheme of immobilizing biological factors via binding to the gels' heparin-binding sites will be more successful in promoting neurite extension.

In summary, since the protein-*graft*-PEG material described in this doctoral thesis fulfilled some essential requirements toward functioning as a matrix for nerve regeneration, such as suitable physical properties, apparent lack of local toxicity, cell adhesivity, proteolytic degradability, and ease of handling, the hope is that possible future experiments will prove the material's successful performance in supporting improved nerve repair *in vivo*. Toward this end, it might prove conducive to incorporate or immobilize additional adhesion and/or growth factors, and it might be helpful or even necessary to pre-seed the matrix with suitable supporting cells, such as autologous Schwann cells or neural stem cells.

Versatility of Protein-*graft*-PEG Hydrogels

In closing, it is worth to re-emphasize protein-*graft*-PEG hydrogels' very versatile nature that stems from the exchangeable protein elements that lie at the matrices' core. Any protein fragment, provided that it remains or becomes water soluble after PEGacrylation, can be rendered in a hydrogel form and thus impart its function to the matrix of which it has become a part. Different protein components with different adhesive or degradative specificities can be incorporated in hydrogels to promote regeneration of specific target tissues, the difference to oligopeptide-based hydrogels being that much more complex and complete biological functionality can potentially be harnessed. Given the possibility to incorporate an amount and variety of biological information only limited by Nature's own repertoire, perhaps future protein-*graft*-PEG hydrogels –possibly patterned– even hold promise as three-dimensional scaffolds for the manufacture of entire artificial organs grown from differentiated donor cells or stem cells. This was foreshadowed when fibroblasts -as a model cell type for ingrowth into protein-*graft*-PEG hydrogels- attached to, migrated within, apparently proliferated in, and eventually completely colonized the matrix (Figure 5.10, Chapter 5).

REFERENCES

1. Archibald, S. J., Krarup, C., Shefner, J., Li, S. T., and Madison, R. D. (1991). A collagen-based nerve guide conduit for peripheral nerve repair: an electrophysiological study of nerve regeneration in rodents and nonhuman primates. J. Comp. Neurol. **306**, 685-96.

2. Seckel, B. R. (1990). Enhancement of peripheral nerve regeneration. Muscle Nerve **13**, 785-800.

3. Kakinoki, R., Nishijima, N., Ueba, Y., Oka, M., Yamamuro, T., and Nakamura, T. (1998). Nerve regeneration over a 20-mm gap through a nerve conduit containing blood vessels in rats: the influence of interstump distance on nerve regeneration. J. Neurosurg. Sci. **42**, 11-21.

4. Navarro, X. (2001). (by personal communication).

5. Horowitz, B., Prince, A. M., Horowitz, M. S., and Watklevicz, C. (1993). Viral safety of solvent-detergent treated blood products. Dev. Biol. Stand. **81**, 147-61.

6. Kjaergard, H. K., and Weis-Fogh, U. S. (1994). Autologous fibrin glue for sealing vascular prostheses of high porosity. Cardiovasc. Surg. **2**, 45-7.

7. Fawcett, J. W., and Keynes, R. J. (1990). Peripheral Nerve Regeneration. Annu. Rev. Neurosci. **13**, 43-60.

8. Nathaniel, E. J., and Pease, D. C. (1963). Degenerative changes in rat dorsal roots during Wallerian degeneration. J. Ultrastruct. Res. **9**, 511-532.

9. Sunderland, S., and Bradley, K. C. (1952). Perineurium of peripheral nerves. Anat. Res. **113**, 125-141.

10. Thomas, P. K. (1963). The connective tissue of peripheral nerve: an electron microscope study. J. Anat. **97**, 35-44.

11. Bunge, R. P., and Bunge, M. B. (1983). Interactions between Schwann cell function and extracellular matrix production. Trends Neurosci. **7**, 499-505.

12. Cornbrooks, C. J., Carey, D. J., McDonald, J. A., Timple, R., and Bunge, R. P. (1983). In vivo and in vitro observations on laminin production by Schwann cells. Proc. Natl. Acad. Sci. USA **80**, 3850-3854.

13. Foehring, R. C., Sypert, G. W., and Munson, J. B. (1986). Properties of self-reinnervated motor units of medial gastrocnemius of cat. II. Axotomized motoneurons and time course of recovery. J. Neurophysiol. **55**, 947-65.

14. Gordon, T. (1983). Dependence of peripheral nerves on their target organs. *In:* Somatic and Autonomic Nerve-Muscle Interactions, G. Burnstock, R. A. O'Brien and G. Vrbov'a, eds. (Amsterdam: Elsevier), pp. 289-325.

15. Kuno, M., Miyata, Y., and Munoz-Martinez, E. J. (1974). Differential reaction of fast and slow alpha-motoneurones to axotomy. J. Physiol. **240**, 725-39.

16. Smith, P. A., Shapiro, J., Gurtu, S., Kelly, M. E. M., and Gordon, T. (1988). The response of ganglionic neurons to axotomy. *In:* Neurology and Neurobiology. The Current Status of Peripheral Nerve Regeneration, T. Gordon, R. B. Stein and P. A. Smith, eds. (New York: Alan R. Liss), pp. 15-23.

17. Ebadi, M., Bashir, R. M., Heidrick, M. L., Hamada, F. M., Refaey, H. E., Hamed, A., Helal, G., Baxi, M. D., Cerutis, D. R., and Lassi, N. K. (1997). Neurotrophins and their receptors in nerve injury and repair. Neurochem. Int. **30**, 347-74.

18. Lewin, G. R., and Barde, Y. A. (1996). Physiology of the neurotrophins. Annu. Rev. Neurosci. **19**, 289-317.

19. Davies, A. M. (1994). The role of neurotrophins in the developing nervous system. J. Neurobiol. **25**, 1334-48.

20. Jessell, T. M. (1991). Cell Migration and Axon Guidance. *In:* Princliples of Neural Science, Third Edition, E. R. Kandel, J. H. Schwartz and T. M. Jessell, eds. (Norwalk: Appleton & Lange), pp. 908-928.

21. Nicholls, J. G., Martin, A. R., and Wallace, B. G. (1992). From neuron to brain. *In:* Neuronal development and the formation of synaptic connections (Sunderland, Massachusetts: Sinauer Associates, Inc.), pp. 339-387.

22. Daniloff, J. K., Levi, G., Grumet, M., Rieger, F., and Edelman, G. M. (1986). Altered expression of neuronal cell adhesion molecules induced by nerve injury and repair. J. Cell Biol. **103**, 929-45.

23. Martini, R., and Schachner, M. (1988). Immunoelectron microscopic localization of neural cell adhesion molecules (L1, N-CAM, and myelin-associated glycoprotein) in regenerating adult mouse sciatic nerve. J. Cell Biol. **106**, 1735-46.

24. Previtali, S. C., Feltri, M. L., Archelos, J. J., Quattrini, A., Wrabetz, L., and Hartung, H. (2001). Role of integrins in the peripheral nervous system. Prog. Neurobiol. **64**, 35-49.

25. Ruoslahti, E., and Pierschbacher, M. D. (1986). Arg-Gly-Asp: a versatile cell recognition signal. Cell **44**, 517-8.

26. Tashiro, K., Sephel, G. C., Greatorex, D., Sasaki, M., Shirashi, N., Martin, G. R., Kleinman, H. K., and Yamada, Y. (1991). The RGD containing site of the mouse laminin A chain is active for cell attachment, spreading, migration and neurite outgrowth. J. Cell Physiol. **146**, 451-9.

27. Venstrom, K. A., and Reichardt, L. F. (1993). Extracellular Matrix 2: Role of extracellular matrix molecules and their receptors in the nervous system. FASEB J. **7**, 996-1003.

28. Neugebauer, K. M., Emmett, C. J., Venstrom, K. A., and Reichardt, L. F. (1991). Vitronectin and thrombospondin promote retinal neurite outgrowth: developmental regulation and role of integrins. Neuron **6**, 345-58.

29. Mecham, R. P. (1991). Receptors for laminin on mammalian cells. FASEB J. **5**, 2538-2546.

30. Graf, J., Ogle, R. C., Robey, F. A., Sasaki, M., Martin, G. R., Yamada, Y., and Kleinman, H. K. (1987). A pentapeptide from the laminin B1 chain mediates cell adhesion and binds the 67,000 laminin receptor. Biochemistry **26**, 6896-900.

31. Graf, J., Iwamoto, Y., Sasaki, M., Martin, G. R., Kleinman, H. K., Robey, F. A., and Yamada, Y. (1987). Identification of an amino acid sequence in laminin mediating cell attachment, chemotaxis, and receptor binding. Cell **48**, 989-96.

32. Charonis, A. S., Skubitz, A. P., Koliakos, G. G., Reger, L. A., Dege, J., Vogel, A. M., Wohlheuter, R., and Furcht, L. T. (1988). A novel synthetic peptide of the B1 chain of laminin with heparin-binding and cell adhesion-promoting activities. J. Cell Biol. **107**, 1253-1260.

33. Tashiro, K., Sephel, G. C., Weeks, B., Sasaki, M., Martin, G. R., Kleinman, H. K., and Yamada, Y. (1989). A synthetic peptide containing the IKVAV sequence in the A chain of laminin mediates cell attachment, migration, and neurite outgrowth. J. Biol. Chem. **264**, 16174-16182.

34. Sephel, G. C., Tashiro, K., Sasaki, M., Kandel, S., Yamada, Y., and Kleinman, H. K. (1989). A laminin-pepsin fragment with cell attachment and neurite outgrowth activity at distinct sites. Dev. Biol. **135**, 172-81.

35. Sephel, G. C., Tashiro, K. I., Sasaki, M., Greatorex, D., Martin, G. R., Yamada, Y., and Kleinman, H. K. (1989). Laminin A chain synthetic peptide which supports neurite outgrowth. Biochem. Biophys. Res. Commun. **162**, 821-9.

36. Kleinman, H. K., Ogle, R. C., Cannon, F. B., Little, C. D., Sweeney, T. M., and Luckenbill-Edds, L. (1988). Laminin receptors for neurite formation. Proc. Natl. Acad. Sci. USA **85**, 1282-1286.

37. Douville, P. J., Harvey, W. I., and Carbonetto, S. (1988). Isolation and partial characterization of high affinity laminin receptors in neural cells. J. Biol. Chem. **263**, 14964-14969.

38. Kleinman, H. K., Weeks, B. S., Cannon, F. B., Sweeney, T. M., Sephel, G. C., Clement, B., Zain, M., Olson, M. O., Jucker, M., and Burrous, B. A. (1991). Identification of a 110-kDa nonintegrin cell surface laminin-binding protein which recognizes an A chain neurite-promoting peptide. Arch. Biochem. Biophys. **290**, 320-325.

39. Jucker, M., Walker, L. C., Kibbey, M. C., Kleinman, H. K., and Ingram, D. K. (1993). Localization of a Laminin-Binding Protein in Brain. Neuroscience **56**, 1009-1022.

40. Luckenbill-Edds, L., Kaiser, C. A., Rodgers, T. R., and Powell, D. D. (1995). Localization of the 110 kDa receptor for laminin in brains of embryonic and postnatal mice. Cell Tissue Res. **279**, 371-377.

41. Kleinman, H. K., Graf, J., Iwamoto, Y., Sasaki, M., Schasteen, C. S., Yamada, Y., Martin, G. R., and Robey, F. A. (1989). Identification of a second active site in laminin for promotion of cell adhesion and migration and inhibition of in vivo melanoma lung colonization. Arch. Biochem. Biophys. **272**, 39-45.

42. Massia, S. P., Rao, S. S., and Hubbell, J. A. (1993). Covalently immobilized laminin peptide Tyr-Ile-Gly-Ser-Arg (YIGSR) supports cell spreading and co-localization of the 67-kilodalton laminin receptor with alpha-actinin and vinculin. J. Biol. Chem. **268**, 8053-9.

43. Clemence, J. F., Ranieri, J. P., Aebischer, P., and Sigrist, H. (1995). Photoimmobilization of a bioactive laminin fragment and pattern-guided selective neuronal cell attachment. Bioconjug. Chem. **6**, 411-7.

44. Matsuzawa, M., Weight, F. F., Potember, R. S., and Liesi, P. (1996). Directional neurite outgrowth and axonal differentiation of embryonic hippocampal neurons are promoted by a neurite outgrowth domain of the B2-chain of laminin. Int. J. Dev. Neurosci. **14**, 283-295.

45. Reichardt, L. F., and Tomaselli, K. J. (1991). Extracellular Matrix Molecules and Their Receptors: Functions in Neural Development. Annu. Rev. Neurosci. **14**, 531-70.

46. Martini, R. (1994). Expression and functional roles of neural cell surface molecules and extracellular matrix components during development and regeneration of peripheral nerves. J. Neurocytology **23**, 1-28.

47. Davis, G. E., Klier, F. G., Engvall, E., Cornbrooks, C., Varon, S., and Manthorpe, M. (1987). Association of Laminin with Heparin and Chondroitin Sulfate-bearing Proteoglycans in Neurite-promoting Factor Complexes from Rat Schwannoma Cells. Neurochem. Res. **12**, 909-921.

48. Skubitz, A. P. N., McCarthy, J. B., Charonis, A. S., and Furcht, L. T. (1988). Localization of Three Distinct Heparin-binding Domains of Laminin by Monoclonal Antibodies. J. Biol. Chem. **263**, 4861-4868.

49. Jackson, R. L., Busch, S. J., and Cardin, A. D. (1991). Glycosaminoglycans: molecular properties, protein interactions, and role in physiological processes. Physiol. Rev. **71**, 481-539.

50. Tessler, S., Rockwell, P., Hicklin, D., Cohen, T., Levi, B. Z., Witte, L., Lemischka, I. R., and Neufeld, G. (1994). Heparin modulates the interaction of VEGF165 with soluble and cell associated flk-1 receptors. J. Biol. Chem. **269**, 12456-61.

51. Hantaz-Ambroise, D., Vigny, M., and Koenig, J. (1987). Heparan sulfate proteoglycan and laminin mediate two different types of neurite outgrowth. J. Neurosci. **7**, 2293-304.

52. Hayashi, K., Madri, J. A., and Yurchenco, P. D. (1992). Endothelial cells interact with the core protein of basement membrane perlecan through beta 1 and beta 3 integrins: an adhesion modulated by glycosaminoglycan. J. Cell. Biol. **119**, 945-59.

53. Perris, R., and Johansson, S. (1990). Inhibition of neural crest cell migration by aggregating chondroitin sulfate proteoglycans is mediated by their hyaluronan-binding region. Dev. Biol. **137**, 1-12.

54. Oohira, A., Matsui, F., and Katoh-Semba, R. (1991). Inhibitory effects of brain chondroitin sulfate proteoglycans on neurite outgrowth from PC12D cells. J. Neurosci. **11**, 822-7.

55. Snow, D. M., Lemmon, V., Carrino, D. A., Caplan, A. I., and Silver, J. (1990). Sulfated proteoglycans in astroglial barriers inhibit neurite outgrowth in vitro. Exp. Neurol. **109**, 111-30.

56. Ferguson, T. A., and Muir, D. (2000). MMP-2 and MMP-9 increase the neurite-promoting potential of schwann cell basal laminae and are upregulated in degenerated nerve. Mol. Cell. Neurosci. **16**, 157-67.

57. Ruoslahti, E. (1989). Proteoglycans in cell regulation. J. Biol. Chem. **264**, 13369-72.

58. Siconolfi, L. B., and Seeds, N. W. (2001). Induction of the plasminogen activator system accompanies peripheral nerve regeneration after sciatic nerve crush. J. Neurosci. **21**, 4336-47.

59. Siconolfi, L. B., and Seeds, N. W. (2001). Mice lacking tPA, uPA, or plasminogen genes showed delayed functional recovery after sciatic nerve crush. J. Neurosci. **21**, 4348-55.

60. Hantgan, R. R., Francis, C. W., and Marder, V. J. (1994). Fibrinogen Structure and Physiology. *In:* Hemostasis and Thrombosis: Basic Principles and Clinical Practice, Third Edition, R. W. Colman, J. Hirsh, V. J. Marder and E. W. Salzman, eds. (Philadelphia: J. B. Lippincott Company), pp. 277-300.

61. Estreicher, A., Wohlwend, A., Belin, D., Schleuning, W., and Vassalli, J. (1989). Characterization of the cellular binding site for the urokinase type plasminogen activator. J. Biol. Chem. **264**, 1180-1189.

62. Pittman, R., Ivins, J., and Buettner, H. (1989). Neuronal plasminogen activators: cell surface binding sites and involvement in neurite outgrowth. J. Neurosci. **9**, 4269-4286.

63. Hafteck, J., and Thomas, P. K. (1968). Electron-microscope observations on the effects of localized crush injuries on the connective tissues of peripheral nerve. J. Anat. **103**, 233-243.

64. Kimmel, D. I., and Moyer, E. K. (1947). Dorsal roots following anastomosis of the central stumps. J. Comp. Neurol. **87**, 289-319.

65. Fine, E. G., Valentini, R. F., and Aebischer, P. (2000). Nerve Regeneration. *In:* Principles of Tissue Engineering, R. P. Lanza, R. Langer and J. Vacanti, eds.: Academic Press), pp. 785-798.

66. Sunderland, S. (1991). Nerve Injuries and Their Repair (London: Churchill-Livingstone).

67. Krause, T. L., and Bittner, G. D. (1990). Rapid morphological fusion of severed myelinated axons by polyethylene glycol. Proc. Natl. Acad. Sci. USA **87**, 1471-1475.

68. Lore, A. B., Hubbell, J. A., Bobb, D. S., Jr., Ballinger, M. L., Loftin, K. L., Smith, J. W., Smyers, M. E., Garcia, H. D., and Bittner, G. D. (1999). Rapid induction of functional and morphological continuity between severed ends of mammalian or earthworm myelinated axons. J. Neurosci. **19**, 2442-54.

69. Suematsu, N. (1989). Tubulation for peripheral nerve gap: its history and possibility. Microsurgery **10**, 71-74.

70. Williams, L. R., Danielsen, N., Müller, H., and Varon, S. (1988). Influence of the acellular fibrin matrix on nerve regeneration success within the silicone chamber model. *In:* Neurology and Neurobiology. The Current Status of Peripheral Nerve Regeneration, T. Gordon, R. B. Stein and P. A. Smith, eds. (New York: Alan R. Liss), pp. 111-122.

71. Aebischer, P., Guenard, V., and Valentini, R. F. (1990). The morphology of regenerating peripheral nerves is modulated by the surface microgeometry of polymeric guidance channels. Brain Res. **531**, 211-8.

72. Valentini, R. F., and Aebischer, P. (1993). The role of materials in designing nerve guidance channels and chronic neural interfaces. *In:* Robotics and Biological Systems: Towards a New Bionics?, P. Dario, G. Sandini and P. Aebischer, eds. (New York: Springer Verlag), pp. 625-636.

73. Aebischer, P., Guenard, V., and Brace, S. (1989). Peripheral nerve regeneration through blind-ended semipermeable guidance channels: effect of the molecular weight cutoff. J. Neurosci. **9**, 3590-5.

74. den Dunnen, W. F. A., van der Lei, B., Robinson, P. H., Holwerda, A., Pennings, A. J., and Schakenraad, J. M. (1995). Biological performance of a degradable poly(lactic acid-ε-caprolactone) nerve guide: Influence of tube dimensions. J. Biomed. Mat. Res. **29**, 757-766.

75. Fansa, H., Keilhoff, G., Wolf, G., and Schneider, W. (2001). Tissue engineering of peripheral nerves: A comparison of venous and acellular muscle grafts with cultured Schwann cells. Plast. Reconstr. Surg. **107**, 485-94; discussion 495-6.

76. Stensaas, L., Bloch, L. M., Garcia, R., and Sotelo, J., Jr. (1989). Snug tubular enclosures reduce extrafascicular axonal escape at peripheral nerve repair sites. Exp. Neurol. **103**, 135-45.

77. Bouhadir, K. H., Lee, K. Y., Alsberg, E., Damm, K. L., Anderson, K. W., and Mooney, D. J. (2001). Degradation of partially oxidized alginate and its potential application for tissue engineering. Biotechnol. Prog. **17**, 945-50.

78. Williams, L. R., Danielsen, N., Muller, H., and Varon, S. (1987). Exogenous matrix precursors promote functional nerve regeneration across a 15-mm gap within a silicone chamber in the rat. J. Comp. Neurol. **264**, 284-290.

79. Ahmed, Z., Underwood, S., and Brown, R. A. (2000). Low concentrations of fibrinogen increase cell migration speed on fibronectin/fibrinogen composite cables. Cell Motil. Cytoskeleton **46**, 6-16.

80. Underwood, S., Afoke, A., Brown, R. A., MacLeod, A. J., Shamlou, P. A., and Dunnill, P. (2001). Wet extrusion of fibronectin-fibrinogen cables for application in tissue engineering. Biotechnol. Bioeng. **73**, 295-305.

81. Madison, R. D., da Silva, C., Dikkes, P., Sidman, R. L., and Chiu, T. H. (1987). Peripheral nerve regeneration with entubulation repair: comparison of biodegradeable nerve guides versus polyethylene tubes and the effects of a laminin-containing gel. Exp. Neurol. **95**, 378-90.

82. Madison, R. D., Da Silva, C. F., and Dikkes, P. (1988). Entubulation repair with protein additives increases the maximum nerve gap distance successfully bridged with tubular prostheses. Brain Res. **447**, 325-34.

83. Keynes, R. J., Hopkins, W. G., and Huang, L. H. (1984). Regeneration of mouse peripheral nerves in degenerating skeletal muscle: guidance by residual muscle fibre basement membrane. Brain Res. **295**, 275-81.

84. Fawcett, J. W., and Keynes, R. J. (1986). Muscle basal lamina: a new graft material for peripheral nerve repair. J. Neurosurg. **65**, 354-63.

85. Glasby, M. A., Gschmeissner, S. G., Hitchcock, R. J., and Huang, C. L. (1986). The dependence of nerve regeneration through muscle grafts in the rat on the availability and orientation of basement membrane. J. Neurocytol. **15**, 497-510.

86. Feneley, M. R., Fawcett, J. W., and Keynes, R. J. (1991). The role of Schwann cells in the regeneration of peripheral nerve axons through muscle basal lamina grafts. Exp. Neurol. **114**, 275-85.

87. Matsumoto, K., Ohnishi, K., Kiyotani, T., Sekine, T., Ueda, H., Nakamura, T., Endo, K., and Shimizu, Y. (2000). Peripheral nerve regeneration across an 80-mm gap bridged by a polyglycolic acid (PGA)-collagen tube filled with laminin-coated collagen fibers: a histological and electrophysiological evaluation of regenerated nerves. Brain Res. **868**, 315-328.

88. Schense, J. C., Bloch, J., Aebischer, P., and Hubbell, J. A. (2000). Enzymatic incorporation of bioactive peptides into fibrin matrices enhances neurite extension. Nature Biotechnol. **18**, 415-9.

89. Sakiyama-Elbert, S. E., and Hubbell, J. A. (2000). Development of fibrin derivatives for controlled release of heparin- binding growth factors. J. Control. Release **65**, 389-402.

90. Sakiyama-Elbert, S. E., and Hubbell, J. A. (2000). Controlled release of nerve growth factor from a heparin-containing fibrin-based cell ingrowth matrix. J. Control. Release **69**, 149-58.

91. Sakiyama-Elbert, S. E., Panitch, A., and Hubbell, J. A. (2001). Development of growth factor fusion proteins for cell-triggered drug delivery. FASEB J. **15**, 1300-2.

92. Guenard, V., Kleitman, N., Morrissey, T. K., Bunge, R. P., and Aebischer, P. (1992). Syngeneic Schwann cells derived from adult nerves seeded in semipermeable guidance channels enhance peripheral nerve regeneration. J. Neurosci. **12**, 3310-20.

93. Rodriguez, F. J., Verdu, E., Ceballos, D., and Navarro, X. (2000). Nerve guides seeded with autologous schwann cells improve nerve regeneration. Exp. Neurol. **161**, 571-84.

94. Meyer, M., Matsuoka, I., Wetmore, C., Olson, L., and Thoenen, H. (1992). Enhanced synthesis of brain-derived neurotrophic factor in the lesioned peripheral nerve: different mechanisms are responsible for the regulation of BDNF and NGF mRNA. J. Cell Biol. **119**, 45-54.

95. Hughes, P. M., and Perry, V. H. (2000). The role of macrophages in degeneration and regeneration in the peripheral nervous system. *In:* Degeneration and Regeneration in the Nervous System, N. R. Saunders and K. M. Dziegielewska, eds. (Amsterdam: Harwood Academic Publishers), pp. 263-283.

96. Bellamkonda, R., Ranieri, J. P., Bouche, N., and Aebischer, P. (1995). Hydrogel-based three-dimensional matrix for neural cells. J. Biomed. Mat. Res. **29**, 663-71.

97. Labrador, R. O., Buti, M., and Navarro, X. (1995). Peripheral nerve repair: role of agarose matrix density on functional recovery. Neuroreport **6**, 2022-6.

98. Bellamkonda, R., Ranieri, J. P., and Aebischer, P. (1995). Laminin oligopeptide derivatized agarose gels allow three-dimensional neurite extension in vitro. J. Neurosci. Res. **41**, 501-9.

99. Borkenhagen, M., Clemence, J. F., Sigrist, H., and Aebischer, P. (1998). Three-dimensional extracellular matrix engineering in the nervous system. J. Biomed. Mat. Res. **40**, 392-400.

100. Sufan, W., Suzuki, Y., Tanihara, M., Ohnishi, K., Suzuki, K., Endo, K., and Nishimura, Y. (2001). Sciatic nerve regeneration through alginate with tubulation or nontubulation repair in cat. J. Neurotrauma **18**, 329-38.

101. Kataoka, K., Suzuki, Y., Kitada, M., Ohnishi, K., Suzuki, K., Tanihara, M., Ide, C., Endo, K., and Nishimura, Y. (2001). Alginate, a bioresorbable material derived from brown seaweed, enhances elongation of amputated axons of spinal cord in infant rats. J. Biomed. Mat. Res. **54**, 373-84.

102. Vacanti, J. P., Morse, M. A., Saltzman, W. M., Domb, A. J., Perez-Atayde, A., and Langer, R. (1988). Selective cell transplantation using bioabsorbable artificial polymers as matrices. J. Pediatr. Surg. **23**, 3-9.

103. Barrera, D. A., Zylstra, E., Lansbury, P. T., and Langer, R. (1993). Synthesis and RGD peptide modification of a new biodegradable copolymer system: Poly(lactic acid-*co*-lysine). J. Am. Chem. Soc. **115**, 11010-11011.

104. Cook, A. D., Hrkach, J. S., Gao, N. N., Johnson, I. M., Pajvani, U. B., Cannizzaro, S. M., and Langer, R. (1997). Characterization and development of RGD-peptide-modified poly(lactic acid-*co*-lysine) as an interactive, resorbable biomaterial. J. Biomed. Mat. Res. **35**, 513-523.

105. Hern, D. L., and Hubbell, J. A. (1998). Incorporation of adhesion peptides into nonadhesive hydrogels useful for tissue resurfacing. J. Biomed. Mat. Res. **39**, 266-76.

106. Elbert, D. L., and Hubbell, J. A. (2001). Conjugate Addition Reactions Combined with Free-Radical Cross-Linking for the Design of Materials for Tissue Engineering. Biomacromolecules **2**, 430-441.

107. Healy, K. E., Rezania, A., and Stile, R. A. (1999). Designing biomaterials to direct biological responses. Ann. NY Acad. Sci. **875**, 24-35.

108. Stile, R. A., and Healy, K. E. (2001). Semi-Interpenetrating Polymer Networks for Tissue Engineering. *In:* 5th Annual Hilton Head Workshop on Engineering Tissues, R. M. Nerem, ed. (Hilton Head Island, S.C., USA).

109. McGrath, K. P., Tirrell, D. A., Kawai, M., Mason, T. L., and Fournier, M. J. (1990). Chemical and biosynthetic approaches to the production of novel polypeptide materials. Biotechnol. Prog. **6**, 188-92.

110. Kiick, K. L., Weberskirch, R., and Tirrell, D. A. (2001). Identification of an expanded set of translationally active methionine analogues in Escherichia coli. FEBS Lett. **502**, 25-30.

111. Sharma, N., Furter, R., Kast, P., and Tirrell, D. A. (2000). Efficient introduction of aryl bromide functionality into proteins in vivo. FEBS Lett. **467**, 37-40.

112. Petka, W. A., Harden, J. L., McGrath, K. P., Wirtz, D., and Tirrell, D. A. (1998). Reversible hydrogels from self-assembling artificial proteins. Science **281**, 389-92.

113. Krejchi, M. T., Atkins, E. D., Waddon, A. J., Fournier, M. J., Mason, T. L., and Tirrell, D. A. (1994). Chemical sequence control of beta-sheet assembly in macromolecular crystals of periodic polypeptides. Science **265**, 1427-32.

114. Cantor, E. J., Atkins, E. D., Cooper, S. J., Fournier, M. J., Mason, T. L., and Tirrell, D. A. (1997). Effects of amino acid side-chain volume on chain packing in genetically engineered periodic polypeptides. J. Biochem. (Tokyo) **122**, 217-25.

115. Panitch, A., Matsuki, K., Cantor, E. J., Cooper, S. J., Atkins, E. D. T., Fournier, M. J., Mason, T. L., and Tirrell, D. A. (1997). Poly(L-alanylglycine): Multigram-Scale

Biosynthesis, Crystallization, and Structural Analysis of Chain-Folded Lamellae. Macromolecules **30**, 42-49.

116. Panitch, A., Yamaoka, T., Fournier, M. J., Mason, T. L., and Tirrell, D. A. (1999). Design and Biosynthesis of Elastin-like Artificial Extracellular Matrix Proteins Containing Periodically Spaced Fibronectin CS5 Domains. Macromolecules **32**, 1701-1703.

117. Welsh, E. R., and Tirrell, D. A. (2000). Engineering the Extracellular Matrix: A Novel Approach to Polymeric Biomaterials. I. Control of the Physical Properties of Artificial Protein Matrices Designed to Support Adhesion of Vascular Endothelial Cells. Biomacromolecules **1**, 23-30.

118. van Hest, J. C., and Tirrell, D. A. (1998). Efficient introduction of alkene functionality into proteins in vivo. FEBS Lett. **428**, 68-70.

119. Chang, C. D., and Meienhofer, J. (1978). Solid-phase peptide synthesis using mild base cleavage of N alpha-fluorenylmethyloxycarbonylamino acids, exemplified by a synthesis of dihydrosomatostatin. Int. J. Pept. Protein Res. **11**, 246-9.

120. Ulbrich, K., Zacharieva, E. I., Obereigner, B., and Kopecek, J. (1980). Polymers containing enzymatically degradable bonds V. Hydrophilic polymers degradable by papain. Biomaterials **1**, 199-204.

121. Krinick, N. L., Sun, Y., Joyner, D., Spikes, J. D., Straight, R. C., and Kopecek, J. (1994). A polymeric drug delivery system for the simultaneous delivery of drugs activatable by enzymes and/or light. J. Biomat. Sci. Polym. Ed. **5**, 303-24.

122. Suzuki, Y., Tanihara, M., Nishimura, Y., Suzuki, K., Kakimaru, Y., and Shimizu, Y. (1997). A novel wound dressing with an antibiotic delivery system stimulated by microbial infection. ASAIO J. **43**, M854-7.

123. Tanihara, M., Suzuki, Y., Nishimura, Y., Suzuki, K., Kakimaru, Y., and Fukunishi, Y. (1999). A novel microbial infection-responsive drug release system. J. Pharm. Sci. **88**, 510-4.

124. West, J. L., and Hubbell, J. A. (1999). Polymeric Biomaterials with Degradation Sites for Proteases Involved in Cell Migration. Macromolecules **32**, 241-244.

125. Sperinde, J. J., and Griffith, L. G. (1997). Synthesis and Characterization of Enzymatically-Cross-Linked Poly(ethylene glycol) Hydrogels. Macromolecules **30**, 5255-5264.

126. Pratt, A. B. (2001). Cell-Responsive Synthetic Biomaterials Formed *In Situ*. *In:* Division of Chemistry and Chemical Engineering; Ph.D. Thesis (Pasadena: California Institute of Technology).

127. Pratt, A. B., and Hubbell, J. A. (2001). Synthetic Extracellular Matrices for *in situ* Tissue Engineering. *submitted for publication.*

128. Harris, J. M., and Zalipsky, S. (1997). Poly(ethylene glycol): Chemistry and Biological Applications. *In:* ACS Symposium Series (Washington, DC).

129. Kelly, J. P. (1991). The Neural Basis of Perception and Movement. *In:* Principles of Neural Science, Third Edition, E. R. Kandel, J. H. Schwartz and T. M. Jessell, eds. (Norwalk: Appleton & Lange), pp. 283-295.

130. Cotman, C. W., Cribbs, D. H., and Kahle, J. (1994). Toward Establishing Neural Networks in Culture. *In:* Enabling Technologies for Cultured Neural Networks, D. A. Stenger and T. M. McKenna, eds. (Academic Press, Inc.), pp. 3-22.

131. Connolly, P. (1994). Bioelectronic interfacing: micro- and nano-fabrication techniques for generating predetermined molecular arrays. TIBTECH **12**, 123-127.

132. Curtis, A., Wilkinson, C., and Breckenridge, L. (1994). Living Nerve Nets. *In:* Enabling Technologies for Cultured Neural Networks, D. A. Stenger and T. M. McKenna, eds. (Academic Press, Inc.), pp. 99-120.

133. Kovacs, G. T. A. (1994). Introduction to Theory, Design, and Modeling of Thin-Film Microelectrodes for Neural Interfaces. *In:* Enabling Technologies for Cultured Neural Networks, D. A. Stenger and T. M. McKenna, eds. (Academic Press, Inc.), pp. 121-165.

134. Kumar, A., Biebuyck, H. A., and Whitesides, G. M. (1994). Patterning Self-Assembled Monolayers: Applications in Materials Science. Langmuir **10**, 1498-1511.

135. Stenger, D. A., Georger, J. H., Dulcey, C. S., Hickman, J. J., Rudolph, A. S., Nielsen, T. B., McCort, S. M., and Calvert, J. M. (1992). Coplanar Molecular Assemblies of Amino- and Perfluorinated Alkylsilanes: Characterization and Geometric Definition of Mammalian Cell Adhesion and Growth. J. Am. Chem. Soc. **114**, 8435-8442.

136. Matsuda, T., and Sugawara, T. (1996). Control of cell adhesion, migration, and orientation on photochemically microprocessed surfaces. J. Biomed. Mat. Res. **32**, 165-173.

137. Corey, J. M., Wheeler, B. C., and Brewer, G. J. (1996). Micrometer Resolution Silane-Based Patterning of Hippocampal Neurons: Critical Variables in Photoresist and Laser Ablation Processes for Substrate Fabrication. IEEE Trans. Biomed. Engr. **43**, 944-955.

138. Taborelli, M., Eng, L., Descouts, P., Ranieri, J. P., Bellamkonda, R., and Aebischer, P. (1995). Bovine serum albumin conformation on methyl and amine functionalized surfaces compared by scanning force microscopy. J. Biomed. Mat. Res. **29**, 707-14.

139. Drumheller, P. D., and Hubbell, J. A. (1994). Polymer networks with grafted cell adhesion peptides for highly biospecific cell adhesive substrates. Anal. Biochem. **222**, 380-8.

140. Drumheller, P. D. (1994). Polymer Networks of Poly(Ethylene Glycol) as Biospecific Cell Adhesive Substrates (The University of Texas at Austin).

141. Drumheller, P. D., and Hubbell, J. A. (1995). Densely crosslinked polymer networks of poly(ethylene glycol) in trimethylolpropane triacrylate for cell-adhesion-resistant surfaces. J. Biomed. Mat. Res. **29**, 207-15.

142. Jeon, S. I., Lee, J. H., Andrade, J. D., and De Gennes, P. G. (1991). Protein-Surface Interactions in the Presence of Polyethylene Oxide: I. Simplified Theory. J. Colloid and Interface Sci. **142**, 149-158.

143. Jeon, S. I., and Andrade, J. D. (1991). Protein-Surface Interactions in the Presence of Polyethylene Oxide: II. Effect of Protein Size. J. Colloid and Interface Sci. **142**, 159-166.

144. Sigrist, H., Collioud, A., Clemence, J. F., Gao, H., Luginbühl, R., Sänger, M., and Sundarababu, G. (1995). Surface Immobilization of Biomolecules by Light. Optical Engineering **34**, 2339-2348.

145. Huebsch, J. B., Fields, G. B., Triebes, T. G., and Mooradian, D. L. (1996). Photoreactive analog of peptide FN-C/H-V from the carboxy-terminal heparin-binding domains of fibronectin supports endothelial cell adhesion and spreading on biomaterial surfaces. J. Biomed. Mat. Res. **31**, 555-567.

146. Massia, S. P., and Hubbell, J. A. (1991). Human endothelial cell interactions with surface-coupled adhesion peptides on a nonadhesive glass substrate and two polymeric biomaterials. J. Biomed. Mat. Res. **25**, 223-42.

147. Freshney, R. I. (1987). Culture of Animal Cells, Second Edition Edition (New York: Alan R. Liss, Inc.).

148. Ruoslahti, E., and Pierschbacher, M. D. (1987). New perspective in cell adhesion: RGD and integrins. Science **238**, 491-497.

149. Hubbell, J. A. (1995). Biomaterials in tissue engineering. Biotechnology (NY) **13**, 565-76.

150. Hubbell, J. A. (1999). Bioactive biomaterials. Curr. Opin. Biotechnol. **10**, 123-9.

151. Tyler-Cross, R., Sobel, M., Marques, D., and Harris, R. B. (1994). Heparin binding domain peptides of antithrombin III: analysis by isothermal titration calorimetry and circular dichroism spectroscopy. Protein Sci. **3**, 620-7.

152. Elbert, D. L., Pratt, A. B., Lutolf, M. P., Halstenberg, S., and Hubbell, J. A. (2001). Protein delivery from materials formed by self-selective conjugate addition reactions. J. Control. Release **76**, 11-25.

153. Zhao, X., and Harris, J. M. (1998). Novel Degradable Poly(ethylene glycol) Hydrogels for Controlled Release of Protein. J. Pharm. Sci. **87**, 1450-1458.

154. Modhaddam, M. J., and Matsuda, T. (1993). Molecular Design of Three-Dimensional Artificial Extracellular Matrix: Photosensitive Polymers Containing Cell Adhesive Peptide. J. Polym. Sci., Part A: Polymer Chemistry **31**, 1589-1597.

155. Kamath, K. R., and Park, K. (1995). Study on the Release of Invertase from Enzymatically Degradable Dextran Hydrogels. Polymer Gels and Networks **3**, 243-254.

156. Mathur, A. M., Moorjani, S. K., and Scranton, A. B. (1996). Methods for Synthesis of Hydrogel Networks: A Review. J. Macromol. Sci. Rev. Macromol. Chem. Phys. **C36**, 405-430.

157. Peppas, N. A., Keys, K. B., Torres-Lugo, M., and Lowman, A. M. (1999). Poly(ethylene glycol)-containing hydrogels in drug delivery. J. Control. Rel. **62**, 81-87.

158. Hill-West, J. L., Dunn, R. C., and Hubbell, J. A. (1995). Local release of fibrinolytic agents for adhesion prevention. J. Surg. Res. **59**, 759-63.

159. Morpurgo, M., Veronese, F. M., Kachensky, D., and Harris, J. M. (1996). Preparation of characterization of poly(ethylene glycol) vinyl sulfone. Bioconjug. Chem. **7**, 363-8.

160. Andersson, S. G., and Kurland, C. G. (1990). Codon preferences in free-living microorganisms. Microbiol. Rev. **54**, 198-210.

161. Ausubel, F., Brent, R., Kingston, R. E., Moore, D. D., Seidman, J. G., Smith, J. A., and Struhl, K. (1995). Short Protocols in Molecular Biology, Third Edition (John Wiley & Sons, Inc.).

162. Novagen, I. (1997). pET System Manual, 7th Edition (Madison, WI, USA: Novagen, Inc.).

163. Pomroy, N. C., and Deber, C. M. (1998). Solubilization of hydrophobic peptides by reversible cysteine PEGylation. Biochem. Biophys. Res. Commun. **245**, 618-21.

164. Pomroy, N. C., and Deber, C. M. (1999). Conjugation of polyethylene glycol via a disulfide bond confers water solubility upon a peptide model of a protein transmembrane segment. Anal. Biochem. **275**, 224-30.

165. Veronese, F. M. (2001). Peptide and protein PEGylation: a review of problems and solutions. Biomaterials **22**, 405-17.

166. Yu, S. M., Conticello, V. P., Zhang, G., Kayser, C., Fournier, M. J., Mason, T. L., and Tirrell, D. A. (1997). Smectic ordering in solutions and films of a rod-like polymer owing to monodispersity of chain length. Nature **389**, 167-70.

167. Parkhe, A. D., Cooper, S. J., Atkins, E. D., Fournier, M. J., Mason, T. L., and Tirrell, D. A. (1998). Effect of local sequence inversions on the crystalline antiparallel beta-sheet lamellar structures of periodic polypeptides: implications for chain-folding. Int. J. Biol. Macromol. **23**, 251-8.

168. ExPASy Molecular Biology Server: ProtParam tool: Institut Suisse de Bioinformatique (1999).

169. Hiraoka, N., Allen, E., Apel, I. J., Gyetko, M. R., and Weiss, S. J. (1998). Matrix metalloproteinases regulate neovascularization by acting as pericellular fibrinolysins. Cell **95**, 365-77.

170. Matsuno, H., Stassen, J. M., Vermylen, J., and Deckmyn, H. (1994). Inhibition of integrin function by a cyclic RGD-containing peptide prevents neointima formation. Circulation **90**, 2203-6.

171. Noiri, E., Gailit, J., Sheth, D., Magazine, H., Gurrath, M., Muller, G., Kessler, H., and Goligorsky, M. S. (1994). Cyclic RGD peptides ameliorate ischemic acute renal failure in rats. Kidney Int. **46**, 1050-8.

172. Greene, L. A., and Tischler, A. S. (1976). Establishment of a noradrenergic clonal line of rat adrenal pheochromocytoma cells which respond to nerve growth factor. Proc. Natl. Acad. Sci. USA **73**, 2424-8.

173. Tischler, A. S., and Greene, L. A. (1975). Nerve growth factor-induced process formation by cultured rat pheochromocytoma cells. Nature **258**, 341-2.

174. Greene, L. A. (1978). Nerve Growth Factor Prevents the Death and Stimulates the Neuronal Differentiation of Clonal PC12 Pheochromocytoma Cells in Serum-Free Medium. J. Cell Biol. **78**, 747-755.

175. Brewer, G. J., Torricelli, J. R., Evege, E. K., and Price, P. J. (1993). Optimized Survival of Hippocampal Neurons in B27-Supplemented Neurobasal™, a New Serum-free Medium Combination. J. Neurosci. Res. **35**, 567-76.

176. Bottenstein, J. E. (1985). (Cell Culture in the Neurosciences). *In:* Cell Culture in the Neurosciences, J. E. Bottenstein and A. L. Harvey, eds. (New York and London: Plenum Press), pp. p. 3.

177. Herbert, C. B., Bittner, G. D., and Hubbell, J. A. (1996). Effects of fibinolysis on neurite growth from dorsal root ganglia cultured in two- and three-dimensional fibrin gels. J. Comp. Neurol. **365**, 380-91.

178. Skene, J. H. (1989). Axonal growth-associated proteins. Annu. Rev. Neurosci. **12**, 127-56.

179. Meiri, K. F., Pfenninger, K. H., and Willard, M. B. (1986). Growth-associated protein, GAP-43, a polypeptide that is induced when neurons extend axons, is a component of growth cones and corresponds to pp46, a major polypeptide of a subcellular fraction enriched in growth cones. Proc. Natl. Acad. Sci. USA **83**, 3537-41.

180. Sigma-Aldrich, I. (1999). Monoclonal Anti-GAP-43, Product Information (www.sigma-aldrich.com).

181. DiMilla, P. A., Stone, J. A., Quinn, J. A., Albelda, S. M., and Lauffenburger, D. A. (1993). Maximal migration of human smooth muscle cells on fibronectin and type IV collagen occurs at an intermediate attachment strength. J Cell Biol **122**, 729-37.

182. Schense, J. C., and Hubbell, J. A. (2000). Three-dimensional migration of neurites is mediated by adhesion site density and affinity. J Biol Chem **275**, 6813-8.

183. Busby, T. F., Argraces, W. S., Brew, S. A., Pechik, I., Gilliland, G. L., and Ingham, K. C. (1995). Heparin Binding by Fibronectin Module-III-13 Involves Six

Discontinuous Basic Residues Brought Together to Form a Cationic Cradle. J. Biol. Chem. **270**, 18558-18562.

184. Waite, K. A., Mugnai, G., and Culpg, L. A. (1987). A Second Cell-Binding Domain on Fibronectin (RGDS-Independent) for Neurite Extension of Human Neuroblastoma Cells. Exp. Cell Res. **169**, 311-327.

185. Brinkley, M. (1992). A Brief Survey of Methods for Preparing Protein Conjugates with Dyes, Haptens, and Cross-Linking Reagents. Bioconjugate Chem. **3**, 2-13.